INFRARED AND RAMAN SPECTROSCOPY STUDY OF LAYERED SYSTEMS

by

JIAN LI

A dissertation submitted to the Graduate Faculty in Physics in partial fulfillment of the requirements for the degree of Doctor of Philosophy
The City University of New York

2013

This manuscript has been read and accepted for the Graduate Faculty in Physics in satisfaction of the dissertation requirement for the degree of Doctor of Philosophy

Prof. Jiufeng J. Tu

Date — **Chair of Examining Committee**

Prof. Steven G. Greenbaum

Date — **Executive Officer**

Prof. Joseph L. Birman

Dr. Christopher C. Homes

Prof. Carlos A. Meriles

Prof. Sergey A. Vitkalov

Supervisory Committee

THE CITY UNIVERSITY OF NEW YORK

Abstract

INFRARED AND RAMAN SPECTROSCOPY STUDY OF LAYERED SYSTEMS

by

Jian Li

Adviser: Jiufeng Tu

Optical spectroscopy studies the interaction between light (photon) and matter. During such interaction, different processes such as reflection, transmission, scattering, absorption or fluorescence can occur. Among all the optical spectroscopic techniques, infrared (IR) and Raman spectroscopy are most commonly used. In an Infrared process, photons are absorbed. The required light source emits polychromatic Infrared light and when it passes through or being reflected by the sample the light is partially absorbed. The frequency dependent absorption allows one to study the electronic and vibrational structure of the sample. On the other hand, the Raman spectroscopy is second order in nature where the photon is scattered instead of being absorbed. A monochromatic light source is used instead of a continuous spectrum. Generally, the dominate effect in an optical process is absorption and transmission

but a (small) portion of photons are scattered. A small fraction of photons change their energy/wavelength during the scattering. Depending on the scale of the change in energy, those inelastic scatterings can be categorized into Brillouin scattering and Raman scattering. Although sharing the same mechanism, different energy scale require completely different experimental setups for Brillouin scattering and Raman scattering.

In the study of infrared and Raman spectroscopy, group theory is a very helpful tool. The calculation of absolute intensity of an optical transition is rather difficult and sometimes infeasible, especially for crystal vibrations. Group theory is the mathematical language that describes the symmetry property of the physical system. Selection rules based on symmetry consideration had been predicted. Group theory, especially representation theory, is an important branch of condensed matter physics.

Both theoretical and experimental results of my PhD research are presented. The topics being covered are: infrared study of iron based superconductor $BaFe_{1.85}Co_{0.15}As_2$; the study of Raman scattering with Laguerre-Gaussian (LG) beam.

Acknowledgments

I would like to express the deepest appreciation to Dr. Jiufeng J. Tu, who supported my PhD study and more importantly, introduced me to the world of physics. Without him, my dream of pursuing higher education would not be possible. I would also like to thank Dr. Joseph L. Birman for providing the vision, encouragement and advise necessary for me to proceed through the doctoral program and complete my dissertation. Special thanks go to my committee members, Dr. Christopher C. Homes, Dr. Carlos A. Meriles, Dr. Yuhang Ren and Dr. Sergey A. Vitkalov for their support and guidance.

Contents

List of Tables

List of Illustrations

Chapter 1

Group Theory

Symmetries exist everywhere. Group theory is the mathematical language describing the symmetries. IN the field of physics, group theory finds its applications in many branches. Famous examples are: the SU(2), U(3) group for free space; crystallographic point groups for molecules; crystallographic space groups for crystals; O(3) group for atomic physics. In this chapter, after a brief introduction of the history of the application of group theory in physics, some important areas of group theory, especially crystallographic point group and space group will be presented. Many other important areas, such as continuous groups, symmetric groups, full rotation groups, are not included.

1.1 Brief introduction and history

Currently, there are vigorous research activities in group theory applications in physics. This was not the case before the pioneer work by H. Weyl [1] and E. P. Wigner [2] in the 1920s and 1930s. Early interest of group theory is mainly confined in a quite small region, namely the periodic structures of crystals. J. F. C. Hessel [3] identified all the 32 crystallographic point groups in the year 1830 where only the rotational symmetry is considered. In 1890, Schonflies [4] and Fedorov [5] determined the 230 crystallographic space groups independently. Those studies solved the early problems that was raised by Steno [6] in 1669. In 1931, Wigner published the book *Gruppentheorie*

und ihre Anwendung auf die Quantenmechanik der Atomspektren, which is referred to some people as "the bible of group theory". Winger himself became familiar with group theory as a result of his interest in crystallography. After that, group theory has been applied in more and more fields of physics. One noticeable application is one of the greatest triumphs of human – relativity, to which Einstein successfully applied the *Lorentz group*.

The application of group theory in physics can be simply demonstrated by the standard example: $\int f(x)dx = 0$ if $f(x)$ is an odd function. Instead of doing the actual integral, simple symmetry consideration indicates that this is zero. This is one simplest example of group theory. In reality more symmetry operations besides *inversion* exist in the physical system under study and group theory predicts go/no go rules that are called *selection rules*.

1.2 Structure of abstract group

A *group* is a collection of elements $A,\ B,\ C,\ \cdots$ with certain group multiplication:

1. the set is closed under group multiplication.

2. the associate law holds.

3. identity element E exists.

4. inverse element exists.

Due to limitation of space, only finite groups are considered here. That is, the number of elements $A,\ B,\ C,\ \cdots$ is finite. Many important infinite groups, including continuous groups, can be found in standard textbooks. If the group multiplication

	E	A	B	C	D	F
E	E	A	B	C	D	F
A	A	E	D	F	B	C
B	B	F	E	D	C	A
C	C	D	F	E	A	B
D	D	C	A	B	F	E
F	F	B	C	A	E	D

Table 1.1 : Multiplication table for group G_6^2.

is commutative, the group is *Abelian*. In the following subsections we list concepts that are crucial for understanding an abstract group.

1.2.1 Multiplication table

The structure of the group are determined by its multiplication table. Two groups with the same multiplication table is isomorphic. A typical group multiplication table is given in table 1.1. It gives the product of an element from the row and an element from the column, such as $AB = D$. It is also clear that this group is not Abelian since $AB \neq BA$.

1.2.2 Rearrangement theorem

If the whole set of elements is multiplied by one same element within the group, each group element appears exactly once. In other words, multiplying each element by A_k merely rearranges the elements.

1.2.3 Subgroups

For some cases, a collection of elements within a large group $\mathscr{G}$ also forms a group $\mathscr{S}$. This smaller collection of elements are called *subgroup* of the original, larger group. A set of elements $\mathscr{S}X$ is called *right coset* if X is not in $\mathscr{S}$. It can be proved that two right cosets of $\mathscr{S}$ is either identical or have no elements in common. This leads to the conclusion that the order g of the subgroup $\mathscr{S}$ must be integral divisor of the order h of the large group $\mathscr{G}$, the ratio of the two order, h/g being the *index* of $\mathscr{S}$ in $\mathscr{G}$.

1.2.4 Class structure

The conjugate elements for element A is formed by XAX^{-1} where X is any element of the group $\mathscr{G}$. The collection of elements conjugate with each other forms a *class*. The identity element E forms a class itself. Any other classes other than E do not form subgroup. The way that a group $\mathscr{G}$ is divided into different classes is called *class structure*. Elements belonging to the same class have the same physical meaning. Accordingly, the *factor group* of $\mathscr{G}$ with respect to $\mathscr{S}$ can also be defined.

1.3 Representation of groups

1.3.1 Representation

The representation of a group is a set of matrices $D(g)$ that have one-to-one correspondence to group elements that satisfy

$$D(A)D(B) = D(AB) \tag{1.1}$$

Those matrices the satisfy the multiplication table. The dimensionality of the matrices is called the *dimensionality* of the representation. Infinite sets of matrices exist

to represent one group. Those can be decomposed into smaller matrices are called *reducible* and those cannot be decomposed are called *irreducible*.

1.3.2 Orthogonality theorem

It can be proved that the irreducible representations of a group satisfy the following *orthogonality theorem*:

$$\sum_g \bar{D}^{(i)}(g)_{\mu\nu} D^{(j)}(g)_{\alpha\beta} = \frac{h}{l_i} \delta_{i,j} \delta_{\mu\alpha} \delta_{\nu\beta} \tag{1.2}$$

where the summation g runs over all group elements and the matrix $\bar{D}^{(i)}(g)$ is the complex conjugate of $D^{(i)}(g)$.

1.3.3 Character table

The definition of the representation, $D(A)D(B) = D(AB)$, can not determine the matrices uniquely. A whole set of representations after unitary transformation is still a representation. Two sets of irreducible representations that can be connected by unitary transformation are equivalent. To make this arbitrary less annoying, the traces of the matrices are used since they are invariant under unitary transformation. Therefore the *character* of the ith representation is:

$$\chi^{(i)}(g) = \mathrm{Tr} D^{(i)}(g) = \sum_{\mu=1}^{l_i} D^{(i)}_{\mu\mu}(g) \tag{1.3}$$

Application the orthogonality theorem for representations shows that elements within one class have the same character. The orthogonality theorem for representations now becomes orthogonality theorems for characters:

$$\sum_k \bar{\chi}^{(i)}(\mathscr{C}_k) \chi^{(j)}(\mathscr{C}_k) = \frac{h}{N_k} \delta_{i,j}, \tag{1.4a}$$

$$\sum_i \bar{\chi}^{(i)}(\mathscr{C}_k) \chi^{(i)}(\mathscr{C}_l) = \frac{h}{N_k} \delta_{k,l} \tag{1.4b}$$

Based on this theorem, the characters for all irreducible representations can be obtained systematically and it has been done and tabulated.

1.3.4 Basis functions

A set of functions, $\psi^{(i)_k}$, are said to be the basis function of irreducible representation $D^{(i)}$ if

$$P_g \psi_\kappa^{(i)} = \sum_{\lambda=1}^{l_i} \psi_\lambda^i D^{(i)}(g)_{\lambda\kappa} \tag{1.5}$$

Following this definition, an orthogonal theorem is found for basis functions that two functions belonging to different irreducible representations or different rows of the same representation are orthogonal:

$$(\psi_\kappa^{(i)}, \psi_{\kappa'}^{(i')}) = \delta_{ii'}\delta_{\kappa\kappa'} \sum_{\lambda=1}^{l_i} (\psi_\lambda^{(i)}, \psi_\lambda^{(i)}) l_i^{-1} \tag{1.6}$$

It shows that the scalar product is independent of κ. According, two kinds of projection operators can be defined:

$$\mathscr{P}_{\lambda\kappa}^{(i)} = \frac{l_i}{h} \sum_g \bar{D}_{\lambda\kappa}^{(i)} P_g, \tag{1.7a}$$

$$\mathscr{P}^{(i)} = \sum_\kappa \mathscr{P}_{\kappa\kappa}^{(i)} = \frac{l_i}{h} \sum_g \bar{\chi}^{(i)} P_g \tag{1.7b}$$

so that when working on basis function

$$\mathscr{P}_{\lambda\kappa}^{(i)} \psi_{\kappa'}^{(j)} = \delta_{ij}\delta_{\kappa\kappa'} \psi_{\lambda'}^{(j)} \tag{1.8a}$$

$$\mathscr{P}^{(i)} \psi_{\kappa'}^{(j)} = \delta_{ij} \sum_\kappa \psi_\kappa^{(j)} \tag{1.8b}$$

The idea is that when projection operators works on any function, the output are the basis functions that transform according to certain irreducible representation. This serves as the corner stone of later analysis on Raman tensors for LG beam.

1.4 Group theory application in physics

1.4.1 Quantum mechanics and wave functions

In quantum mechanics, a physical system is described by its Hamiltonian $\mathscr{H}$. Some Hamiltonians have invariant properties therefore the Hamiltonian operator commute with some spatial operations. The set of complete commuting operators are said to form *the group of the Schrodinger equation*.

Schrodinger equation is generally in the form of $\mathscr{H}\psi_n = E_n\psi_n$ where E_n and ψ_n are the eigenvalue and eigenstates of the Hamiltonian operator. The commuting transformation operators have such properties:

$$P_g\mathscr{H}\psi_n = P_gE_n\psi_n \tag{1.9a}$$

$$\mathscr{H}P_g\psi_n = E_nP_g\psi_n \tag{1.9b}$$

From this we see that function $P_g\psi_n$ obtained by operating symmetry operators on eigenfunctions will also be an eigenfunction with the same energy. This set of functions obtained this way forms a complete basis space for the group of Schrodinger equation. Same energy means degeneracy. Those degeneracy forced by symmetry are called *normal degeneracy*. There could exist other degenerating functions that can not be connected with each other by symmetry operation and they are called *accidental degeneracy*. A classical example of accidental degeneracy is the degeneracy of $2s$ and $2p$ orbital functions in hydrogen-like atom. The eigenfunctions of energy E_n form basis set for the irreducible representation of the group of the Schrodinger equations.

It should be noted that the physical problem that group theory deals with does not confined into eigenvalue problems of Hamiltonian operators. Classical situation, such as molecule vibration and crystal vibration can also be handled by group theory ele-

gantly [7]. In that case, the Hamiltonian is the total potential and the eigenfunctions are the normal modes.

1.4.2 Selection rules

Having identified eigenstates as basis functions of the corresponding group, one further step is to establish the selection rules, *i.e.*, the transitions between those eigenstates. For invariant operators, the matrix elements $(\psi_{\kappa'}^{(i')}, \mathscr{H}\psi_{\kappa'}^{(i')})$ vanish between functions belonging to different irreducible representations or to different rows of the same unitary representation. For some physical system, perturbations break the original symmetry. For those invariant operators, the matrix element $(\psi_{\kappa'}^{(i')}, \mathscr{H}'\psi_{\kappa'}^{(i')})$ vanish unless the representation $D^{i'}$ is found in the direct product $D^{i} \times D^{\mathscr{H}'}$.

Those strong restrictions on the non-zero transitions are called *selection rules*. They depend only on the symmetry properties of the physical system. Other information of the interaction besides symmetry is irrelevant for this go/no go selection rules. The intensity of the transition sure depends on interaction details besides symmetry properties.

1.5 Crystallographic point group

A crystallographic point group is a set of symmetry operations with a central point fixed that leaves the pattern unchanged. Crystallographic means these point groups have their origin in crystal which limits the number of rotations to 2-fold, 3-fold, 4-fold and 6-fold. Different combinations of rotations with reflection lead to a total of 32 point groups.

1.5.1 List of the 32 crystallographic point group

Due to historical reasons, different notations exist in the literature. The Hermann-Mauguin notation (full and short), the Shubnikov notation and Schoenflies notations are most commonly used. The Hermann-Mauguin notation is sometimes called international notation. The 32 point groups are tabulated in tab .1 in different notations. These 32 point groups are categorized into 7 crystal systems: triclinic, monoclinic, orthorhombic, tetragonal, trigonal, hexagonal and cubic. All point groups are subgroups of O_h and D_{6h}.

1.5.2 Character tables

The character tables of those point groups can be found in any group theory text book, the standard one being *The Properties of the Thirty-Two Point Groups* [8] by G. F. Koster *et al.*

1.6 Crystallographic space groups

The major difference between point group and space group is that there is no fixed point in space groups. The presence of the translational symmetry greatly complicate the situation, for the irreducible representations of space groups are difficult to obtain and to use.

The space groups are a collection of spatial transformations. In a three dimensional world, both translation and rotation can be one dimensional, two dimensional and three dimensional. To form space groups, the dimensionality of the translation must be equal to or smaller than the dimensionality of the rotation. As a result, there are 6 different types of space groups and they are listed in table 1.2. Those groups

Dimension	name of the space group	number of the groups
(1,1)	line groups	2
(2,1)	frieze groups	7
(3,1)	rod groups	75
(2,2)	wallpaper groups	17
(3,2)	layer groups	80
(3,3)	Fedorov groups	230

Table 1.2 : Space groups of different dimension.

with unequal lattice dimension and rotation dimension are called *subperiodic* space groups. The 230 (3,3) Fedorov group and the 17 (2,2) wallpaper group are introduced in following sections.

Most generally, a space group operation is $\{\varphi|\mathbf{t}(\varphi)\}$, where φ is rotational operation and $\mathbf{t}(\varphi)$ is translational operation associated with rotation φ. $\{\varphi|\mathbf{t}(\varphi)\}$ represents the spatial operation: $\{\varphi|\mathbf{t}(\varphi)\}\cdot\mathbf{r}=\varphi\cdot\mathbf{r}+\mathbf{t}(\varphi)$. The product of two symmetry operations is $\{\varphi_1|\mathbf{t}_1(\varphi_1)\}\cdot\{\varphi_2|\mathbf{t}_2(\varphi_2)\}=\{\varphi_1\cdot\varphi_2|\mathbf{t}_1(\varphi_1)+\varphi_1\cdot\mathbf{t}_2(\varphi_2)\}$. The complete set of $\{\varphi|\mathbf{t}(\varphi)\}$ is space group $\mathscr{G}$. Let $\mathbf{R_L}$ denote lattice vectors and the complete set of $\mathbf{R_L}$ forms the translational group $\mathscr{I}$. In case $\mathbf{t}(\varphi)=\mathbf{R_L}$, the space group is symmorphic. If $\mathbf{t}(\varphi)=\mathbf{R_L}+\tau$, where $\tau\notin\mathscr{I}$, the group is non-symmorphic. The representation theory of non-symmorphic is much more difficult to handle.

1.6.1 The 230 (3,3) Fedorov groups

Same as the 32 point groups, different notations exist for 230 space groups. International notation and Schoenflies notations are most widely used. In table .2 the

list of 230 space groups are given, categorized according to crystal systems. Besides Shubnikov and Schoenflies notations, each space group are numbered and can be quoted using this number. In the international notation, the first part is a capital letter indicating the translational symmetry of the lattice. P, C, F, I representation simple, base-centered, face-centered and body-centered Bravais lattices. The second part indicates the rotational symmetry of the crystal. m, 2, 3, 4, $\bar{3}$ and $\bar{4}$ are signs of pure rotation and reflection; a, b, c, d, n, 2_1, 3_1, 3_2, 4_1, 4_2 and 4_3 are signs of glide planes and screw axis, which in turn are signs of non-symmorphic space groups. A detailed description of each space group, including the list of symmetry operation and the list of Wyckoff positions [9], is given by [10]. The following volumes in the same series by IUCr (International Union of Crystallography) are also useful.

1.6.2 The 17 (2,2) wallpaper groups

The 17 wallpaper groups are listed in table .3. The standard notation for wallpaper groups are IUC notation, IUC standing for the international Union of Crystallography. The notations have the same meaning as in (3,3) case.

1.7 Representation of space groups

The main difference between point group and space group is the presence of translation symmetry in space groups. Infinitely large number of translational symmetry makes the representation theory complicated. In this section, the method of getting irreducible representation and characters of space groups are introduced. It is presented for (3,3) Fedorov groups. Its application to (2,2) wallpaper group is similar but easier.

1.7.1 Character table of (3,3) Fedorov group

The number of symmetry operations in any space group is the product of the number of rotational operations times the number of primitive cell in the sample. The number of rotational operations can be $s = 1, 2, 3, 4, 6, 12, 16, 24, 48$. The number of primitive cell in a crystal is $(N_1 \times N_2 \times N_3)$ and periodic boundary conditions are assumed. With $(N_1 \times N_2 \times N_3 \times s)$ elements, the representation theory of space group must be handled with the introduction of Brillouin zone. There are $N_1 \times N_2 \times N_3$ Brillouin zone points and the irreducible representations are labeled by Brillouin zone point $\mathbf{k}$. At each Brillouin point, the full group $\mathscr{G}$ reduce to a smaller, handleable group $\mathscr{G}_{\mathbf{k}}$. The full irreducible representation of $\mathscr{G}$ can be *induced* from the irreducible representations of $\mathscr{G}_{\mathbf{k}}$. Following irreducible representation, the character table can be obtained. This method will be briefly introduced below in this section. In practice, this is not an easy job, especially for the Brillouin points on the surface of the Brillouin zone of the non-symmorphic space groups, where the irreducible representation of $\mathscr{G}_{\mathbf{k}}$ can not be simply read out from the corresponding point group [11]. Outstanding and exhaustive literatures (Kovalev [12], Zak [13], Miller and Love [14], Cracknell and Davis [15].) exist on this topic where both the matrices and the characters of irreducible representations are tabulated. Even with the help of those tables, the representation theory of crystallographic space groups is not easy because of the chaos in notation.

The goal of getting irreducible representations of space groups is to find for each symmetry operation $\{\varphi|\mathbf{t}(\varphi)\}$ a matrix $D^{(\bigstar k)(m)}(\{\varphi|t(\varphi)\})$ so that $D^{(\bigstar k)(m)}(\{\varphi_1|\mathbf{t}(\varphi_1)\})$ $\cdot\, D^{(\bigstar k)(m)}(\{\varphi_2|\mathbf{t}(\varphi_2)\}) = D^{(\bigstar k)(m)}(\{\varphi_1 \cdot \varphi_2|\mathbf{t}_1(\varphi_1)+\varphi_1\cdot\mathbf{t}_2(\varphi_2)\})$. $\bigstar k$ is label for Brillouin zone point and m is label for the mth irreducible representation at $\bigstar k$ point. Rotational operations brings wave function with wave vector k to wave functions at

wave vectors $\{\varphi \cdot k\}$. Some of these wave vector is equivalent as k: $\{\varphi_i \cdot k\} = k + B_H$, where B_H is any reciprocal lattice vector. The inequivalent set of $\{\varphi \cdot k\}$ is defined as *star of* k and each inequivalent one of $\{\varphi \cdot k\}$ is called an *arm* of the star. Those symmetry operations $\{\varphi|\mathbf{t}(\varphi)\}$ that $\{\varphi_i \cdot k\} = k + B_H$ defines a new group $\mathscr{G}_k$. It is called *group of wave vector* k and is a subgroup of $\mathscr{G}$. The representation of wave vector group $\mathscr{G}_k$ can be obtained from their corresponding point groups in most cases. The only exception is at Brillouin boundary point of non-symmorphic groups. For any point inside Brillouin zone or any symmorphic space group, the representation $D^{(k)(m)}(\{\varphi|\mathbf{t}(\varphi)\})$ is simply $D^{(k)(m)}(\varphi) \times e^{-\mathrm{i}k\cdot\mathbf{t}(\varphi)}$, where $D^{(k)(m)}(\varphi)$ is representation of the point group at wave vector k. The representation theory at Brillouin zone boundary points of non-symmorphic space groups can be obtained using *little group method* or theory of *ray representation*. This trouble can not be avoided because all the interesting physics happen at those high symmetry point due to the high density of states. The space group $\mathscr{G}$ can be decomposed to $\mathscr{G}_k$ in the form of $\mathscr{G} = \mathscr{G}_k + \cdots + \{\varphi_\sigma|\mathbf{t}_\sigma\}\mathscr{G}_k + \cdots + \{\varphi_s|\mathbf{t}_s\}\mathscr{G}_k$, where s is the number of arms in $\bigstar k$ and φ_σ is an operation that brings k to its inequivalent point. Define *dotted matrix* $\dot{D}^{(k)(m)}(\{\varphi|\mathbf{t}\})$:

$$\dot{D}^{(k)(m)}(\{\varphi|\mathbf{t}\}) = \begin{cases} 0 & \text{if } \{\varphi|\mathbf{t}\} \text{ is not in } \mathscr{G}_k \\ D^{(k)(m)}(\{\varphi|\mathbf{t}\}) & \text{if } \{\varphi|\mathbf{t}\} \text{ is in } \mathscr{G}_k. \end{cases} \tag{1.10}$$

The $D^{(\bigstar k)(m)}$ of $\mathscr{G}$ can be induced from $D^{(k)(m)}$ of $\mathscr{G}_k$. It is in a block structure with σ and τ as indices for blocks where φ_σ and φ_σ are operations that bring k to its inequivalent positions.

$$D^{(\bigstar k)(m)}(\{\varphi|\mathbf{t}\})_{\sigma\tau} = \dot{D}^{(k)(m)}(\{\varphi_\sigma|\mathbf{t}_\sigma\}^{-1} \cdot \{\varphi|\mathbf{t}\} \cdot \{\varphi_\tau|\mathbf{t}_\tau\}). \tag{1.11}$$

The matrix $D^{(\bigstar k)(m)}$ is in block form where each block is a matrix from $D^{(k)(m)}$ of $\mathscr{G}_k$. $D^{(\bigstar k)(m)}$ is $s \times s$ the size of $D^{(k)(m)}$ where s is the number of arms in $\bigstar k$. The

character of $D^{(\bigstar k)(m)}$ is :

$$\chi^{(\bigstar k)(m)}(\{\varphi|\mathbf{t}\}) = \sum_{\sigma} \dot{\chi}^{(k)(m)}(\{\varphi_\sigma|\mathbf{t}_\sigma\}^{-1} \cdot \{\varphi|\mathbf{t}\} \cdot \{\varphi_\sigma|\mathbf{t}_\sigma\}). \tag{1.12}$$

where the *dotted character* is defined as:

$$\dot{\chi}^{(k)(m)}(\{\varphi|\mathbf{t}\}) = \begin{cases} 0 & \text{if } \{\varphi|\mathbf{t}\} \text{ is not in } \mathscr{G}_k \\ \chi^{(k)(m)}(\{\varphi|\mathbf{t}\}) & \text{if } \{\varphi|\mathbf{t}\} \text{ is in } \mathscr{G}_k. \end{cases}$$

1.7.2 Character table of (2,2) wallpaper group

Same as (3,3) Fedorov group, the wallpaper groups can be either symmorphic or nonsymmorphic. The irreducible representations of wallpaper groups can be obtained the same way as space groups. Due to relatively simpler two dimensional Brillouin zone and small number (17) of groups, the irreducible representations of wallpaper groups is represented in one review article [16] instead of intimidating books. Note the labeling of Brillouin zone high symmetry points maybe different according to different authors.

1.8 Crystallographic double groups

Up until now, in the discussion of electrons, a single function with spatial coordinate is used to describe one electron state. This is not true in reality because the electrons are spin half particles and their wave functions are *spinors*. In other words, the real wave function of an electron has two components. The spinors can not be described by the irreducible representations of ordinary groups introduced in previous chapters and the concept of *double group* must be used to deal with spinors.

The full derivation of double group and its representation theory is long and complicated. An "artificial" yet effective way of introducing double group is through

the *three dimensional rotational group* $O(3)$. The character of any operation in O_3 is $\chi_J(\alpha) = \frac{\sin(J+\frac{1}{2})\alpha}{\sin(\alpha/2)}$. When J is an integer or zero, the character of operation α is the same as operation $(\alpha + 2\pi)$. However, when J is half-integer, the above rule does not hold and $\chi_J(\alpha + 2\pi) = -\chi_J(\alpha)$. There exists an additional operation, rotation by 2π, that in single group is the identity operator but in double group which describes spinors of spin half particles, is not the identity. It is due to the homomorphism between $SU(2)$ and $O(3)$. The rotation by 2π is labelled $\bar{E}$. $\bar{E}$ commutes with all spatial operations. The combination of $\bar{E}$ with all other ordinary spatial operations doubles the size of the group. This is where the name double groups comes from. The corresponding representations of the double group are called *double representations* due to double group or *two valued representations*. Single electron wave function actually belongs to double representations.

There are 32 crystallographic double point groups. The character tables of the double groups can also be worked out despite the relatively larger size of the group. The basis functions for single groups involves only (x, y, z) but the basis functions for double groups are combination of (x, y, z) and spinor ψ. It should be noted that time reversal has not introduced yet and Kramers theorem does not apply so far although according to the character tables all the double representations seems to be degenerate. There are few exception that double representations are non-degenerate.

1.9 Time reversal and magnetic group

The discussion on point group and space groups so far focus only on spatial symmetries of the the physical system. However, besides spatial operation, time reversal θ is a different kind of transformation:

$$\theta : t \mapsto -t \tag{1.13}$$

For a particle with spin J, $\theta = \exp -i\pi \frac{J_y}{\hbar} K$ where J_y is the y component of the particle's spin and K is the complex conjugate operation. Its effects on position and momentum operators are $\theta x \theta^{-1} = x$ and $\theta p \theta^{-1} = -p$. A physical system with even (including zero) or odd electrons is described by Schrodinger equation or Dirac equation. Being different in nature, Schrodinger equation and Dirac equation behave differently under time reversal operations θ. It can be shown that:

$$\theta^2 = 1 \quad : \quad \text{even number of electrons} \tag{1.14a}$$

$$\theta^2 = -1 : \quad \text{odd number of electrons} \tag{1.14b}$$

When studying atoms, molecules and crystals, the effect of the time reversal operator θ is to change the direction of the spin. Obviously, for physical system without magnetic momentum, the introduction of θ doubles the number of symmetry operations in the group. And for a system with magnetic momentum, θ itself is not an symmetry operation but it becomes one when combined with spatial operations. Different combinations exist and the ordinary point groups and space groups can be extended to magnetic point groups and magnetic space groups with the introduction of θ. Those two magnetic groups will be given in the next two subsections. Due to the unpopularity of the wallpaper group, its corresponding magnetic group is not well studied. Only the magnetic groups of the Fedorov space groups are given.

1.9.1 Magnetic crystallographic point group

Suppose two crystallographic point group $\mathscr{G}$ and $\mathscr{H}$. A magnetic crystallographic point group $\mathscr{M}$ must be of the three structures:

1. $\mathscr{M} = \mathscr{G}$

2. $\mathscr{M} = \mathscr{G} \oplus \theta\, \mathscr{G}$

3. $\mathscr{M} = \mathscr{H} \oplus \theta\ (\mathscr{G} - \mathscr{H})$

Type (1) is the ordinary point group, where time reversal is not considered. There are 32 of these. Type (2) describes a physical system without (permanent) magnetic momentum. The magnetic group is simply the ordinary point group plus elements that are formed by spatial operation associated with time reversal. Obviously there are 32 of type (2) magnetic point groups. They are sometimes called "gray" group. Type (3) magnetic groups are formed by splitting one point group $\mathscr{G}$ into two: $\mathscr{H}$ and $\mathscr{G} - \mathscr{H}$. There are 58 different ways of splitting the 32 point groups. The totally number of magnetic crystallographic point group is 122. The magnetic crystallographic point groups are also called Shubnikov [17] point groups.

1.9.2 Magnetic crystallographic space group

Magnetic crystallographic space groups are also called Shubnikov [17] space groups. There are four ways of introducing time reversal into crystallographic space groups:

1. $\mathscr{M} = \mathscr{G}$

2. $\mathscr{M} = \mathscr{G} \oplus \theta\ \mathscr{G}$

3. $\mathscr{M} = \mathscr{H} \oplus \theta\ \{\alpha_i|\tau_i\}\ \mathscr{H} = \mathscr{H} \oplus \theta\ (\mathscr{G} - \mathscr{H})$

4. $\mathscr{M} = \mathscr{H} \oplus \theta\ \{e|t_0\}\ \mathscr{H}$

The first two type of magnetic space groups are trivial and each type contains 230 space groups. Type (3) corresponds to the splitting a Fedorov space group in two and associate half with time reversal and there are 674 of such Shubnikov space groups. Type (4) describes black and white lattice, where the element $\{e|t_0\}$ is a pure fractional transition. By fractional one means that t_0 is not a lattice vector in group

$\mathscr{G}$. There are 517 such type of Shubnikov space groups. The combination of the four types gives a total of 1651. The full list of the 122 Shubnikov point groups and the 1651 Shubnikov space groups can be found in standard textbooks.

1.9.3 Co-representation

Although anti-unitary time reversal orator θ is included, the magnetic groups are still group and they have irreducible representations. Except for the type (1) magnetic point groups and magnetic space groups, a general magnetic group is of the form:

$$\mathscr{M} = \mathscr{H} \oplus \mathbf{a_0}\mathscr{H} \tag{1.15}$$

Here, $\mathbf{a_0}$ is a fixed anti-unitary operator that $\mathbf{a_0} = \theta\mathbf{u_0}$, $\mathbf{u_0}$ being a corresponding fixed unitary operator in $\mathscr{H}$. Also, we use $\mathbf{u}$ to denote the unitary operations from $\mathscr{H}$ and use $\mathbf{a}$ to denote the anti-unitary operator $\mathbf{a} = \theta\mathbf{u}$. For type (2) magnetic point groups and type (2) magnetic space groups, $\mathbf{a_0}$ can be chosen to be time reversal operator θ and for type (3) magnetic point groups and type (3), (4) magnetic space groups, $\mathbf{a_0}$ is θ associated with some spatial operation: $\mathbf{a_0} = \theta\{\alpha|\tau\}$.The anti-unitary operator is both anti-linear and anti-unitary:

$$\mathbf{a_0}(c_1 f + c_2 g) = \bar{c}_1 \mathbf{a_0} f + \bar{c}_2 \mathbf{a_0} g \tag{1.16a}$$

$$(\mathbf{a_0} f, \mathbf{a_0} g) = (g, f) \tag{1.16b}$$

The representation theory of magnetic groups has been solved by Wigner [18] and later by Dimmock and Wheeler [19]. To distinguish from representations of ordinary groups, the irreducible representations of magnetic groups are called *irreducible co-representations*. Due to the anti-unitary nature of the half the operators,the definition

of co-representation $M^i(\mathbf{g}=\mathbf{u},\mathbf{a})$ is different from the definition of ordinary group:

$$M^i(\mathbf{u_1})M^i(\mathbf{u_2}) = M^i(\mathbf{u_1 u_2}) \tag{1.17a}$$

$$M^i(\mathbf{u})M^i(\mathbf{a}) = M^i(\mathbf{ua}) \tag{1.17b}$$

$$M^i(\mathbf{a})\bar{M}^i(\mathbf{u}) = M^i(\mathbf{au}) \tag{1.17c}$$

$$M^i(\mathbf{a_1})\bar{M}^i(\mathbf{a_2}) = M^i(\mathbf{a_1 a_2}) \tag{1.17d}$$

The irreducible co-representation for $\mathscr{M} = \mathscr{H} \oplus \mathbf{a_0}\mathscr{H}$ can be built up from the irreducible representation of its unitary part $\mathscr{H}$. Suppose all the irreducible representations $D^i(\mathbf{u})$ of $\mathscr{H}$ have been obtained already. It can be shown that the co-representation $M^i(\mathbf{g})$ of $\mathscr{M}$ is related to $D^i(\mathbf{u})$:

Case (a)

$M^i(\mathbf{u}) = D^i(\mathbf{u})$; $M^i(\mathbf{a}) = D^i(\mathbf{a a_0^{-1}})\beta$.

$\beta\beta^* = D^i(\mathbf{a_0^2})$.

Case (b)

$$M^i(\mathbf{u}) = \begin{pmatrix} D^i(\mathbf{u}) & 0 \\ 0 & D^i(\mathbf{u}) \end{pmatrix};\ M^i(\mathbf{a}) = \begin{pmatrix} 0 & D^i(\mathbf{a a_0^{-1}})\beta \\ -D^i(\mathbf{a a_0^{-1}})\beta & 0 \end{pmatrix}.$$

$\beta\beta^* = -D^i(\mathbf{a_0^2})$.

Case (c)

$$M^i(\mathbf{u}) = \begin{pmatrix} D^i(\mathbf{u}) & 0 \\ 0 & \bar{D}^i(\mathbf{a_0^{-1} u a_0}) \end{pmatrix};\ M^i(\mathbf{a}) = \begin{pmatrix} 0 & D^i(\mathbf{a a_0}) \\ \bar{D}^i(\mathbf{a_0^{-1} a}) & 0 \end{pmatrix}.$$

The criterion for the co-representation being case (a), (b) or (c) is:

$$\sum_{\mathbf{a}} \chi^i(\mathbf{a^2}) = \begin{cases} +n & \text{case (a)} \\ -n & \text{case (b)} \\ 0 & \text{case (c)} \end{cases} \tag{1.18}$$

The summation is over all the anti-unitary operators. Taking into account the defination $\mathbf{a_0} = \theta\mathbf{u_0}$ and the fact that time reversal commutes with all spatial operators, the above criterion can be transformed into a form of summations over unitary operators:

$$\sum_{\mathbf{u}} \chi^i(\mathbf{u_0 u u_0 u}) = \begin{cases} +\omega n & \text{case (a)} \\ -\omega n & \text{case (b)} \\ 0 & \text{case (c)} \end{cases} \tag{1.19}$$

where $\omega = 1$ for even number of electrons and $\omega = -1$ for odd number of electrons. For type (2) magnetic point groups and magnetic space groups, the representative anti-unitary operator is time reveral operator θ itself. In this case, the $\mathbf{u_0}$ becomes the identity and the above criterion simplifies to:

$$\sum_{\mathbf{u}} \chi^i(\mathbf{u_0^2}) = \begin{cases} +\omega n & \text{case (a)} \\ -\omega n & \text{case (b)} \\ 0 & \text{case (c)} \end{cases} \tag{1.20}$$

It is the *Frobenius-Schur* test [20, 21] that they discovered while working on *real representations*. The three cases in the discussion of real representation (real and equivalent; equivalent but not real; not equivalent) are special situations of type (2) magnetic group. Obviously in case (b) and (c) the dimensionality of the co-representation of the magnetic group is twice the dimensionality of its corresponding unitary group. This phenomena is called time reversal induced *additional degeneracy*. It should not be confused with the *double group* where no time reversal symmetry is introduced. So far we have introduced the theory of co-representation. It will be applied to magnetic point group and magnetic space groups below.

magnetic point groups

There are 122 magnetic crystallographic point groups in three types. the co-representations of the magnetic crystallographic point groups $\mathscr{M} = \mathscr{H} \oplus \mathbf{a_0}\mathscr{H}$ is obtained by inducing from representations of the corresponding crystallographic point group $\mathscr{H}$ once the case to which $\mathscr{M}$ belong is known. The co-representation for the 32 type (1) magnetic crystallographic point groups is the same as the both the single and double representation of the corresponding crystallographic point groups.

For type (2) magnetic crystallographic point groups, the anti-unitary representative is time reversal itself. The co-representation results has been worked out using criterion 1.20. For case (a), the representation remains the same. For case (b), the representation stick together with itself, making the dimensionality of the co-representation twice the dimensionality of the point group. For case (c), two representations stick together. When more than two case (c) representations exist in one group, confusion can be avoided that two representations who stick together are complex conjugates.

The time reversal induced additional degeneracy has great impact on the electronic states. Careful inspection of the 32 type (2) magnetic crystallographic point groups show that all co-representations for double group is at least two-fold degenerate. This is the well known *Kramers theorem* that the energy levels of systems with an odd number of electrons are at least doubly degenerate, no matter how low the symmetry of the system is, as long as there is no external magnetic field that breaks the time reversal symmetry, in which case the system should be described by type (3) magnetic crystallographic point groups. The original Kramers theorem was derived from different routine [22].

The remaining 58 type (3) magnetic crystallographic point groups does not contain

time reversal itself therefore co-representation of these groups should be obtained from criterion 1.19 for both the single and double representations.

magnetic space groups

In principle, the co-representations of the crystallographic magnetic space groups $\mathscr{M} = \mathscr{H} \oplus \mathbf{a_0}\mathscr{H}$ is obtained by inducing from representations of the corresponding crystallographic space group $\mathscr{H}$. The major difficulty is that in the criterion, the summation is over infinite number of group elements. Further simplifications, using the orthogonality properties of the Fourier series, are required to make the criterion practical. This has been done to type (2) crystallographic magnetic space groups where time reversal itself presents. The derivation can be found in reference [11]. Only the results are listed here:

$$\sum_{p=1}^{g_p} \dot{\chi}^{(\kappa)(m)}(\{\psi_p|\tau_p\}^2)\Delta = \begin{cases} |\mathbf{P}(\mathbf{k})| & \text{case (a)} \\ -|\mathbf{P}(\mathbf{k})| & \text{case (b)} \\ 0 & \text{case (c)} \end{cases} \tag{1.21}$$

where the dotted character are defined in previous sections; $\mathbf{P}(\mathbf{k})$ is the number of elements in group of wavevector $\mathbf{P}(\mathbf{k})$ and

$$\Delta = \begin{cases} 1 & \text{if} \quad \psi_p \cdot \kappa = -\kappa + \mathbf{K} \\ 0 & \text{otherwise} \end{cases} \tag{1.22}$$

In other words, the symbol Δ is zero if $-k$ is not equivalent with k. A more special case is that the $\bigstar -k$ is not equivalent with $\bigstar k$, in which all Δs becomes zero and the co-representation belongs to case (3). Therefore for space groups without inversion symmetry, the co-representations of the space group, taking into account of

time reversal, is twice the size of the representation of the space group without time reversal. The doubling in size is due to the sticking together of representations from $\bigstar k$ and $\bigstar -k$. A physical system, without external magnetic field, is time reversal invariant. The full symmetry for this system contains time reversal operator therefore belongs to type (2) crystallographic magnetic point group and space group. The co-representation of such groups is called *physically irreducible representation.*

1.10 Electronic states

1.10.1 Electronic state in atom and molecule

For a physical system without translational symmetry, the index of the irreducible representations does not require momentum k and should be 1 fold in symmetry. In molecules, an electronic states is said to belong to, say, E_g representation. In atoms, an electronic states is said to be $3p$ states, where p is the index for symmetry and 3 is the index for energy that has no symmetry origin.

1.10.2 Electronic state in crystal

In the presence of periodic lattice structure, translational operations are added to the group that describes the symmetry of the physical system. The symmetry of the electronic wave function in crystal is labeled with two induces: k and Γ_i.

In single electron approximation, the Hamiltonian of an electron in crystal is:

$$[-\frac{\hbar^2}{2m}\nabla^2 + V(\mathbf{r})]\phi_n(\mathbf{k},\mathbf{r}) = \varepsilon_n\phi_n(\mathbf{k},\mathbf{r}) \tag{1.23}$$

and the potential $V(\mathbf{r})$ is invariant under the operation of the group of Schrodinger equation:

$$P_g V(\mathbf{r}) P_g^{-1} = V(\mathbf{r}) \tag{1.24}$$

Due to the translational symmetry of the group, the wave functions must have the form of *Bloch functions*:

$$\phi_n(\mathbf{k},\mathbf{r}) = e^{i\mathbf{k}\cdot\mathbf{r}}u_n(\mathbf{r}) \quad \text{with} \quad u_n(\mathbf{r}+\mathbf{R_L}) = u_n(\mathbf{r}) \tag{1.25}$$

Upon substitution, the Schrodinger equation now becomes:

$$-\frac{\hbar^2}{2m}\nabla^2 u_n(\mathbf{r}) + [V(\mathbf{r}) + \frac{\hbar}{m}\mathbf{k}\cdot\mathbf{p}]u_n(\mathbf{r}) = (\varepsilon_n - \frac{\hbar^2\mathbf{k}^2}{2m})u_n(\mathbf{r}) \tag{1.26}$$

This is called *pseudo-Schrodinger equation*. And the symmetry of the new Hamiltonian with $u_n(\mathbf{r})$ as eigenstates reduce from the whole group $\mathscr{G}$ to the group of wave vector $\mathscr{G}_\mathbf{k}$ when $\mathbf{k}$ is non-zero. In other words, at Brillouin points away from zone center, the irreducible representations of the wave functions are irreducible representations of the group at Brillouin zone point $\mathbf{k}$.

The irreducible representation obtained this way belongs to the single groups. To take into account of electron spin, the additional spinor is added to the irreducible representation. The double representation according to which spinors transform can be found in Koster [8] because the $\phi(1/2, \pm 1/2)$ is clearly shown in the basis functions. The product of a single representation and a double representation is a double representation. Then the time reversal operator is taken into account and for some cases, such as systems without inversion symmetry, two representations stick together to form a co-representation that is twice as large.

1.11 Vibrational states

1.11.1 Vibration in molecules

This section deals with molecular vibrations. A classical model is a good starting point and quantum mechanical treatment will be presented once the normal coordinate is

obtained. Suppose a molecule has symmetry $\mathscr{G}$. The αth component of the position of the atom i away from it equilibrium position in the molecule is labeled $\mathbf{r}^i_\alpha$. The potential energy of the molecule for small vibration can be kept only up to second order, first ordering being zero. The equations of motions for the system is:

$$m_i \frac{\partial^2 \mathbf{r}^i_\alpha}{\partial t^2} = -\sum_{j\beta} V^{ij}_{\alpha\beta} \mathbf{r}^j_\beta \tag{1.27}$$

$V^{ij}_{\alpha\beta}$ is the force constant. Define *force matrix* $D^{ij}_{\alpha\beta} = \frac{V^{ij}_{\alpha\beta}}{\sqrt{m_i m_j}}$ and use trial solution $\mathbf{r}^i_\alpha = \frac{\mathbf{u}^i_\alpha}{\sqrt{m_i}} e^{i\omega t}$, the equation of motion becomes:

$$\sum_{j\beta} D^{ij}_{\alpha\beta} \mathbf{u}^j_\beta - \omega^2 \mathbf{u}^i_\alpha = 0 \tag{1.28}$$

Apparently $D^{ij}_{\alpha\beta}$ inherits the symmetry properties of the potential energy of the system there is invariant under transformation of the group $\mathscr{G}$. Solving eigenvalues and eigenstates gives all the energies and normal modes of the vibration. It can be shown rigorously [7] that 6 (for non-linear molecules) or 5 (for linear molecules) of the eigenvalues are zero and they correspond to the translation and rotation of the molecule.

The force constant matrix $D^{ij}_{\alpha\beta}$ is invariant under group $\mathscr{G}$ therefore the equation of motion 1.28 can be analyzed with group theory. The results are based on different sets of atoms (that transforms to each other under symmetry operation) in the molecule. For one set of n atoms, assign each atom with three vectors in x, y, z direction. The positions of atoms form a representation for group $\mathscr{G}$ called *atomic equivalence representation* and the $3n$ vectors assigned on them form a bigger representation of group $\mathscr{G}$ called *mechanical representation*. The character $\chi^{AER}(g)$ for atomic equivalence representation is easy: it is the number of atoms sitting on their original position under operation P_g. The mechanical representation is simply the

direct product of atomic equivalence representation and *vector representation*, which is what x, y, z belong in group $\mathscr{G}$:

$$\chi^{\text{mech}}(g) = \chi^{\text{AER}}(g) \cdot \chi^{\text{vector}}(g) \tag{1.29}$$

Repeat the same for the all sets of atoms in the molecule, the *total mechanical representation* is obtained. The decomposition of total mechanical representation gives all the modes for the molecule. Taken away the translational mode and rotational mode, the rest are vibrational modes for the molecule. The translational mode is a vector that transforms as x, y, z and the rotational mode is a pseudo-vector that transforms as R_x, R_y, R_z.

The eigenstates of the molecule vibration can also be obtained with group theory. Applying the projection operators for different irreducible representations to the anyone of the basis of mechanical representation yield the vibrational modes. This vibrational modes are called *normal modes* and each normal mode is associated with one vibration frequency. The mathematical expression for normal modes in terms of $\mathbf{r}_\alpha^i$ is called *normal coordinate* and the normal mode belongs to the λth branch of the lth irreducible representation is: $Q_{l\lambda}$. The atomic displacements corresponding to this normal mode is:

$$\mathbf{r}_\alpha^i(l\lambda) = \frac{1}{\sqrt{m_i}} Q_{l\lambda} e^{-i\omega t} \tag{1.30}$$

The acutal atomic displacement in the molecule is the linear combination of different normal modes. The coefficient of linear combination is determined by initial position and initial velocity of the atoms in the molecule because the equation of motion is second order in nature.

The above analysis is based completely on classical equation of motion of the

atoms. Once the normal modes in the classical case are known, the classical Hamiltonian, which is the summation of kinetic and potential energy, is:

$$\mathscr{H} = T + V = \frac{1}{2}\sum_{l=1}^{3N}(\dot{\mathbf{Q}}_l)^2 + \frac{1}{2}\sum_{l=1}^{3N}{\omega_l}^2{\mathbf{Q}_l}^2 \tag{1.31}$$

The corresponding quantum-mechanical problem is also easy:

$$\frac{1}{2}(\mathbf{P}_l^2 + \omega_l^2\mathbf{Q}_l^2)\psi_l = E_l\psi_l \tag{1.32}$$

The solutions are the well known harmonic oscillator. Due to multiple normal modes, the solution of the Schrodinger equation is the product of many single harmonic oscillator:

$$E = \sum_k (n_l + \frac{1}{2})\hbar\omega_l \tag{1.33a}$$

$$V = \prod_l N_{n_l} H_{n_l}(\sqrt{\frac{\omega_l}{\hbar}}\mathbf{Q}_l)e^{-(\frac{\omega_l\mathbf{Q}_l^2}{2\hbar})} \tag{1.33b}$$

n_l is the quantum number of oscillator l, N_{n_l} are the normalizing constants and H_{n_l} are the Hermite polynomials. For the first excited state, $n_l = 1$ and $H_{n_l}(\sqrt{\frac{\omega_l}{\hbar}}\mathbf{Q}_l) \propto \mathbf{Q}_l$. Therefore for low excitation, the wavefunction belongs to the irreducible representation of the normal mode $\mathbf{Q}_l$.

1.11.2 Vibration in crystals: phonons

Both the classical and quantum-mechanical treatment of vibration in crystal is the same as the treatment in molecules. The major difficulty again rise from the periodic structure: infinite number of atoms makes the above analysis impractical. The idea of momentum space is applied again and the infinitely large force matrix reduce to acceptable size. After that, normal modes and normal coordinations can be worked out based on symmetry considerations.

Suppose the crystal has symmetry $\mathscr{G}$. The αth component of the position of the atom i in the nth primitive cell, away from it equilibrium position, is labeled $\mathbf{r}_\alpha^{(ni)}$. The potential energy of the crystal for small vibration can be kept only up to second order, first ordering being zero. The equations of motions for the system is:

$$m_i \frac{\partial^2 \mathbf{r}_\alpha^{(ni)}}{\partial t^2} = -\sum_{(mj)\beta} V_{\alpha\beta}^{(ni)(mj)} \mathbf{r}_\beta^{(mj)} \tag{1.34}$$

$V_{\alpha\beta}^{(ni)(mj)}$ is the force constant. Define *force matrix* $D_{\alpha\beta}^{(ni)(mj)} = \frac{V_{\alpha\beta}^{(ni)(mj)}}{\sqrt{m_i m_j}}$ and use trial solution $\mathbf{r}_\alpha^{(ni)} = \frac{\mathbf{u}_\alpha^{(ni)}}{\sqrt{m_i}} e^{i\omega t}$, the equation of motion becomes:

$$\sum_{(mj)\beta} D_{\alpha\beta}^{(ni)(mj)} \mathbf{u}_\beta^{(mj)} - \omega^2 \mathbf{u}_\alpha^{(ni)} = 0 \tag{1.35}$$

For ther crystal, there are $N_1 \times N_2 \times N_3$ primitive cells and within each cell there are s atoms. As a result, the dimensionality of the force constant matrix is $3sN$ by $3sN$, and there are $3sN$ equations of motions. Solving the eigenvalue and eigenstates of $3sN$ by $3sN$ is formidable and more importantly, not necessary. Transform the equations of motion into momentum space through the following transformations:

$$\mathbf{u}_\alpha^i(\mathbf{q}) = \mathbf{u}_\alpha^{(ni)}(\mathbf{r}) e^{-i\mathbf{q}\cdot\mathbf{R_n}} \tag{1.36a}$$

$$D_{\alpha\beta}^{ij}(\mathbf{q}) = \sum_n D_{\alpha\beta}^{(ni)(mj)}(\mathbf{r}) e^{i\mathbf{q}\cdot(\mathbf{R_n}-\mathbf{R_m})} \tag{1.36b}$$

and now the equations of motion is reduced to s by using orthogonality theorem between Fourier series:

$$\sum_{j\beta} D_{\alpha\beta}^{ij}(\mathbf{q}) \mathbf{u}_\beta^j(\mathbf{q}) - \omega^2 \mathbf{u}_\alpha^i(\mathbf{q}) = 0 \tag{1.37}$$

Group theory can now be applied and the phonon modes can be classified to its irreducible representations. The label for the eigenstates belonging to the λth branch of the lth irreducible representation is $\mathbf{Q}_\alpha^i(\mathbf{q}|l\lambda)$ and the actual atomic displacement

for this phonon mode is:

$$\mathbf{r}_{\alpha}^{(ni)}(\mathbf{r}|l\lambda) = \frac{1}{\sqrt{m_i}}\mathbf{Q}_{\alpha}^{i}(\mathbf{q}|l\lambda)e^{i(\mathbf{q}\cdot\mathbf{R_n}-\omega t)} \tag{1.38}$$

The real phonon mode is a linear combination of different phonon modes. The coefficient of the linear combination is determined by the initial position and velocity of the atoms in the crystal.

The determination of phonon symmetry for crystals is very similar to molecules. Both atomic equivalence representation and mechanical representation are defined and the decomposition of mechanical representation gives all the phonon modes. No translational and rotational modes need to be eliminated.

For zone center phonon, the character of the atomic equivalence representation is the number of atoms that is not moving or being moved to its equivalent positions. Equivalent means that the two points can be connected with a full Bravais lattice of the primitive cell. The mechanical representation is the direct product of atomic equivalence representation and vector representation: $\chi^{\text{mech}}(g) = \chi^{\text{AER}}(g) \cdot \chi^{\text{vector}}(g)$. The whole analysis is done in the corresponding point group of the space group.

The analysis of phonon structure at Brillouin zone point k is done in the point group of the group of wavevector $\mathscr{G}_k$. For phonon modes at Brillouin point k away from zone center, additional factors are needed to get the atomic equivalence representation. The character of the atomic equivalence representation is the number of atoms that is not moving or being moved to its equivalent positions *times* a factor that is $e^{i\mathbf{k}\cdot(\mathbf{R_n}-\mathbf{R'_n})}$. $\mathbf{R_n}$ and $\mathbf{R'_n}$ are the original and new position of the nth atom in the set under study. Note that this additional factor is only for the atoms that can be shifted to equivalent positions.

The mechanical representation is the direct product of atomic equivalence representation and vector representation. To be mentioned is that, for some non-

symmorphic space groups, at the surface of the Brillouin zone, the "vector representation" is not a representation. See for example table 30 on page 389 of reference [11] where (x, y, z) are only unacceptable representations of the covering group. Luckily, this non-representation nature of (x, y, z) does not affect the derivation of mechanical representation: (x, y, z) still have characters under the symmetry operations (rotation and reflection part only) and $\chi^{\text{mech}}(g) = \chi^{\text{AER}}(g) \cdot \chi^{(x,y,z)}(g)$. At any Brillouin zone point, a total dimensionality of $3s$ is expected for phonon modes. Of those $3s$ branches, 3 are acoustic phonons and $3s - 3$ are optical phonons. Optical phonons correspond to the stretching mode of the atoms therefore their energy are usually higher than acoustic phonons. The 3 acoustic phonons are connected with sound velocities in the solid for they correspond to the atomic movements in one direction. At special cases, mostly in the vicinity of structural phase transitions, one optical branch may become *soft mode* [23] whose frequency is reduced to that of acoustic phonons.

1.12 Direct product and Clebsch-Gordan coefficient

1.12.1 Direct product

Suppose a group $\mathscr{G}$ with its basis functions ψ_j^μ and ψ_l^ν. When an operator works on one one set of basis, the irreducible representations are the transform matrix:

$$P_g \psi_j^\mu = \sum_i \psi_i^\mu D_{ij}^\mu(g) \tag{1.39a}$$

$$P_g \phi_l^\nu = \sum_k \phi_k^\nu D_{kl}^\nu(g) \tag{1.39b}$$

When the operator works on the product of $\psi_j^\mu \cdot \phi_l^\nu$:

$$P_g(\psi_j^\mu \cdot \phi_l^\nu) = \sum_{ik} \psi_j^\mu \cdot \phi_l^\nu D_{ij}^\mu(g) D_{kl}^\nu(g) \tag{1.40a}$$

$$\equiv \sum_{ik} \psi_j^\mu \cdot \phi_l^\nu D_{ik,jl}^{\mu\nu}(g) \tag{1.40b}$$

The *direct product* and the character for direct product are defined:

$$D_{ik,jl}^{\mu\nu}(g) = D_{ij}^\mu(g) D_{kl}^\nu(g) \tag{1.41a}$$

$$\chi_{ik,jl}^{\mu\nu}(g) = \chi_{ij}^\mu(g) \cdot \chi_{kl}^\nu(g) \tag{1.41b}$$

The representation of the direct product is also called *product representation* or *kronecker product*. It is generally reducible and the decomposition of product representation can be easily done.

When μ and ν are the same representation, the direct product can be separated into two kinds: *symmetric direct product* $[D^\mu \times D^\mu]$ and *antisymmetric direct product* $\{D^\mu \times D^\mu\}$ with $D^\mu \times D^\mu = [D^\mu \times D^\mu] + \{D^\mu \times D^\mu\}$. Symmetric and antisymmetric means that the wavefunctions in the product remains or changes its sign under change of particle. The matrices for symmetric and antisymmetric products are:

$$[D^\mu \times D^\mu(g)]_{kl,ij} = \frac{1}{2}[D_{ki}^\mu(g) D_{lj}^\mu(g) + D_{li}^\mu(g) D_{kj}^\mu(g)] \tag{1.42a}$$

$$\{D^\mu \times D^\mu(g)\}_{kl,ij} = \frac{1}{2}[D_{ki}^\mu(g) D_{lj}^\mu(g) - D_{li}^\mu(g) D_{kj}^\mu(g)] \tag{1.42b}$$

and the characters for both representations are:

$$[\chi^\mu \times \chi^\mu(g)] = \frac{1}{2}[(\chi^\mu(g))^2 + \chi(g^2)] \tag{1.43a}$$

$$\{\chi^\mu \times \chi^\mu(g)\} = \frac{1}{2}[(\chi^\mu(g))^2 - \chi(g^2)] \tag{1.43b}$$

Both products can be decomposed into summations of irreducible representations of the group.

1.12.2 Reduction coefficient

The decomposition of direct product, symmetric direct product and antisymmetric direct product is easy. The results has been tabulated (in reference [24] for example) for all crystallographic point groups. The decompositon of the direct product of space groups is not an easy job. There are different ways to determine the reduction coefficient and method of linear algebraic equations is the most straightforward one [11]. The reduction coefficients $(\bigstar km \bigstar k'm'|\bigstar k''m'')$ are defined as:

$$D^{(\bigstar k \otimes \bigstar k')(m \otimes m')} = \sum_{\bigstar k''} \sum_{m''} (\bigstar km \bigstar k'm'|\bigstar k''m'') D^{(\bigstar k'')(m'')}. \tag{1.44}$$

This is equvalent as:

$$\chi^{(\bigstar k)(m)} \chi^{(\bigstar k')(m')} = \sum_{\bigstar k''} \sum_{m''} (\bigstar km \bigstar k'm'|\bigstar k''m'') \chi^{(\bigstar k'')(m'')} \tag{1.45}$$

where $\chi^{(\bigstar k)(m)}$ is the character of representation $D^{(\bigstar k)(m)}$. The first step is to determine which representations are possible based on wave vector selection rules:

$$\bigstar k \otimes \bigstar k' = \sum_{\bigstar k''} (\bigstar k \bigstar k'|\bigstar k'') \bigstar k'' \tag{1.46}$$

This step is done by inspection and only $(\bigstar km \bigstar k'm'|\bigstar k''m'')$ from the non-vanishing wave vectors $\bigstar k''$ need to be considered. Equation 1.45 is then written down for different symmetry elements $\{\varphi|t(\varphi)\}$:

$$\chi^{(\bigstar k)(m)}(\{\varphi|t\}) \chi^{(\bigstar k')(m')}(\{\varphi|t\}) = \sum_{\bigstar k''} \sum_{m''} (\bigstar km \bigstar k'm'|\bigstar k''m'') \chi^{(\bigstar k'')(m'')}(\{\varphi|t\}) \tag{1.47}$$

In those equations, the only unknowns are the coefficients. By choosing as many symmetry elements as needed, the coefficients $(\bigstar km \bigstar k'm'|\bigstar k''m'')$ can be obtained. Once the number of linearly independent equations is equal to the number of coefficients, all coefficients can be determined at once. Before that, not a single coefficient can be determined.

1.12.3 Clebsch-Gordan coefficient

To take the above analysis further the following questions can be asked: what are the coefficients of linear combinations between basis functions:

$$\Psi_s^{(\lambda\tau_\lambda)} = \sum_{jl} \psi_j^\mu \phi_l^\nu (\mu j, \nu l | \lambda \tau_\lambda s) \tag{1.48}$$

λ denotes all the irreducible representations in the direct product of $D^\mu \times D^\nu$ and τ_λ) is a additional label for λ in case more than one λ representation is contained in $D^\mu \times D^\nu$ and τ_λ). The coefficients $(\mu j, \nu l | \lambda \tau_\lambda)$ are usually called *Clebsch-Gordan coefficients* and other names such as *Wigner coefficients* and *vector-addition coefficients* exist. This definition is not unique. Alternatively, the reverse can be defined:

$$\psi_j^\mu \phi_l^\nu = \sum_{\lambda\tau_\lambda} \Psi_s^{(\lambda\tau_\lambda)} (\lambda \tau_\lambda s | \mu j, \nu l) \tag{1.49}$$

The transformation between two sets of basis is unitary the two Clebsch-Gordan coefficients are related:

$$(\lambda \tau_\lambda s | \mu j, \nu l) = \overline{(\mu j, \nu l | \lambda \tau_\lambda s)} \tag{1.50}$$

The standard method of obtaining Clebsch-Gordan coefficients is through the full determination of matrices of the irreducible representations. It can be shown that:

$$D_{ij}^\mu(g) D_{kl}^\nu(g) (\mu j, \nu l | \lambda \tau_\lambda s) = (\mu i, \nu k | \lambda \tau_\lambda s') D_g^{\lambda\tau_\lambda}(g) \tag{1.51}$$

therefore the Clebsch-Gordan coefficients are components of the translation matrices connecting the direct product and its reduced form.

So far, only a sketch is given on crystallographic groups. Many interesting topics, such as symmetric group, and useful applications, such as crystal fields, Laudau phase transition, are not covered due to the limitation of space and time. The points that emphasized will be helpful in later chapters. Different selection rules in infrared

spectroscopy and Raman spectroscopy are going to be discussed after the principles of both physical processes are introduced.

Chapter 2

Infrared Spectroscopy

Infrared light (IR) is light in the infrared region in the electromagnetic spectrum, roughly between 10 cm^{-1} and 14000 cm^{-1}. Usually it is divided into three sub-regions: 14000 cm^{-1} – 4000 cm^{-1} for near-IR, 4000 cm^{-1} – 400 cm^{-1} for mid-IR and 400 cm^{-1} – 10 cm^{-1} for far-IR. Infrared spectroscopy use infrared light source to study the vibrational and electronic energy levels of the molecules and crystals. The typical energy of the vibrational mode in molecules and crystals is within this region. This energy range is also ideal for studying the free electron response, interband transition of small-gap semiconductors as well as superconducting gaps and density-wave gaps. During the interaction with matter, light can be reflected, transmitted, absorbed and scattered. Infrared spectroscopy focus on the absorption of light. Being first order in nature, the intensity of absorption is much higher than light scattering therefore the scattered light can be ignored in infrared spectroscopy.

In practice the reflectivity or transmissivity is measured and well developed formalism converts the reflectivity or transmissivity to material parameters that characterize the molecules or crystals under study. Of all material parameters, the real part of conductivity σ_1 is of central interest because of its direct connection with photon absorption.

Different regions of Infrared spectroscopy require different sources, detectors, windowns and maybe spectrometers. A detailed description of such experimental tech-

niques can be found in reference [25, 26].

2.1 Electrodynamics of solids

The macroscopic, phenomenological [27] description of light, both with and without the presence of matter, is the Maxwell's equations. The Maxwell's equations have simple and elegant solutions in vacuum, namely the plane waves. The presence of matter introduces several material parameters that are in general functions of both frequency ω and wavevector q. In many cases the *long wavelength approximation* is used that the wave length of light is much larger than the lattice constant therefore only the $q = 0$ part of the optical parameters and response functions are interesting. Those parameters, such as dielectric function ϵ, conductivity σ and refractive index N, are connected with each other. In different models different parameter sets are used because of their convenience in that situation. Being response functions in nature, the real and imaginary part of the optical parameters are also connected, through the well known Kramers-Kronig relation [28, 29]. The Maxwell's equations have different forms in case of Gaussian units or SI units are used although the physics remains the same. Here, the Gaussian units are used.

2.1.1 Maxwell's equations

Maxwell's equations in vacuum

Maxwell's equations [30] are a set of differential equations that describes the macroscopic behavior of the electromagnetic waves. In case of vacuum:

$$\nabla \times \mathbf{E}(\mathbf{r},\, \mathrm{t}) + \frac{1}{c}\frac{\partial \mathbf{B}(\mathbf{r},t)}{\partial t} = 0 \tag{2.1a}$$

$$\nabla \cdot \mathbf{B}(\mathbf{r},t) = 0 \tag{2.1b}$$

$$\nabla \times \mathbf{B}(\mathbf{r},\, \mathrm{t}) - \frac{1}{c}\frac{\partial \mathbf{E}(\mathbf{r},t)}{\partial t} = \frac{4\pi}{c}\mathbf{J}_{\mathrm{total}}(\mathbf{r},t) \tag{2.1c}$$

$$\nabla \cdot \mathbf{E}(\mathbf{r},t) = 4\pi\rho_{\mathrm{total}}(\mathbf{r},t) \tag{2.1d}$$

$\mathbf{E}$, $\mathbf{B}$, $\mathbf{J}$, ρ are electric field, magnetic induction, current density and charge density. c is the speed of light in vacuum. The meaning of the subscript "total" is explained when dealing with Maxwell's equations with matter. The form of the equations suggest the definition of two potential fields: the vector potential $\mathbf{A}(\mathbf{r},\, \mathrm{t})$ and scalar potential $\Phi(\mathbf{r},t)$:

$$\mathbf{B}(\mathbf{r},t) = \nabla \times \mathbf{A}(\mathbf{r},t) \tag{2.2a}$$

$$\mathbf{E}(\mathbf{r},t) + \frac{1}{c}\frac{\partial \mathbf{A}(\mathbf{r},t)}{\partial t} = -\nabla\Phi(\mathbf{r},t) \tag{2.2b}$$

The substitution of both equations back into the Maxwell's equations yield the following:

$$\nabla^2\Phi = -4\pi\rho \tag{2.3a}$$

$$\nabla^2\mathbf{A} = -\frac{4\pi}{c}\mathbf{J} \tag{2.3b}$$

In the derivation of the above equations, the Coulomb gauge is used:

$$\nabla \cdot \mathbf{A} = 0 \tag{2.4}$$

If the absence of free current $\mathbf{J}$ and external charge ρ is further assumed, the Maxwell's equations have plane wave solutions.

Maxwell's equations in the medium

In the presence of matter, the Maxwell's equations change the form and new variables are introduced:

$$\nabla \times \mathbf{E}(\mathbf{r},\, \mathrm{t}) + \frac{1}{c}\frac{\partial \mathbf{B}(\mathbf{r},t)}{\partial t} = 0 \tag{2.5a}$$

$$\nabla \cdot \mathbf{B}(\mathbf{r},t) = 0 \tag{2.5b}$$

$$\nabla \times \mathbf{H}(\mathbf{r},\, \mathrm{t}) - \frac{1}{c}\frac{\partial \mathbf{D}(\mathbf{r},t)}{\partial t} = \frac{4\pi}{c}\mathbf{J}_{\mathrm{cond}}(\mathbf{r},t) \tag{2.5c}$$

$$\nabla \cdot \mathbf{D}(\mathbf{r},t) = 4\pi\rho_{\mathrm{ext}}(\mathbf{r},t) \tag{2.5d}$$

$\mathbf{D}$, $\mathbf{E}$, $\mathbf{B}$, $\mathbf{H}$ are the electric displacement, electric field strength, magnetic induction and magnetic field strength. $\mathbf{D}$ and $\mathbf{H}$ are connected with $\mathbf{E}$ and $\mathbf{B}$ through:

$$\mathbf{D} = \epsilon\mathbf{E} = (1 + 4\pi\chi_e)\mathbf{E} = \mathbf{E} + 4\pi\mathbf{P} \tag{2.6a}$$

$$\mathbf{B} = \mu\mathbf{H} = (1 + 4\pi\chi_m)\mathbf{E} = \mathbf{H} + 4\pi\mathbf{M} \tag{2.6b}$$

$\mathbf{P}$ and $\mathbf{M}$ are the dipole moment density (or polarization density) and magnetic moment density (or magnetization). ϵ, χ_e, μ and χ_m are dielectric constant (or permittivity), dielectric susceptibility, permeability and magnetic susceptibility. In most situations the permeability μ for materials are close to 1 unless for magnetic materials, which is not the focus here. The presence of a medium leads to electric dipoles, magnetic moments, polarization charges and induced currents and both current and charge may have more than one component:

$$\mathbf{J}_{\mathrm{total}} = \sigma\mathbf{E} = \mathbf{J}_{\mathrm{cond}} + \mathbf{J}_{\mathrm{bound}} = \mathbf{J}_{\mathrm{cond}} + \frac{\partial \mathbf{P}}{\partial t} + c\nabla \times \mathbf{M} \tag{2.7a}$$

$$\rho_{\mathrm{total}} = \rho_{\mathrm{ext}} + \rho_{\mathrm{pol}} = \rho_{\mathrm{ext}} - \nabla \cdot \mathbf{P} \tag{2.7b}$$

In the above analysis, the dielectric constant is assumed to be a scalar. This is only true for glass or crystals with cubic symmetry. Crystals with other symmetry properties have tensorial dielectric constant which leads to *birefringence* in optics.

Frequency and wave vector dependence of response functions

The optical parameter are frequency dependent and they are related to response functions. The response function $G(\mathbf{r}-\mathbf{r}', t-t')$ describes the response of the homogeneous system $X(\mathbf{r}, t)$ to an external stimulus $f(\mathbf{r}', t')$

$$X(\mathbf{r}, t) = \iint_{-\infty}^{\infty} G(\mathbf{r} - \mathbf{r}', t - t') f(\mathbf{r}', t') \mathrm{d}t' \mathrm{d}\mathbf{r}' \tag{2.8}$$

It means that the response at point $\mathbf{r}$ at time t is related to the stimulus at any point $\mathbf{r}$**'** at any time t'. The Fourier transform in both frequency and wave vector space of the above equation is:

$$X(\mathbf{q}, \omega) = G(\mathbf{q}, \omega)\ f(\mathbf{q}, \omega) \tag{2.9}$$

This general relation can be simplified to special cases and correspondingly their Fourier transforms:

$$G(\mathbf{r} - \mathbf{r}', t - t') = \delta(\mathbf{r}, \mathbf{r}') G(t - t') \Rightarrow X(\omega) = G(\omega)\ f(\omega) \tag{2.10a}$$

$$G(\mathbf{r} - \mathbf{r}', t - t') = \delta(t, t') G(\mathbf{r} - \mathbf{r}') \Rightarrow X(\mathbf{q}) = G(\mathbf{q})\ f(\mathbf{q}) \tag{2.10b}$$

The first case without $\mathbf{q}$ dependence is the *local approximation* where the response at $\mathbf{r}$ is only related to stimulus at that point. The response with $\mathbf{q}$ are therefore called *non-local effect*. Similarly, the inclusion of frequency dependence in response function is called *retardation effect* because the response at time t is related to stimulus at any time t'.

Solutions of Maxwell's equations in the medium

When there is no external charge, Maxwell's equations in the medium can be simplified into two equations on $\mathbf{E}$ and H only:

$$\nabla^2\mathbf{E} - \frac{\epsilon_1\mu_1}{c^2}\frac{\partial^2\mathbf{E}}{\partial t^2} - \frac{4\pi\mu_1\sigma_1}{c^2}\frac{\partial\mathbf{E}}{\partial t} = 0 \tag{2.11a}$$

$$\nabla^2\mathbf{H} - \frac{\epsilon_1\mu_1}{c^2}\frac{\partial^2\mathbf{H}}{\partial t^2} - \frac{4\pi\mu_1\sigma_1}{c^2}\frac{\partial\mathbf{E}}{\partial t} = 0 \tag{2.11b}$$

Compared with wave equations for vacuum, one additional term exist for both $\mathbf{E}$ and $\mathbf{H}$. This term involves first order derivative of the field and corresponds to the *dissipation* of the wave: Both $\mathbf{E}$ and $\mathbf{H}$ are damping. When σ_1, the real part of conductivity, is zero, the dissipation terms vanish and the wave equations have plane wave form as in vacuum although the parameters, such as ϵ and μ, change the speed of light. As a result, it is important to distinguish metal ($\sigma_1 \neq 0$) and insulator ($\sigma_1 = 0$) in the discussion of electrodynamics of solids.

2.1.2 Connection between optical constants

The three complex, frequency and wavevector dependent optical parameters, dielectric constant ϵ, index of refraction N and electric conductivity σ, determine the optical properties of solids that some are transparent while others are opaque and some surfaces are reflecting while others are absorbing [31].

The three parameters are connected with each other and the knowledge of one enables the determination of the others. The complex forms of the three parameters are: dielectric constant $\epsilon = \epsilon_1 + i\epsilon_2$; index of refraction $N = n + ik$ and electric

	Dielectric constant ϵ	Conductivity σ	Refractive index N
ϵ		$\epsilon_1 = 1 - \frac{4\pi\sigma_2}{\omega}$	$\epsilon_1 = n^2 - k^2$
		$\epsilon_2 = \frac{4\pi\sigma_1}{\omega}$	$\epsilon_2 = 2nk$
σ	$\sigma_1 = \frac{\omega\epsilon_2}{4\pi}$		$\sigma_1 = \frac{nk\omega}{2\pi}$
	$\sigma_2 = (1-\epsilon_1)\frac{\omega}{4\pi}$		$\sigma_2 = (1-n^2+k^2)\frac{\omega}{4\pi}$
N	$n = \sqrt{\frac{(\epsilon_1^2+\epsilon_2^2)^{1/2}}{2} + \frac{\epsilon_1}{2}}$	$n = \sqrt{\frac{[(1-\frac{4\pi\sigma_2}{\omega})^2+(\frac{4\pi\sigma_1}{\omega})^2]^{1/2}}{2} + \frac{1}{2} - \frac{2\pi\sigma_2}{\omega}}$	
	$k = \sqrt{\frac{(\epsilon_1^2+\epsilon_2^2)^{1/2}}{2} + \frac{\epsilon_1}{2}}$	$k = \sqrt{\frac{[(1-\frac{4\pi\sigma_2}{\omega})^2+(\frac{4\pi\sigma_1}{\omega})^2]^{1/2}}{2} - \frac{1}{2} + \frac{2\pi\sigma_2}{\omega}}$	

Table 2.1 : Relations between optical parameters.

conductivity $\sigma = \sigma_1 + i\sigma_2$. The connection between them are:

$$\epsilon = N^2 \tag{2.12a}$$

$$\epsilon = 1 - \frac{4\pi i\sigma}{\omega} \tag{2.12b}$$

The connection between dielectric constant and conductivity is the direct result of Maxwell's equations:

$$\nabla \times (\nabla \times \mathbf{E}) = -\nabla^2\mathbf{E} = \frac{\omega^2}{c^2}(1 + \frac{4\pi i\sigma}{\omega})\mathbf{E} = \frac{\omega^2}{c^2}\epsilon(\omega)\mathbf{E} \tag{2.13}$$

The complete relation between the three optical parameters are in table 2.1 where the permeability μ_1 is taken as 1 as magnetic materials is not considered.

At the interface of two materials with different optical parameters, reflection, refraction and transmission would occur. Given the optical parameters, the relative of intensity of reflection, refraction and transmission can be obtained for different incident angle and light polarization. The results are well known in standard textbooks such as Jackson [32] and Born [33] and the results are not included here. However, one important parameter has to be emphasised. The *reflectance* R is defined as the power

reflected at a surface. In most simple and common situation, consider that light is normally incident from vacuum on a medium. Reflectance R and its corresponding phase change θ are therefore [23]:

$$R = \frac{|\mathbf{E}^{\text{refl}}|^2}{|\mathbf{E}^{\text{inci}}|^2} = |\frac{1-N}{1+N}|^2 = \frac{(1-n)^2+k^2}{(1+n)^2+k^2} \tag{2.14a}$$

$$\tan\theta = -\frac{2k}{1-n^2-k^2} \tag{2.14b}$$

From this it can see that the reflectance is always less than zero. For good metals, the large conductivity leads to bigger k than n and the reflectance R is close to one. This is the reason why metals looks shiny. It is also true that high reflectance (shiny) surfaces indicate high absorption inside the medium. On the other hand, an transparent crystal, where the absorption coefficient is small inside, tends to have less reflective surfaces. Of course, all optical parameters are frequency independent. They are taken as constant here because only the appearance of a solid is discussed and they can be approximately considered as frequency independent in visible light region. At frequencies higher than the plasma frequency, metal cease to show high reflectance. The optical parameters for metal will be studied in more detail in later sections after the introduction of Drude model.

2.1.3 Kramers-Kronig relation; sum rules

Due to causality, the real and imaginary parts of a response functions are connected through the Kramers-Kronig relation [28, 29]. Suppose a response function $G(\mathbf{r}, \mathbf{r}', t, t')$ (or simply $G(t-t')$) and its Fourier transform $G(\omega)$. The real and imag-

inary part of $G(\omega) = G_1(\omega) + iG_2(\omega)$ are connected through:

$$G_1(\omega) = \frac{1}{\pi}\mathscr{P}\int_{-\infty}^{\infty}\frac{G_2(\omega')}{\omega' - \omega}\mathrm{d}\omega' \tag{2.15a}$$

$$G_2(\omega) = -\frac{1}{\pi}\mathscr{P}\int_{-\infty}^{\infty}\frac{G_1(\omega')}{\omega' - \omega}\mathrm{d}\omega' \tag{2.15b}$$

The integrals with $\mathscr{P}$ symbols are principle value integrals. It can be shown that the conductivity $\sigma(\omega) = \sigma_1(\omega) + i\sigma_2(\omega)$ and the modified dielectric functions $\epsilon(\omega) - 1 = \epsilon_1(\omega) - 1 + i\epsilon_2(\omega)$ are both response functions.

Another important Kramers-Kronig application is the Reflectance and its partner phase function. The *phase change* θ of the reflectance $R(\omega)$:

$$\theta(\omega) = \frac{\omega}{\pi}\int_0^{\infty}\frac{\ln\{R(\omega')\} - \ln\{R(\omega)\}}{\omega^2 - \omega'^2}\mathrm{d}\omega' \tag{2.16}$$

Experimentally, the reflectance is measured over a wide range of spectrum and the phase change θ is therefore fully determined. The knowledge of reflectance and phase change allows the determination of all other otical parameters over the entire frequency region.

2.2 Photon lattice interaction

In the above discussions, the properties of the solid is expressed in term of frequency dependent optical parameters. The microscopic study of solid and its interaction with light must be carried out to give the forms of the optical parameters. In most situations, there are two kinds of interactions: photon lattice interaction and photon electron interaction. The energy scale of photon lattice interaction, especially inelastic scatterings are smaller than that of electronic origin therefore photon lattice interaction and photon electron interaction are separable in energy. Plus, due to the

relatively small mass of electrons compared with atoms, the intensity of electronic response in much higher than lattice response in general. As a result, For metals and semiconductors, although both interactions exist but only the electronic response are important, except for some phonon mode in the spectrum that has lattice origin in the low frequency region. On the other hand, for insulators, the lack of free electrons makes the photon lattice interaction dominate. In this section, the photon lattice interaction is discussed. There are two angles to approach: from lattice point of view that the equation of motion is coupled with electromagnetic fields therefore gives optical parameters; and from photon point of view that both elastic and inelastic scattering of photons take place.

2.2.1 Infrared selection rules for phonons

The normal modes Q_l are elementary excitations of a system's Hamiltonian without taking into account of electronic degree of freedom. Group theory can be applied to the Hamiltonian to obtain the normal modes according to their symmetries. The wave function are a normal mode Q_l is a n_lth order Hermite function with a Gaussian envelope and an appropriate normalizing factor:

$$\psi_{n_l}(Q_l) = [\sqrt{\frac{2n_l}{\hbar}}\frac{1}{2^{n_l}(n_l!)}]^{\frac{1}{2}} e^{-\frac{\pi n_l Q_l^2}{\hbar}} H_{n_l}(\sqrt{\frac{2\pi n_l}{\hbar}}Q_l) \tag{2.17}$$

At lowest excited state, $n_l = 1$ and $\psi_1(Q_l) \propto Q_l$ therefore the vibrational state has the same symmetry as the normal mode. This is not the case for higher excited states that the wavefunction does not simply transform as the direct product of two normal modes: additional terms exist from the Hermite functions. For normal degeneracy situation, more than one branch exist in the manifold and $Q_{l\lambda}$ is used instead of Q_l.

In the first order, dipole approximation, the interaction between photon and lattice/molecular vibration transforms as a dipole moment $\boldsymbol{\mu}$ therefore vector representation $D(\mathbf{r})$. Usually, the system is assumed to be at its ground state before interacting with photon and after the interaction, only one single phonon l is excited. Therefore the matrix element for this transition is:

$$< 0010\cdots|\boldsymbol{\mu}|0000\cdots > \tag{2.18}$$

Group theory selection rules predicts that this transition is not allowed if Q_l is not contained in the vector representation $D(\mathbf{r})$. In other words, if the representation of $D(Q_l)$ of the normal mode Q_l is not $D(\mathbf{r})$, this mode is not active in a first order, direct photon absorption process. Those phonon modes that are active are called *polar phonons* and the rest are *non-polar*.

2.2.2 Phonon polariton

The polar phonons interact strongly with photon therefore their equation of motion in the presence of light need to be modified. Huang [34] was the first one to study the coupling between lattice and photon.

Before introducing the coupled equations between long wavelength optical mode and photons, the difference between LO and TO is discussed. The fact that the frequency of the longitudinal optical mode is bigger than transverse optical mode can be obtained from the following simple picture. For longitudinal optical mode, the electromagnetic waves imply an electric field that is alternating along the $\mathbf{q}$ direction. The negative and positive ions in the crystal feel the electric field and make certain displacements. The overall effect of the displacements is to create thin layers of

alternating polarization which in turn create an longitudinal electric filed. The polarization induced field applies a stronger restoring force in the standard lattice vibration model. This is not the case for transverse optical mode where the displacements of ions does not build up polarization layers. Bigger force constants means higher frequencies therefore $\omega_{LO} > \omega_{TO}$. The more ionic the crystal is, the greater the difference between ω_{LO} and ω_{TO}. For example, LiF has $\omega_{LO} = 12 \times 10^{13}\text{s}^{-1}$ and $\omega_{TO} = 5.8 \times 10^{13}\text{s}^{-1}$ and less ionic GaAs has $\omega_{LO} = 5.5 \times 10^{13}\text{s}^{-1}$ and $\omega_{TO} = 5.1 \times 10^{13}\text{s}^{-1}$. Covalent crystals, such as Si and C, show no difference in ω_{LO} and ω_{TO}. It should be mentioned that this analysis relics on the $\mathbf{q} \neq 0$ assumption. A more rigorous discussion of the relative frequency of ω_{LO} and ω_{TO} can be found in section 4.1.1 in reference [35].

The phenomenological, macroscopic description of ionic, cubic crystal with two ions per primitive cell is:

$$\frac{\partial^2 \mathbf{W}}{\partial t^2} = b_{11}\mathbf{W} + b_{12}\mathbf{E} \tag{2.19a}$$

$$\mathbf{P} = b_{21}\mathbf{W} + b_{22}\mathbf{E} \tag{2.19b}$$

The vector $\mathbf{W}$ is the relative displacement of the two ions within one primitive cell, normalized with respect to the effective mass $\bar{M}$ and volume of the primitive cell Ω:

$$\mathbf{W} = (\frac{\bar{M}}{\Omega})^{1/2}(\mathbf{u}_+ - \mathbf{u}_-) \tag{2.20}$$

$\mathbf{P}$ is the macroscopic polarization density and $\mathbf{E}$ is the macroscopic electric field. Coefficients b_{11}, b_{12}, b_{21}, b_{22} are independent except that $b_{12} = b_{21}$, a result from symmetry consideration that can be derived from microscopic study of the system. The coefficients can be connected to more intuitive physical quantities.

1. At zero frequency, the relative displacement $\mathbf{W}$ has vanishing time derivatives therefore

$$\mathbf{W} = -\frac{b_{12}}{b_{11}}\mathbf{E} \Rightarrow \mathbf{P} = (b_{22} - \frac{b_{12}^2}{b_{11}})\mathbf{E} \tag{2.21}$$

Compared with the definition of dielectric constants:

$$\mathbf{P} = [\epsilon(0) - 1]\mathbf{E} \tag{2.22}$$

such connection can be established:

$$[\epsilon(0) - 1] = b_{22} - \frac{b_{12}^2}{b_{11}} \tag{2.23}$$

2. At infinitely high frequency, the heavy ions are not able to response with electromagnetic waves. In such situations, $\mathbf{W} = 0$ and

$$\mathbf{P} = b_{22}\mathbf{E} \Rightarrow [\epsilon(\infty) - 1] = b_{22} \tag{2.24}$$

3. When there is no electromagnetic wave, the electric field $\mathbf{E}$ is zero and the frequency of the free oscillator is ω_0

$$\frac{\partial^2 \mathbf{W}}{\partial t^2} = b_{11}\mathbf{W} = -\omega_0^2 \mathbf{W} \Rightarrow b_{11} = -\omega_0^2 \tag{2.25}$$

Our previous analysis shows that the presence of electromagnetic wave change the frequency of longitudinal optical mode and the frequency of transverse optical mode remains. $\omega_0 = \omega_{TO}$. This leads to:

$$b_{11} = -\omega_{TO}^2 \tag{2.26}$$

More rigorous derivation of the relation $\omega_0 = \omega_{TO}$ uses the separation of longitudinal and transverse displacement vector $\mathbf{W} = \mathbf{W}_T + \mathbf{W}_L$:

$$\frac{\partial^2 \mathbf{W}_T}{\partial t^2} = b_{11}\mathbf{W}_T \tag{2.27}$$

The same connection between b_{11} and ω_{TO} is obtained.

It is reasonable to assume that $\mathbf{P}$, $\mathbf{E}$ and $\mathbf{W}$ oscillates at the same frequency ω with amplitude $\mathbf{P}_0$, $\mathbf{E}_0$ and $\mathbf{W}_0$. Then the equations of motion becomes:

$$-\omega^2 \mathbf{W}_0 = b_{11}\mathbf{W}_0 + b_{12}\mathbf{E}_0 \tag{2.28a}$$

$$\mathbf{P}_0 = b_{12}\mathbf{W}_0 + b_{22}\mathbf{E}_0 \tag{2.28b}$$

Combine two equations,

$$\mathbf{P}_0 = [-\frac{b_{12}^2}{b_{11}+\omega^2} + b_{22}]\mathbf{E}_0 \tag{2.29}$$

There are no free charge in the ionic crystal therefore

$$\nabla \cdot \mathbf{D} = 0 \Rightarrow \mathbf{q} \cdot (\mathbf{E}_0 + \mathbf{P}_0) = 0 \tag{2.30}$$

This leads to the equation that describes the optical modes in ionic crystals in the presence of electromagnetic wave:

$$(\mathbf{q} \cdot \mathbf{E}_0)[\epsilon_0 - \frac{b_{12}^2}{b_{11}+\omega^2} + b_{22}] = 0 \tag{2.31}$$

For longitudinal optical mode, $\mathbf{q} \cdot \mathbf{E}_0 \neq 0$ and

$$\epsilon_0 - \frac{b_{12}^2}{b_{11}+\omega_{LO}^2} + b_{22} = 0 \tag{2.32}$$

Express b_{11}, b_{12}, b_{22} in terms of $\epsilon(0)$, $\epsilon(\infty)$, ω_{TO} and ω_{LO} defined in the above equation is connected with ω_{TO}:

$$\omega_{LO}^2 = \frac{\epsilon(0)}{\epsilon(\infty)}\omega_{TO}^2 \tag{2.33}$$

This is the well known LST relation, named after Lyddane, Sachs and Teller.

For transverse optical mode, $\mathbf{q} \cdot \mathbf{E}_0 = 0$. But $\nabla \times \mathbf{E} = -\frac{\partial \mathbf{H}}{\partial t}$ and

$$\mathbf{q} \times \mathbf{E}_0 = \omega \mathbf{H}_0 \tag{2.34}$$

therefore $\mathbf{q}$, $\mathbf{E}$ and $\mathbf{H}$ perpendicular with each other. Also,

$$\nabla \times \mathbf{H} = \frac{\partial \mathbf{D}}{\partial t} \Rightarrow \mathbf{q} \times \mathbf{H}_0 = -\omega(\mathbf{E}_0 + \mathbf{P}_0) \tag{2.35}$$

Combine the above two equations and use the definition of b_{11}, b_{12} and b_{22}:

$$\epsilon(\omega) = \epsilon(\infty) \cdot \frac{\omega_{LO}^2 - \omega^2}{\omega_{TO}^2 - \omega^2} \tag{2.36}$$

Electromagnetic wave between the frequency region of ω_{TO} and ω_{LO} can not propagate because of negative dielectric constant. The definition of index of refraction $ck = n\omega$ gives $c^2k^2 = \epsilon(\omega)\omega^2$. Combined with the dielectric functions, the dispersion relation for the coupled transverse optical mode and light is: (also see figure 2.1)

$$\omega_{\pm} = \frac{1}{2\epsilon(\infty)}[(\epsilon(0)\omega_0^2 + c^2q^2) \pm \sqrt{(\epsilon(0)\omega_0^2 + c^2q^2)^2 - 4\omega_{TO}^2c^2q^2\epsilon(\infty)}] \tag{2.37}$$

The above analysis shows that for longitudinal mode, there is no dispersion relation and $\omega_{LO}(q) = \omega_{LO}$. For transverse mode, the coupling between phonon and photon drastically change the behavior of both. There are two branches in the dispersion relation. The upper branch behaves as phonon with frequency ω_{LO} at low frequency and as photon with dielectric constant $\epsilon(\infty)$ at high frequency. The lower branch behave as photon with dielectric constant $\epsilon(0)$ at low frequency and as phonon with frequency ω_{TO} at high frequency. This coupled system of TO phonon and photon is called phonon polariton.

Remember the starting point of the discussion is the cubic crystal. Group theory predicts that at zone center, the polar phonons are three fold degenerate T_1. Away from zone center, it splits into two fold TO mode and non-degenerate LO mode along high symmetry Brillouin zone lines. However, the terms "zone center TO, LO mode" is used because experimentally the crossing over region is not accessible. Due to the nature of neutrons, the neutron scatterings experiment are probing in ω-q space the part where the crossing over is well finished therefore only the ω_{LO} and ω_{TO} are measured. For Raman scattering, in the usual back scattering or right angle scattering geometry, the crossover region is also not probed as only ω_{LO} and ω_{TO} are measured. At forward scattering geometry, the crossing over region is probed and different frequencies beside ω_{LO} and ω_{TO} are observed.

The above analysis is not confined in cubic crystals. Polaritons exist in other

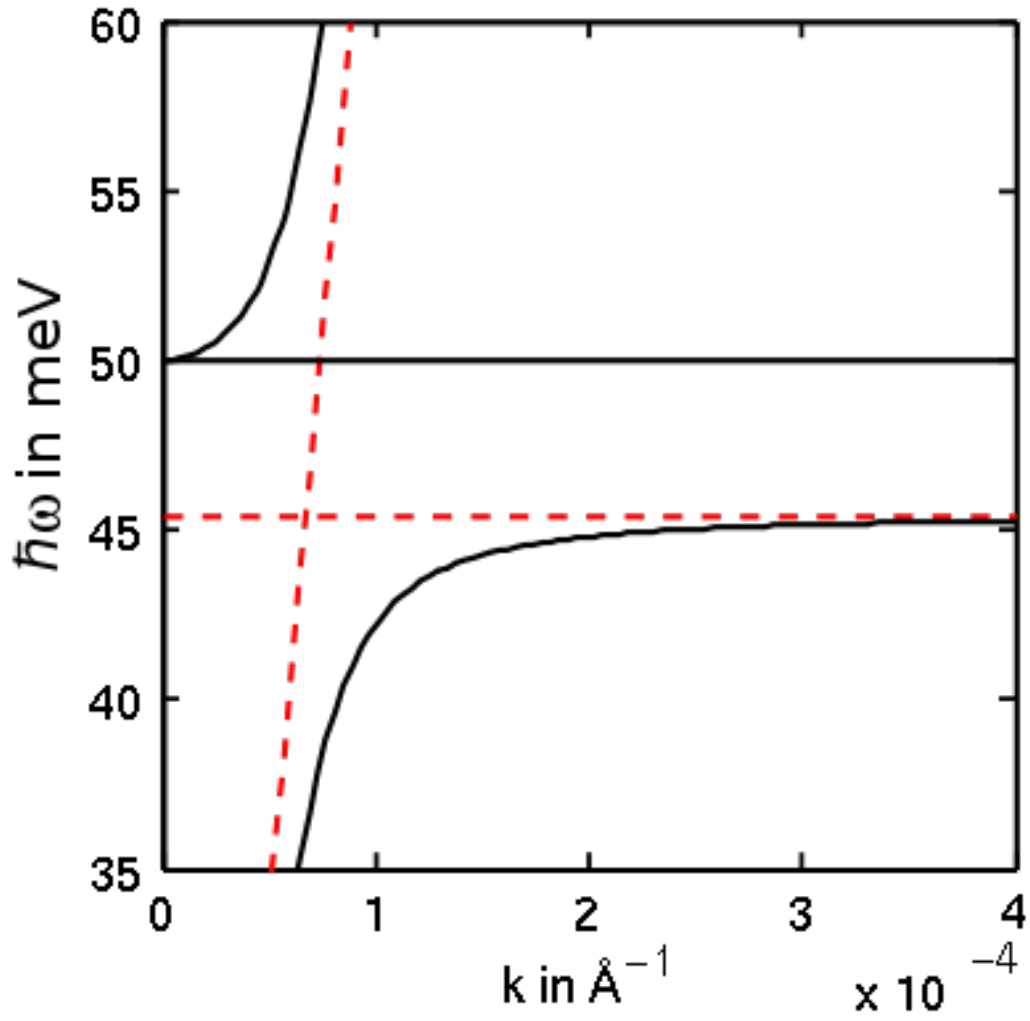

Figure 2.1 : Dispersion relation of phonon polariton for TO mode of cubic crystals. The interaction between photon and polar phonon change the phonon behavior greatly at small wavevector.

crystals systems and those with degenerate phonons mode are splitted by leaving the Brillouin zone center. The splitting of degenerate phonon modes in crystals other than cubic system are discussed by Hayes and Loudon [35, 36].

2.3 Photon electron interaction

After the introduction of interaction between polar phonon and photon, the remaining part is the interaction between electrons and photons. It has completely different formalism and the results does not necessarily confined to the long wave length limit: the complete optical parameter dependence on both frequency and wavevector $\mathbf{q}$ is contained in the formalism. Band theory is a starting point for such discussion therefore metal, semiconductor and broken symmetry states such as superconductor are well fitted in this formalism.

2.3.1 Response function

Longitudinal and transverse response

The four fields $\mathbf{E}$, $\mathbf{D}$, $\mathbf{H}$, $\mathbf{B}$, vector potential $\mathbf{A}$ and current density $\mathbf{J}$ are vectors and they can be separated into longitudinal and transverse components according to their direction with respect to wavevector $\mathbf{q}$, such as $\mathbf{E} = \mathbf{E}_L + \mathbf{E}_T$. This does not introduce new physics but only to bring convenience:

$$\nabla \times \mathbf{E} = \nabla \times \mathbf{E}_T \text{ and } \nabla \cdot \mathbf{E} = \nabla \cdot \mathbf{E}_L \tag{2.38}$$

Separate the vector potential $\mathbf{A}$ and plug it into Maxwell's equations, one obtain such results:

$$\nabla^2\mathbf{A} - \frac{1}{c^2}\frac{\partial^2\mathbf{A}}{\partial t^2} = -\frac{4\pi}{c}\mathbf{J}_T \tag{2.39a}$$

$$\mathbf{E}_L = -i\mathbf{q}\Phi \tag{2.39b}$$

$$\mathbf{E}_T = i\frac{\omega}{c}\mathbf{A} \tag{2.39c}$$

Fluctuation dissipation theorem

In the presence of electromagnetic fields, the Hamiltonian of a physical system is given by:

$$\mathscr{H} = \frac{1}{2m}\sum_i(\mathbf{p} + \frac{e}{c}\mathbf{A})^2 + \sum_{i,j}V_{i,j} + \frac{1}{2}\sum_{(i,j)}\frac{e^2}{|\mathbf{r}_i - \mathbf{r}_j|} - \sum_i e\Phi \tag{2.40}$$

The meanings of the terms are obvious. Expanding the Hamiltonian and neglect second order term A^2, the perturbation Hamiltonian is given by:

$$\mathscr{H}' = \frac{e}{2mc}\sum_i(\mathbf{p}\cdot\mathbf{A} + \mathbf{A}\cdot\mathbf{p}) - \sum_i e\Phi \tag{2.41}$$

The assumption of small A^2 is valid here but in special cases breaks down. The seperation of longitudinal and transverse fields allows one to treat the terms in the perturbation Hamiltonian seperately: $\mathbf{A}\cdot\mathbf{p}$ term for transverse conductivity and $e\Phi$ for longitudinal conductivity. The corresponding Hamiltonian can be written as:

$$\mathscr{H}'_T = -\frac{1}{c}\int \mathbf{J}_T(\mathbf{r})\cdot\mathbf{A}_T(\mathbf{r})\mathrm{d}\mathbf{r} \tag{2.42a}$$

$$\mathscr{H}'_L = \int \rho(\mathbf{r})\Phi(\mathbf{r})\mathrm{d}\mathbf{r} \tag{2.42b}$$

The calculation of transition probability based on Fermi-golden rule leads to the real part of the conductivity for both transverse and longitudinal components:

$$\sigma_{1;L,T}(\mathbf{q},\omega) = \sum_s \frac{1}{\hbar\omega}\int \mathrm{d}t < s|\mathbf{J}_{L,T}(\mathbf{q},0)\overline{\mathbf{J}_{L,T}(\mathbf{q},t)}|s > e^{-i\omega t} \tag{2.43}$$

where summations are over all states in the system. This is the famous *Kubo formula* [37] for conductivity. The real part of the conductivity is connected with the temporal fluctuation of the current density and it is an example of the *fluctuation-dissipation theorem*. A somewhat different expression can be obtained:

$$\sigma_1(\omega) = \frac{e^2}{4\pi^2 m^2 \omega} |\mathbf{p}_{ss'}(\omega)|^2 \int \delta(\hbar\omega - \hbar\omega_{ss'}) \mathrm{d}\mathbf{k} \tag{2.44}$$

$\mathbf{p}$ being the momentum operator and $\int \delta(\hbar\omega - \hbar\omega_{ss'})\mathrm{d}\mathbf{k}$ being proportional to the joint density of states in the transition process. This formula is called *Kubo-Greenwood formula*.

Response function and conductivity

The ultimate goal of the response function discussion is to connect optical parameters with the electronic states in the crystal. The time evolution of the number operator is calculated with electromagnetic fields as perturbation. Both the frequency and wave vector dependence of the electromagnetic wave are kept in the derivation and Bloch forms are assumed for the electronic states in crystal. Use Poisson equation, the number operator analysis leads to the longitudinal dielectric constant:

$$\epsilon_L(\mathbf{q},\omega) = 1 - \lim_{\eta\to 0} \frac{4\pi e^2}{q^2} \sum_{\mathbf{k},ll'} \frac{f(E_{l',\mathbf{k}+\mathbf{q}}) - f(E_{l,\mathbf{k}})}{E_{l',\mathbf{k}+\mathbf{q}} - E_{l,\mathbf{k}} - \hbar\omega - i\hbar\eta} \left| \frac{\int_\Delta \overline{u_{l',\mathbf{k}+\mathbf{q}}} e^{i\mathbf{q}\cdot\mathbf{r}} u_{l,\mathbf{k}} \mathrm{d}\mathbf{r}}{\Delta} \right|^2 \tag{2.45}$$

The integral is taken over one primitive cell, normalized by its volume Δ. This expression of the dielectric function is called *Lindhard function*.

The term $e^{i\mathbf{q}\cdot\mathbf{r}}$ can be replaced in practice by its power expansions:

$$e^{i\mathbf{q}\cdot\mathbf{r}} = 1 + i\mathbf{q}\cdot\mathbf{r} + \cdots \tag{2.46}$$

To the zeroth order, $e^{i\mathbf{q}\cdot\mathbf{r}} = 1$ and this is the *dipole approximation*. The first order $i\mathbf{q}\cdot\mathbf{r}$ would give both magnetic dipole and electric quadrupole. The electric dipole

approximation is most frequently used.

For transverse fields, starting with Hamiltonian $\mathscr{H}'_T = \frac{e}{mc}\mathbf{p}\cdot\mathbf{A}$, calculation on number operator leads to the transverse dielectric constant:

$$\epsilon_T(\mathbf{q},\omega) = 1 - \frac{4\pi N_0 e^2}{\omega^2 m} - \lim_{\eta\to 0}\frac{4\pi e^2}{\omega^2 m^2}\sum_{\mathbf{k},ll'}\frac{f(E_{l',\mathbf{k}+\mathbf{q}}) - f(E_{l,\mathbf{k}})}{E_{l',\mathbf{k}+\mathbf{q}} - E_{l,\mathbf{k}} - \hbar\omega - i\hbar\eta}\left|\frac{\int_\Delta \overline{u_{l',\mathbf{k}+\mathbf{q}}}e^{i\mathbf{q}\cdot\mathbf{r}}u_{l,\mathbf{k}}\mathrm{d}\mathbf{r}}{\Delta}\right|^2 \tag{2.47}$$

The real and imaginary parts of the longitudinal and transverse dielectric constant are straight forward [25]. The conductivity σ can also be easily obtained using table 2.1. In those expressions, Bloch wave is assumed for electrons and the band labelling l, l' allows the calculation on both *intraband* and *interband* transitions which describes metal and semiconductors.

2.3.2 Metals

The Drude mode [38] is a classical model for the transport property of electrons. The electrons are being scattered with an average relaxation time τ which prevents the electric current from going to infinity. It starts with equation of motion of single electron and gives the complex conductivity:

$$\sigma(\omega) = \frac{Ne^2\tau}{m}\frac{1+i\omega\tau}{1+\omega^2\tau^2} \tag{2.48}$$

A typical complex conductivity is given in figure 2.2.

The total area under σ_1 is:

$$\int_0^\infty \sigma_1(\omega)\mathrm{d}\omega = \frac{\pi N e^2}{2m} \tag{2.49}$$

This is the f–sum rule for conductivity. The experimental measurement of σ_1 allows the determination of N/m, the total number of carrier divided by the effective mass.

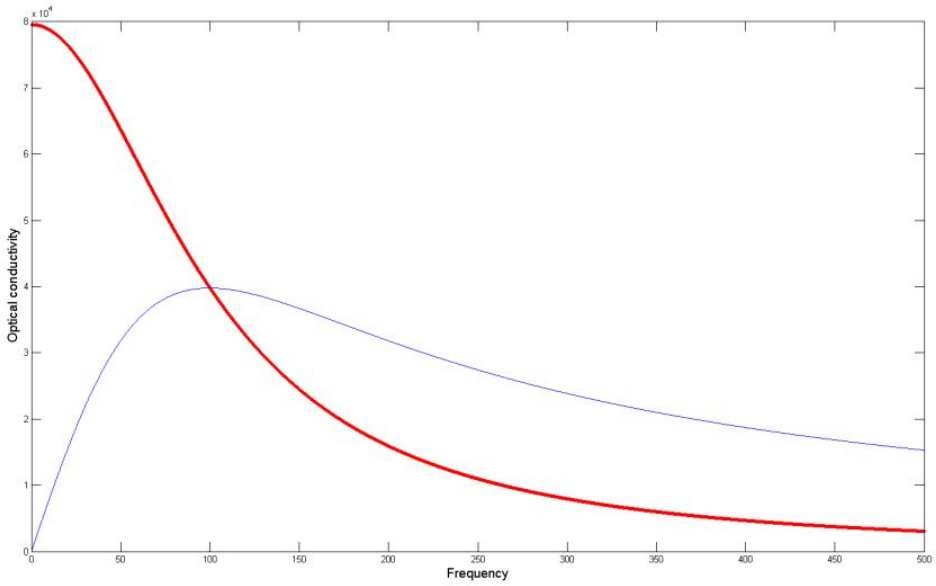

Figure 2.2 : The complex optical conductivity in Drude model. The red, thick line is the real component and the black, thin line is the complex component. The position of the maximum of σ_2 coincide with the position at which σ_1 drop to half its maximum value at the origin.

Accordingly, the *plasma frequency* can be defined as

$$\omega_p = (\frac{4\pi N e^2}{m})^{1/2} \tag{2.50}$$

The frequency at which σ_1 drop to half its maximum is the frequency at which σ_2 reaches its maximum. This frequency is the inverse of relaxation time $1/\tau$ which is defined as the scattering rate γ. In the limit of a "super" conductor, $\gamma \to 0$, the conductivities have the form:

$$\sigma_1(\omega) = \frac{N e^2 \pi}{2m}\delta(0) \quad \text{and} \quad \sigma_2(\omega) = \frac{N e^2}{m\omega} \tag{2.51}$$

The plasma frequency and the scattering rate separates the frequency into three different regions: low frequency Hagen-Rubens regime, intermediate *relaxation regime* and high frequency *transparent regime*. "Transparent" can be seen from the frequency dependent reflectance that before the plasma frequency, Drude metal have reflectance very close to 1 with drastic drop around ω_p. This cliff is called plasma edge and it is usually in the UV or X-ray region for normal metal. Therefore the shiny, reflecting metal for visible light is transparent for high energy photons.

The Drude model does not handle $\mathbf{q}$ dependence. It is a special case (dipole approximation therefore $\mathbf{q} = 0$ limit) of the Kubo formula. More rigorous and general ($\mathbf{q}$ dependent) derivations can be found in reference [25]. The Fermi statistics predicts electron-hole excitation region in the ω-$\mathbf{q}$ diagram and outside this region electron-hole can not be excited therefore a vanishing σ_1.

2.3.3 Semiconductors

Semiconductors have gaps separating their conduction band and valence band. The gaps of semiconductors are smaller that they can be thermally excited. When electromagnetic waves come in, both interband and intraband transitions occur. Both

cases can be studied in the response function formalism with no difficulties. For such transition, the joint density of states are important. Those point with divergently high density of states are called *van Hove singularities*.

The real part of the conductivity σ_1 of semiconductors has two components. One is from the intraband transition, originating from the overall shift of surface sphere, that has features in the low frequency region. The other is from the interband transition, a peak located at frequency corresponding to the energy gap of the semiconductor. The shape of the peak depends on the dispersion of both conduction and valence band, as well as temperature.

2.3.4 Superconductors

Helium was liquefied by Heike Kamerlingh Onnes in the year 1908. Three years later, during the study of resistivity of mercury at low temperature, Onnes discovered superconductivity at 4.2 K. After that many superconducting metals and alloys were discovered, followed by the discovery of many exotic types of superconductors. As of today, mercury thallium barium calcium copper oxide ($Hg_{12}Tl_3Ba_{30}Ca_{30}Cu_{45}O_{125}$, HBCCO) [39] holds the record of highest transition temperature T_c =138 K. The mechanism of conventional superconductors was discovered by Bardeen, Cooper and Schrieffer in 1957 [40]. The Nobel prize winning theory is truly one of the most important triumphs of the quantum theory.

The key of BCS theory [41] is the electron-electron attraction mediated by the exchange of a virtual phonon. When the electron-electron attraction overcomes coulomb repulsion, the Fermi sea becomes unstable: the free electrons form bounded *Cooper pairs* that have opposite spins and momentums. At finite energy, there exist no electronic states to scatter the pairs and the electrons (Cooper pairs) move without

being scattered. To break such pairs, a threshold energy is needed. The energy of the excitations is

$$E_{\mathbf{k}} = \sqrt{\varepsilon_{\mathbf{k}}^2 + \Delta_{\mathbf{k}}^2} \tag{2.52}$$

and the formation of a gap $\Delta_{\mathbf{k}}$ is seen. It should be noted that although the gap is of central interest for superconductors, the gap itself is not the key of superconductivity. Semiconductors have gaps, being usually much larger than superconducting gaps, yet they are not superconducting. Physically it is the global coherence of all electrons that makes a superconductor. BCS defines two basis relations:

$$\Delta = 2\omega_D e^{-\frac{1}{NV}} \quad \text{and} \quad k_B T_c = 1.14\omega_D e^{-\frac{1}{NV}} \tag{2.53}$$

N is the density of electron states at the Fermi surface and V is the electron-electron attraction due to phonon exchange with Debye frequency ω_D as the cut off frequency for phonons. The product of N and V is called the *electron phonon coupling constant* which is a measurement of the electron phonon coupling strength. The above relations eventually lead to the well known ratio between superconducting gap and transition temperature:

$$\frac{2\Delta}{k_B T_c} = 3.52 \tag{2.54}$$

BCS theory also predicts expressions for critical fields and specific heat that agree with experiments.

In a naive way, the conductivity of the superconducting state is obtained by taking $\gamma \to 0$ and

$$\sigma_1(\omega) = \frac{Ne^2\pi}{2m}\delta(0) \quad \text{and} \quad \sigma_2(\omega) = \frac{Ne^2}{m\omega} \tag{2.55}$$

σ_1 is now a delta function located at zero frequency. The sum rule originates from causality therefore are not affected by the superconducting transition. The presence of a superconducting gap rearranges the spectral weight, just as the semiconductor

gaps introduce interband transition peaks. However, part of the rearranged spectral weight for superconductors is now at zero frequency, a region that is experimentally unaccessible. As a result, the term *missing area* is used to describe this part of the spectral weight. Physically it corresponds to the superconducting condensate of cooper pairs. The missing area is the signature of superconductor and in fact the σ_1 measurement by Glover and Tinkham [42] provided the first decisive sigh of superconducting gap.

Not all spectral weight condensates upon entering superconducting state. *Dirty* and *clean* superconductor [43] are defined according to the relative size of two important length scales: the superconducting correlation length ξ and the mean free path of uncondensed electrons l. Correlation length ξ is inversely proportional to superconducting energy gap Δ and the mean free path l is inversely proportional to scattering rate γ. For clean superconductors, $l \ll \xi$ therefore $\gamma \gg 2\Delta$ while in dirty superconductors, $l \gg \xi$ and $\gamma \ll 2\Delta$. It is easy to understand that the optical conductivity σ_1 should be zero at frequencies lower than 2Δ because the presence of the gap Δ requires twice the energy to send a cooper pair from blow the gap to above. 2Δ is sometimes referred as the *optical gap*. In the dirty limit, upon entering superconducting state, a big drop is observed in σ_1 at around $\omega = 2\Delta$ which was originally in the Drude peak ($\gamma \gg 2\Delta$). On the other hand, for clean superconductors, no detectable change of the spectrum is expected at 2Δ upon the superconducting transition. There was no spectral weight because of the narrow Drude peak ($\gamma \ll 2\Delta$) in the normal state. Both dirty and clean superconductors have superconducting condensate therefore missing area in the spectrum except for that the superconducting condensate converges slower in the dirty limit.

To obtain the quantitative behavior of the optical conductivity of the dirty super-

conductors, the electrodynamics was studied by Mattis and Bardeen [44] therefore the name *Mattis-Bardeen formalism*. Recent reviews are in reference [25]. An artificial optical conductivity is shown in figure 2.3. The superconducting condensate is represented by a delta function located at the origin. The half width of the normal state Drude peak γ is 40 a.u., which is bigger than the superconducting gap $2\Delta = 30$ a.u. As a result, the abrupt drop of σ_1 is clearly observed at 30 a.u. which can be taken as an accurate measurement of the superconducting gap 2Δ.

Although the general result $2\Delta/k_BT_c = 3.52$ holds for many superconductor, there are exceptions even before the discovery of unconventional superconductors. This quantitative disagreement apply primarily to lead and mercury. In such systems the electron phonon coupling constant λ is large (≈ 0.35) compared with the rest (≤ 0.2). They are called *strong-coupling superconductors* which leaves the rest *weak-coupling superconductors*. The quantitative deviation from BCS originates from its failure to taken into account of retardation effect: electron phonon coupling should be frequency dependent. Retardation effect is important for strong coupling superconductors. Eliashberg [45] derives an integral equation for frequency dependent gap function $\Delta(\omega)$. McMillan [46] solved such equations using the electron phonon coupling matrix elements of lead and obtained an expression for superconducting transition temperature:

$$T_c \propto \omega_D e^{-\frac{1+\lambda}{\lambda-\mu^*}} \tag{2.56}$$

μ^* is the effective Coulomb potential that BCS failed to take into account. Accordingly, the ratio between gap size and transition temperature is replaced by:

$$\frac{2\Delta}{k_BT_c} = 3.52[1 + c(\frac{T_c}{\omega_D})^2 \ln \frac{\omega_D}{T_c}] \tag{2.57}$$

Both equations reduce to the BCS form in case of weak coupling ($\lambda \ll 1$).

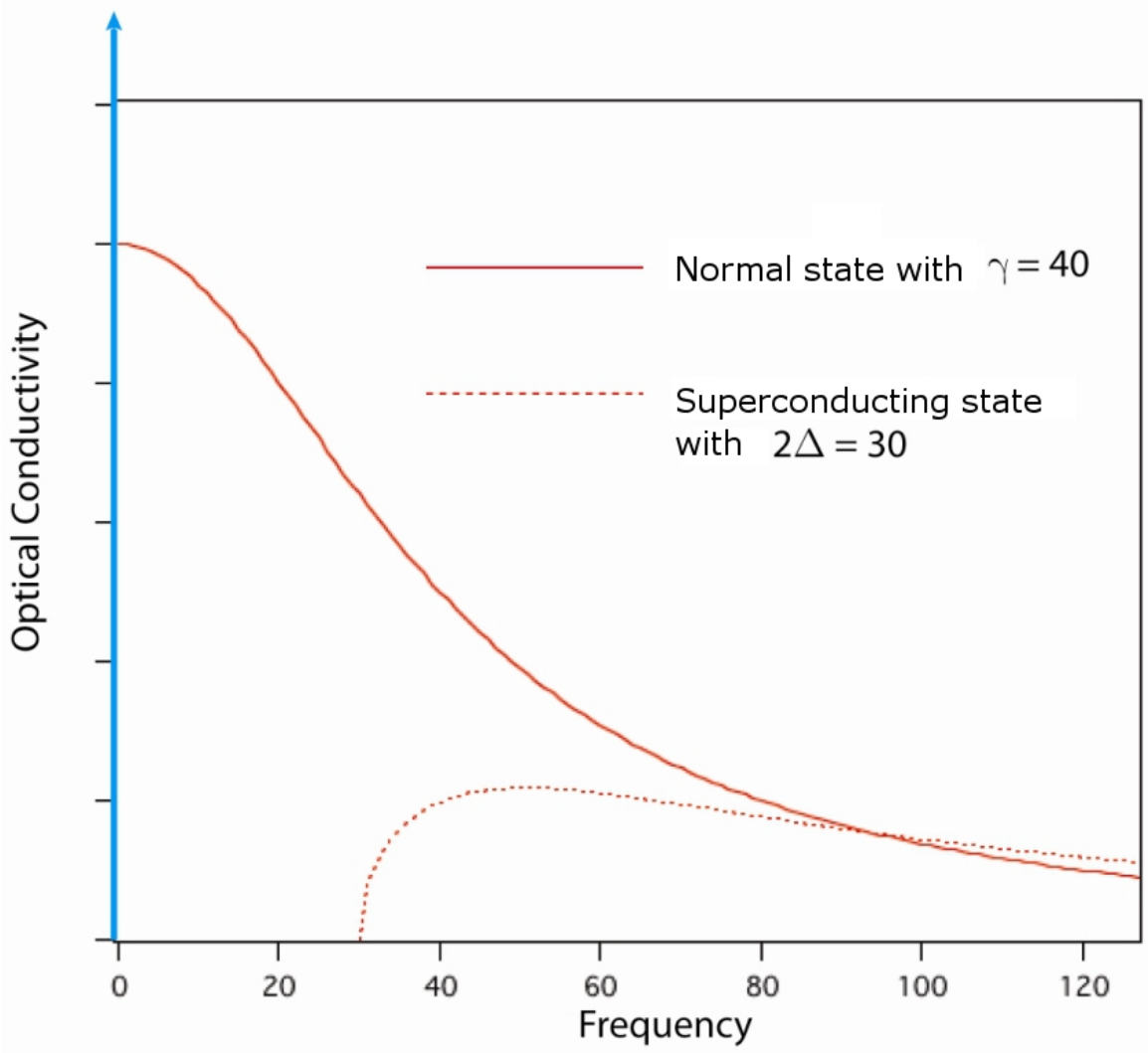

Figure 2.3 : Schematic optical conductivity of σ_1 of conventional (BCS) superconductors in the dirty limit before and after superconducting transition. The shape of σ_1 in superconducting state is quantitatively obtained from the Mattis-Bardeen formalism. The well studied high temperature cuprates and pnictide superconductors are in this category.

In the Eliashberg formalism, the electron phonon coupling constant λ is not simply the product of electron phonon coupling matrix element V and density of states at the Fermi surface N as in the BCS theory. Instead, it is frequency weighted integral of the phonon spectrum function $F(\omega)$ and electron phonon interaction matrix element $\alpha(\omega)$:

$$\lambda = 2\int_0^\infty \frac{\alpha^2(\omega)F(\omega)}{\omega}\mathrm{d}\omega \tag{2.58}$$

The product $\alpha^2(\omega)F(\omega)$ is refered as *electron phonon interaction spectral density*. λ is still the measurement of electron phonon coupling strength. Being a renormalization factor, λ is important for electronic specific heat, electronic density of states around the Fermi surface, effective mass and Fermi velocity [47].

The BCS theory, Eliashberg theory, as well as the BCS based Mattis-Bardeen formalism, apply only to conventional superconductors. Conventional superconductors are phonon-mediated, isotropically gapped with fixed ration between energy gap and transition temperature $2\Delta/kT_c = 3.53$. Unconventional superconductors do not satisfy those conditions. Except two major families of copper based superconductors [48] and iron based superconductors [49, 50], unconventional superconductors also include Fulleride [51], heavy fermions [52] as well as some organic superconductors [53].

The electron phonon coupling constant λ need to be modified to describe the unconventional superconductors. The electron phonon interaction spectral density function $\alpha^2(\omega)F(\omega)$ is replaced by a more general *electron boson interaction spectral density function* $I^2(\omega)\chi(\omega)$:

$$\lambda = 2\int_0^\infty \frac{I^2(\omega)\chi(\omega)}{\omega}\mathrm{d}\omega \tag{2.59}$$

Being frequency dependent, the magnitude of $I^2(\omega)\chi(\omega)$ is a measurement of the strength of electron interaction with bosons. The locations of peaks in $I^2(\omega)\chi(\omega)$

indicate the energy of the excitation through which electrons form cooper pairs.

Infrared spectroscopy allows the determination of $I^2(\omega)\chi(\omega)$ [54]. It is directly related to the optical conductivity:

$$I^2\chi(\omega) = \frac{1}{2\pi}\frac{\mathrm{d}^2}{\mathrm{d}\omega^2}[\omega \mathrm{Re}\frac{1}{\sigma(\omega)}] \tag{2.60}$$

It has been successfully applied to cuprates and the position of the maximum in $I^2(\omega)\chi(\omega)$ identified the spin fluctuation as the glue of cooper pairs [55]. Quite unexpected, the Drude formalism is still useful in the discussion of unconventional superconductors. It is realized by taking the scattering rate both complex and frequency dependent [56]. It is called the *extended Drude formalism* [57]. The scattering rate $1/\tau(\omega)$ and the mass enhancement factor $\lambda(\omega)$ is defined as:

$$\frac{1}{\tau(\omega)} = \frac{\omega_p^2}{4\pi}\mathrm{Re}[\frac{1}{\sigma(\omega)}]; \qquad 1+\lambda(\omega) = \frac{m^*(\omega)}{m_b} = \frac{\omega_p^2}{4\pi\omega}\mathrm{Im}[\frac{1}{\sigma(\omega)}] \tag{2.61}$$

The effective mass enhancement factor $\lambda(\omega)$ obtained through the extended Drude formalism agrees well with specific heat and quantum oscillation measurements [58]. It should be noted that $\lambda(\omega)$, sometimes referred as λ_{tr} due to the transport nature of IR measurement, is an angular average of the "real" electron phonon coupling constant that can be obtained from ARPES measurements. As a result, λ_{tr} could deviate from λ significantly for superconductors with anisotropic gaps. The electrodynamics of high-T_c cuprates can be found in review article by Basov [59].

In this section, important properties of superconductors, such as Meissner effect, thermodynamic properties, London's two-fluid model, type-II superconductors, GinzburgLandau theory and Josephson effect, are not mentioned. They can be found in textbooks.

Chapter 3

Raman Spectroscopy

In 1928, Sir Chandrasekhara Venkata Raman and Kariamanickam Srinivasa Krishnan discoved an inelastic scattering process during the studding of light scattering in liquids [60]. The effect is therefore refereed as "Raman scattering" or "Raman effect". Upon entering solids, most photons get reflected at the surface, transmitted over the other side or get absorbed. A small fraction of the photons are scattered by either the lattice and electrons. Most of the scatterings are elastic that the photons change their direction but not the frequencies. The left small portion of photons, typically 1 in 10^7 [61], will be inelastically scattered. The frequencies of such photons increase or decrease. The change in frequency match vibrational or electronic excitations of the solids and the ratio between red shifted photons and blue shifted photons obey Boltzmann relations. Microscopically, Raman scattering is a second order effect a photon is initially absorbed by the solid and then re-emitted with the creation or destruction of one or many excitations of the solid.

The various optical effect is shown in figure 3.1. It is important to distinguish Raman scattering from both *fluorescence effect* and *Brillouin scattering*. Both Raman and fluorescence effect can be measured on the same Raman spectroscope but they differ in mechanism. In Raman scattering, the photon absorption and emission process are *virtual transitions* that the energies are not necessarily conserved and the characteristic time scale of both transitions are less than one picosecond. The photon absorption and photon emission for fluorescence process are real transitions and their

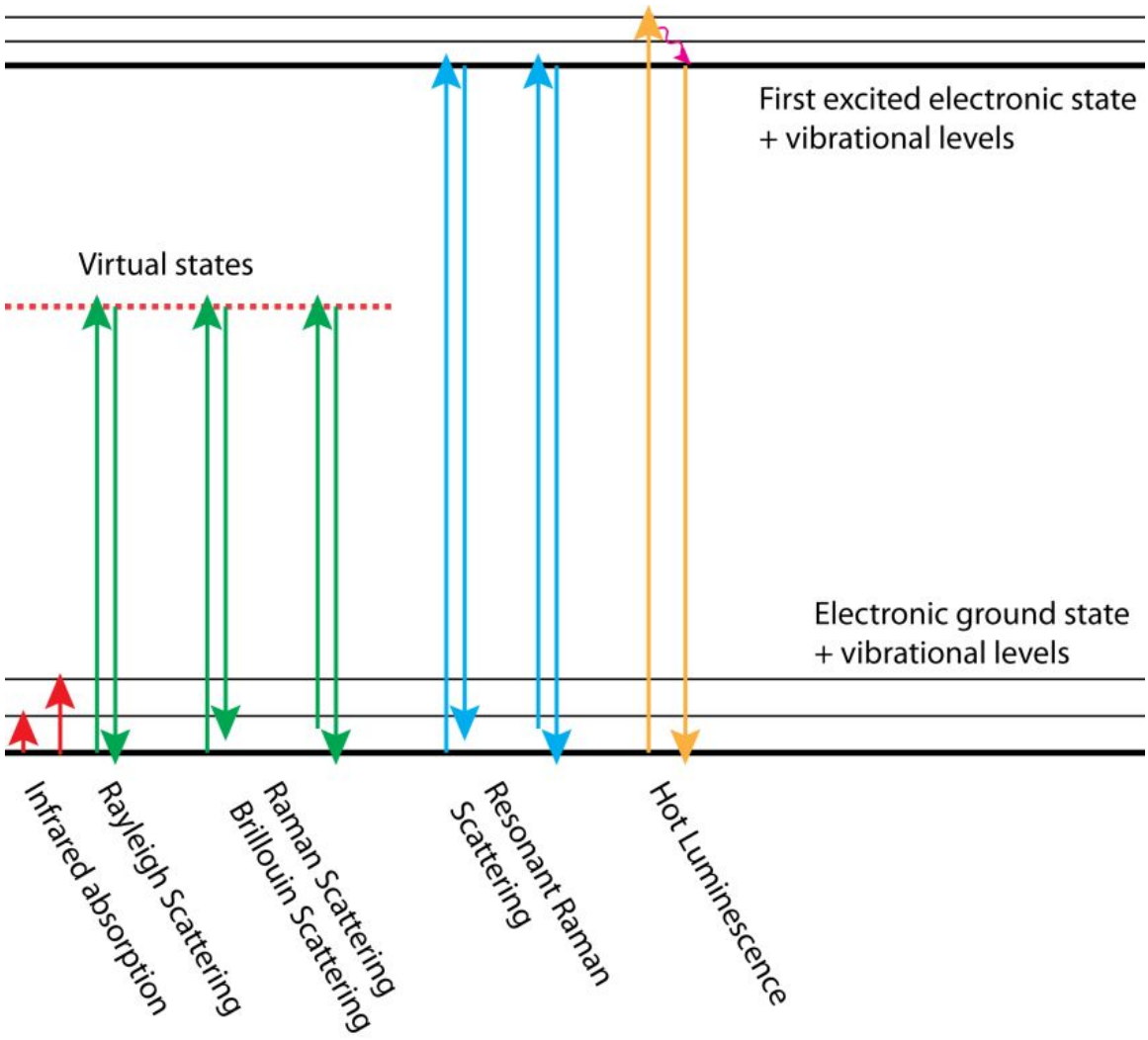

Figure 3.1 : Schematic energy diagram for different optical processes. vibrational energies are much small compared with the separation between electronic levels. As a result, for each electronic level, there are levels with slightly higher energy due to the additional vibrational level. Infrared spectroscopy studies transitions between vibrational levels and the electronic energy level remains the same; Rayleigh scattering, (ordinary) Raman scattering and Brillouin scattering involves virtual electronic state. If the final state is the same as initial state, it is elastic Rayleigh scattering; if one or many phonon are created or annihilated, it is Raman scattering or Brillouin scattering, depending on the energy scale. In those two process, the system before and after has the same electronic energy level but the vibrational levels change; When the energy of the virtual state is near or at the energy levels of the excited states, Raman scattering becomes Resonant and when those transitions becomes *real*, the process is hot luminescence.

time scale is on the order of nanosecond. The incident photon and scattered photon have fixed energy differences in Raman process while the emitted photons have fixed energies in fluorescence. As a result, upon increasing the energy of incident photon, the frequency shift remains and the scattered photon increases its energy while for fluorescence process, the frequency shift increases and scattered photon energy remains. This is an important experimental distinction between the two. Fluorescence is one special form of *luminescence* and in the discussion of optical spectroscopies the two terms interchangeable. On the other hand, the Raman scattering and the Brillouin scattering have the same mechanism. The only difference between the two is the magnitude of the energy shift. For Raman scattering, the energy shift is normally larger than 10 cm^{-1} and usually of order 100 cm^{-1} to 1000 cm^{-1} and for Brillouin scattering typical energy shift is approximately 1 cm^{-1} or less (such as acoustic phonon). The different energy shifts require different experimental setups [62].

Only Raman scattering by phonons are introduced. Raman spectroscopic study of molecule rotation, magnon and electronic excitations are omitted. Both macroscopic and microscopic models exist for the Raman scattering and they will be introduced in the next two sections.

3.1 Macroscopic theory

The inelastic scattering of photons are due to the fluctuation of the medium. The dielectric constant $\chi(\mathbf{r}, t)$ or its Frourier transform $\chi(\mathbf{k}, \omega)$ can be expanded in power series in normal mode $\mathbf{Q}(\mathbf{r}, t) = \mathbf{Q}(\mathbf{q}, \omega_0)\cos(\mathbf{q} \cdot \mathbf{r} - \omega_0 t)$:

$$\chi(\mathbf{k}, \omega, \mathbf{Q}) = \chi_0(\mathbf{k}, \omega) + \frac{\partial \chi}{\partial \mathbf{Q}}\mathbf{Q}(\mathbf{r}, t) \tag{3.1}$$

The polarization $\mathbf{P}$ due to this fluctuation of phonon $\mathbf{Q}$ is therefore:

$$\begin{aligned}
\mathbf{P}(\mathbf{r},t,\mathbf{Q}) &= \mathbf{P}(\mathbf{k},\omega)\cos(\mathbf{k}\cdot\mathbf{r}-\omega t) \\
&= \chi(\mathbf{k},\omega)\mathbf{E}(\mathbf{k},\omega)\cos(\mathbf{k}\cdot\mathbf{r}-\omega t) \\
&= [\chi_0(\mathbf{k},\omega)+\tfrac{\partial\chi}{\partial\mathbf{Q}}\mathbf{Q}(\mathbf{r},t)]\mathbf{E}(\mathbf{k},\omega)\cos(\mathbf{k}\cdot\mathbf{r}-\omega t) \\
&= \chi_0(\mathbf{k},\omega)\mathbf{E}(\mathbf{k},\omega)\cos(\mathbf{k}\cdot\mathbf{r}-\omega t)+\tfrac{\partial\chi}{\partial\mathbf{Q}}\mathbf{Q}(\mathbf{r},t)\mathbf{E}(\mathbf{k},\omega)\cos(\mathbf{k}\cdot\mathbf{r}-\omega t) \\
&= \mathbf{P}_0(\mathbf{r},t)+\tfrac{\partial\chi}{\partial\mathbf{Q}}\mathbf{Q}(\mathbf{q},\omega_0)\cos(\mathbf{q}\cdot\mathbf{r}-\omega_0 t)\mathbf{E}(\mathbf{k},\omega)\cos(\mathbf{k}\cdot\mathbf{r}-\omega t) \\
&= \mathbf{P}_0(\mathbf{r},t)+\tfrac{1}{2}\tfrac{\partial\chi}{\partial\mathbf{Q}}\mathbf{Q}(\mathbf{q},\omega_0)\mathbf{E}(\mathbf{k},\omega) \\
&\qquad\qquad \times\{\cos[(\mathbf{k}+\mathbf{q})\cdot\mathbf{r}-(\omega+\omega_0)t]+\cos[(\mathbf{k}-\mathbf{q})\cdot\mathbf{r}-(\omega-\omega_0)t]\}
\end{aligned}$$

The frequency in the first term $\mathbf{P}_0$ is not changed and it corresponds to the elastic scattering which is also known as Rayleigh scattering. The second term consists of two sinusoidal waves, one with wavevector $(\mathbf{k}+\mathbf{q})$ and frequency $(\omega+\omega_0)$ and the other with wavevector $(\mathbf{k}-\mathbf{q})$ and frequency $(\omega-\omega_0)$. They are called *anti-Stokes* and *Stokes* shifts.

The scattered light can be determined from the frequency and wavevector dependence of polarization using standard dipole radiation theory that intensity of electromagnetic wave is proportional to the square of $\hat{\varepsilon}\cdot\mathbf{P}$. The result can be written down in a transparent way:

$$I_s \propto |\hat{\varepsilon}_I\cdot\frac{\partial\chi}{\partial\mathbf{Q}}\mathbf{Q}\cdot\hat{\varepsilon}_S|^2 \tag{3.2}$$

Here, $\hat{\varepsilon}_I$ and $\hat{\varepsilon}_S$ are the polarization of the incident and scattered light. The quantity $\frac{\partial\chi}{\partial\mathbf{Q}}\mathbf{Q}$ is a second rank tensor and it is usually refereed as the *Raman tensor* $\mathscr{R}$. It is symmetry related and it will be introduced in more details after the microscopic treatment of Raman scattering.

3.2 Microscopic theory

Unlike the infrared absorption process where only vibrational energy levels are involved, in Raman scattering, both electronic and vibrational energy levels participate. To taken into account of both degree of freedoms, the wave functions are, in the Born-Oppenheimer approximation, is in the product of electronic wave function ψ_μ and vibrational wave function $\phi_{\mu,n}$:

$$\Phi_{\mu,n}(\mathbf{r},\mathbf{R}) = \psi_\mu(\mathbf{r},\mathbf{R})\phi_{\mu,n}(\mathbf{R}) \tag{3.3}$$

The μ, n index for phonon is due to the fact that the vibrational wave functions depends on the electronic states. In Raman process, the system is assumed to be at its ground state:

$$\Phi_i = \Phi_{0,0}(\mathbf{r},\mathbf{R}) = \psi_0(\mathbf{r},\mathbf{R})\phi_{0,0}(\mathbf{R}) \tag{3.4}$$

It belongs to the identity representation of the group. After the scattering process, the system is at electric ground state with one additional phonon. The wave function becomes:

$$\Phi_f = \Phi_{0,1}(\mathbf{r},\mathbf{R}) = \psi_0(\mathbf{r},\mathbf{R})\phi_{0,1}(\mathbf{R}) \tag{3.5}$$

There are three steps for the system to go from initial state Φ_i to final state Φ_f. Electromagnetic perturbation makes the system transit from the ground state $\Phi_i = \Phi_{0,0}(\mathbf{r},\mathbf{R})$ to an intermediate state $\Phi_{\text{int}} = \Phi_{\mu,n}(\mathbf{r},\mathbf{R})$ and then come back to the final state $\Phi_f = \Phi_{0,1}(\mathbf{r},\mathbf{R})$ with the emission of a photon with different frequency. The perturbation Hamiltonian is $\mathscr{H}' = \frac{e}{mc}\mathbf{A}\cdot\mathbf{p}$. When dealing with complex fields, additional complex conjugate term is needed. For the convenience of later discussion, the Hamiltonian is written in a more transparent form:

$$\mathscr{H}' = \frac{eA_0}{mc}\hat{\varepsilon}\cdot\mathbf{p} \tag{3.6}$$

$\mathbf{p}$ is the effective momentum operator for both electronic $\mathbf{p}_e$ and vibrational $\mathbf{p}_L$ degree of freedom. Both $\mathbf{p}_e$ and $\mathbf{p}_L$ transform as dipole operators and so is effective momentum operator $\mathbf{p}$. $\hat{\varepsilon}$ is unit vector defined as $\hat{\varepsilon}_{x,y,z} = \frac{\mathbf{x,y,z}}{|\mathbf{r}|}$.

The total transition probability per unit time is given by:

$$\begin{aligned} \omega_{00\to01} &= |\sum_{\text{int}} \frac{<\Phi_f|\mathscr{H}'|\Phi_{\text{int}}><\Phi_{\text{int}}|\mathscr{H}'|\Phi_i>}{E_i - E_{\text{int}}}|^2 \rho(E_f) \\ &= |\sum_{\mu,n} \frac{<\psi_0\phi_{0,1}|\hat{\varepsilon}_S\cdot\mathbf{p}|\psi_\mu\phi_{\mu,n}><\psi_\mu\phi_{\mu,n}|\hat{\varepsilon}_I\cdot\mathbf{p}|\psi_0\phi_{0,0}>}{E_i - E_{\mu,n}}|^2 (\frac{eA_0}{mc})^2 \rho(E_f) \end{aligned} \tag{3.7}$$

After some rearrangement and approximations, the transition probability becomes:

$$\begin{aligned} \omega_{00\to01} &= |\sum_{\mu} \frac{\omega_{\mu,0}^2}{\hbar\omega_i - \hbar\omega_{\mu,0}} < \phi_{0,1}| < \psi_0|\hat{\varepsilon}_S\cdot\mathbf{p}|\psi_\mu >< \psi_\mu|\mathbf{p}\cdot\hat{\varepsilon}_I|\psi_0 > |\phi_{0,0} > |^2 \rho(E_f) \\ &\equiv |\sum_{\mu} < \phi_{0,1}|\hat{\varepsilon}_S\cdot\mathbf{P}\cdot\hat{\varepsilon}_I|\phi_{0,0} > |^2 \rho(E_f) \end{aligned} \tag{3.8}$$

The operator $\mathbf{P}$ is a second order tensor. Based on its definition, it transform as *symmetric second rank tensor operator field*: the symmetrized direct product of two vector representations D^v:

$$D^{\mathbf{P}} = [D^v \times D^v] \tag{3.9}$$

The operator $\mathbf{P}$ can be expanded in normal modes:

$$\mathbf{P} = \mathbf{P}^{(\mathbf{0})} + \sum_{l,\lambda} \mathbf{P}^{(1)}_{l,\lambda}\mathbf{Q}(0|l,\lambda) + \sum_{l,\lambda,l',\lambda'} \mathbf{P}^{(2)}_{l,\lambda,l',\lambda'}\mathbf{Q}(0|l,\lambda)\mathbf{Q}(0|l',\lambda') + \cdots \tag{3.10}$$

Each term in $\mathbf{P}$ must transform the same as $\mathbf{P}$ itself. As a result, the expansion coefficient $\mathbf{P}^{(1)}_{l,\lambda}$ is non zero only if $\mathbf{Q}(0|l,\lambda)$ transform as symmetric second rank tensor operator field. For those normal modes that do satisfy the right symmetry constrain, it get excited and the final vibrational state is the wavefunction of single phonon $\mathbf{Q}(0|l,\lambda)$:

$$|\phi_{0,1} >= \psi_1(Q_l) = [\frac{1}{2\hbar}]^{\frac{1}{4}} e^{-\frac{\pi Q_l^2}{\hbar}} H_1(\sqrt{\frac{2\pi}{\hbar}}Q_l) \tag{3.11}$$

Compared with the initial state $|\phi_{0,0}>$, the net result of photon absorption and photon emission is to create a single phonon in the crystal whose irreducible representation is contained in the symmetrized direct product of two vector representations.

Being a second rank tensor, $\mathbf{P}$ is closely related to the Raman tensor. The Raman tensor $\mathscr{R}$ is defined as the intermediate state averaged value of $\mathbf{P}$:

$$\mathscr{R} = \sum < \phi_{0,1}|\mathbf{P}|\phi_{0,0} > \tag{3.12}$$

As a result, $\mathscr{R}$ has the same symmetry property as $\mathbf{P}$. The scattering rate, expressed in terms of the Raman tensor, is now:

$$I = C|\hat{\varepsilon}_S \cdot \mathscr{R} \cdot \hat{\varepsilon}_I|^2 \tag{3.13}$$

It is clear that only Stokes scattering are discussed but the inclusion of anti-Stokes scattering should be easy. Also, only the single phonon creation is considered therefore the name *first order Raman scattering*. In special cases, the $\mathbf{A} \cdot \mathbf{A}$ term in the perturbation Hamiltonian is also important but only the $\mathbf{A} \cdot \mathbf{p}$ is kept to keep the analysis simple.

The above discussion of Raman scattering analysis is due to Placzek [63] (also see Birman [11]). An alternative formalism is also popular [64]. In this model, the Raman scattering proceeds in three steps: (1) the electromagnetic wave, therefore $\mathscr{H}_{e-rad} = \frac{e}{mc}\mathbf{A} \cdot \mathbf{p}$, excites the ground state $\Phi_i = \Phi_{0,0}(\mathbf{r}, \mathbf{R}) = \psi_0(\mathbf{r}, \mathbf{R})\phi_{0,0}(\mathbf{R})$ to an intermediate state denoted as $\Phi_a = \Phi_{\mu,0}(\mathbf{r}, \mathbf{R}) = \psi_\mu(\mathbf{r}, \mathbf{R})\phi_{\mu,0}(\mathbf{R})$ where the vibrational energy levels are not excited; (2) $\Phi_a = \Phi_{\mu,0}(\mathbf{r}, \mathbf{R})$, upon the electron-phonon coupling interaction $\mathscr{H}_{e-p}$, is scattered into another intermediate state $\Phi_b = \Phi_{\nu,n}(\mathbf{r}, \mathbf{R}) = \psi_\nu(\mathbf{r}, \mathbf{R})\phi_{\nu,n}(\mathbf{R})$ where one vibrational level is excited; (3) the system relax to its final state $\Phi_f = \Phi_{0,n}(\mathbf{r}, \mathbf{R}) = \psi_0(\mathbf{r}, \mathbf{R})\phi_{0,n}(\mathbf{R})$ with the emission of a less

energetic photon, leaving one phonon in the system. Again, this Stokes scattering picture can be extended to anti-Stokes process and for simplicity only first order Raman effect is considered. The scattering probability is:

$$P = (\frac{2\pi}{\hbar})|\sum_{\mu,\nu}\frac{<\psi_0|\mathscr{H}_{e-rad}|\psi_\nu><\psi_\nu|\mathscr{H}_{e-p}|\psi_\mu><\psi_\mu|\mathscr{H}_{e-rad}|\psi_0>}{[\hbar\omega_i-(E_\mu-E_i)][\hbar\omega_i-\hbar\omega_0-(E_\nu-E_i)]}+\cdots|^2\rho(E_f) \tag{3.14}$$

There are totally six different time orders and only one is given explicitly. This expression for the Raman scattering is of little use for the calculation of scattering intensity due to the unknown parameters. However, it is helpful in the discussion of Raman selection rules. Both ψ_μ and ψ_ν transforms according to the vector representation D^v otherwise the matrix elements of $\mathscr{H}_{e-rad}$ becomes zero. For $<\psi_\nu|\mathscr{H}_{e-p}|\psi_\mu>$ to exist, the phonon mode $\mathbf{Q}(0|l,\lambda)$ must be contained within $[D^v\times D^v]$. When exotic incident light are used, ψ_μ and ψ_ν transforms according to certain new representations D' and the phonon mode $\mathbf{Q}(0|l,\lambda)$ must be contained within the direct product of $[D^{'}\times D^{'}]$.

3.3 Raman tensor

The connection between Raman tensor and Clebsh-Gordan coefficients was first studied by Birman [65]. Both equation 3.8 and 3.14 predict selection rules regarding the irreducible representations of the photon operator and phonons: if a phonon to be Raman active,

$$D^{identity}\in[D^{(photon)}\otimes D^{(photon)}]\otimes D^{(phonon)} \tag{3.15}$$

The square bracket indicates symmetric direct product. To take this one step further, for phonons and photons belong to the γth branch of the lth irreducible representation and the Raman selection rules are:

$$\phi_1^{identity}\in\phi_\mu^l\times\phi_{\mu'}^{l'}\times\phi_\lambda^j \quad \text{or} \quad \phi_\lambda^j\in\phi_\mu^l\times\phi_{\mu'}^{l'} \tag{3.16}$$

The polarized incident and scattered photons belong to μth and μ'th branches of the lth and lth representation. λ is the index for the jth phonon branch $\mathbf{Q}(0|j,\lambda)$. For those Raman active phonons, the Raman tensor analysis is based on the Wigner-Eckart theorem that the Raman tensors are the proper Clebsch-Gordan coefficients:

$$\mathscr{R}^{(j,\lambda)}_{\mu,\mu'} = (j,\lambda|l,\mu,l',\mu') \tag{3.17}$$

In ordinary situations, the l and l'th representation is the vector representation because of the dipole approximation in the electron-radiation interaction. μ and μ' are labels for experimental polarization directions such as x, y or xy. This analysis is sufficient for most Raman selection rules. Exceptions are the dipole-quadrupole resonant Raman scattering [66] and Raman scattering with high angular momentum lights. In those unusual situations, one or both l and l' can be different from vector representation and μ and μ' are not simply axial labels.

For ordinary Raman scattering, the experimental configuration are written in the form of scattered photon wave vector, scattering photon polarization, incident photon polarization and incident photon wave vector $\mathbf{k}_S(\epsilon_S,\epsilon_I)\mathbf{k}_I$. From symmetry point of view, the incident and scattered photon wave vectors are irrelevant and the Raman scattering tensors are determined by the photon polarization directions. Analysis on the Raman tensors in 32 crystallographic point groups have been tabulated by [67]. Notice that up until here, all the analysis on Raman tensors are symmetry based and the nature of the excitation are not taken into account. It can be shown [35, 68] that the nature of vibrational excitation impose the following restriction on the Raman tensors that they are symmetric:

$$\mathscr{R}_{i,j} = \mathscr{R}_{j,i} \tag{3.18}$$

On the other hand, the Raman tensors for magnons are antisymmetric:

$$\mathscr{R}_{i,j} = -\mathscr{R}_{j,i} \tag{3.19}$$

Therefore, the Raman tensors [67] need to be symmetrized to be applied to phonons. That is, if $\mathscr{R}_{i,j} = \mathscr{R}_{j,i}$ then nothing should be changed; if $\mathscr{R}_{i,j}$ and $\mathscr{R}_{j,i}$ are different constants, the two constants should be equal; if $\mathscr{R}_{i,j} = -\mathscr{R}_{j,i}$, then both elements vanish. For example, when dealing with phonons, the constant c in Γ_2 mode of C_{6v} point group need to be zero and constants d and e equal for Γ_5 mode of C_{6v} point group. Obviously, for magnons, the Raman tensors would be different compared with phonons. In fact, the antisymmetric restriction on the Raman tensor makes most matrix elements vanish.

The scattering cross section for the lth phonon are determined by the Raman tensors and the polarization directions:

$$\frac{\mathrm{d}\sigma}{\mathrm{d}\Omega} = \sum_{\lambda} |\sum_{i,j} \epsilon_{S,i} \mathscr{R}_{i,j}^{(l,\lambda)} \epsilon_{I,j}|^2 \tag{3.20}$$

The summation over λ is the summation over all branches of the phonon mode in case of degeneracy. The actual value of the matrix elements in the Raman tensors are determined by the details of the interaction.

3.4 Raman scattering by polar phonons

It has been shown in Chapter 2 that the behavior of a phonon, if it is infrared active, change its equation of motion dramatically in the presence of light. For crystals and molecules with a center of inversion symmetry, the infrared active phonons belong to odd representations and Raman active phonons belong to even representations. As a result, the dramatic change of equation of motion for the polar phonons are not

measured by Raman spectroscopy. Of the 32 point groups, only 11 have a center of inversion symmetry and they are called *centrosymmetric*. The rest 21 point groups that lack of inversion symmetry are called *noncentrosymmetric* or *piezoelectric*. In those crystals, the polar excitation at small wavevector forms phonon polaritons. Raman scattering provide the first measurement of the coupled phonon and photon system.

In a Stokes Raman process, both momentum and energy are conserved:

$$\mathbf{q} = \mathbf{k}_I - \mathbf{k}_S \tag{3.21a}$$

$$\omega(\mathbf{q}) = ck_I - ck_S \tag{3.21b}$$

$\omega(\mathbf{q})$ are the dispersion relation of the excitation being measured by Raman scattering. The two conservation laws defined a region in $\omega - q$ space that can be accessed by Raman spectroscopy provided the incident wavevector and energy. Such regions are depicted in figure 3.2. The same diagram is easily obtained for anti-Stokes scattering.

Except for small wavevectors, the polarition has well separated energies for the upper and lower branch. At large scattering angles, the Raman scattering probes only the lower branch with steady (no q dependence) frequency. Typical example are the LO and TO mode of zinc-blende crystals. The cubic T_d lattice predicts three fold degeneracy in Γ_4 phonon but the lack of inversion center induced strong coupling with photon split the mode. At near forward scattering geometry, $\theta \approx 0$ line in the Raman accessible region cuts the lower branch at regions the frequency is q dependent. The scattering angle (therefore wavevector q) dependence in Raman scattering at near forward scattering provide the first evidence of the existence of phonon-polaritions [69]. The upper branch is always above the Raman accessible region therefore can be be measured in this way.

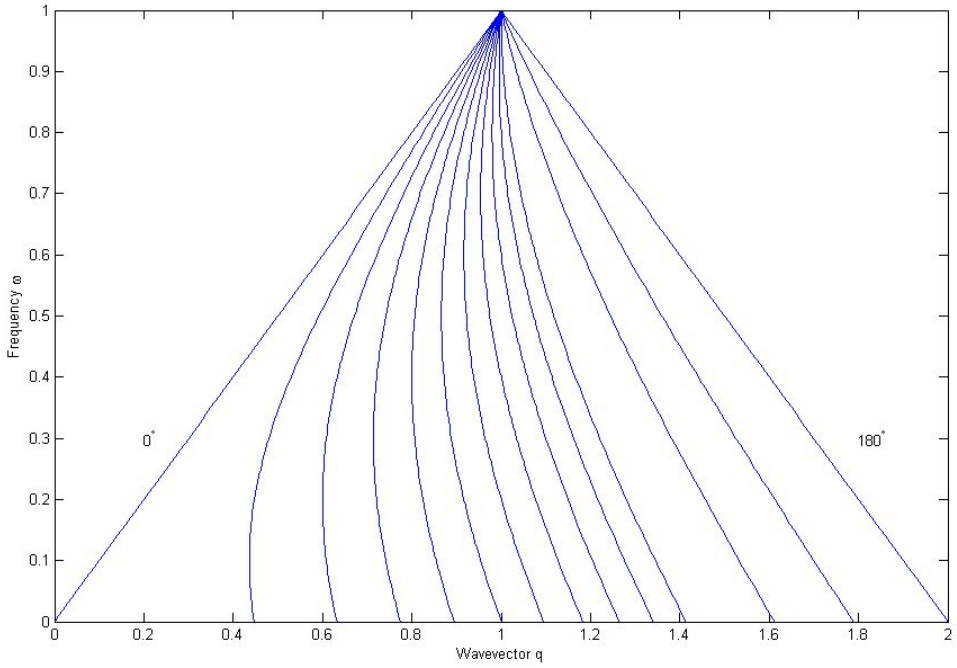

Figure 3.2 : The Raman accessible region at different scattering geometry. The excitations of a physical system will have certain dispersion relation. The cross points of this dispersion of the excitation and the family of Raman lines determines the energy and momentum transfer during the light scattering.

Chapter 4

Infrared Spectroscopic Study on Iron Pnictide Superconductors

Since its discovery by Heike Kamerlingh Onnes in 1911, superconductivity has generated tremendous interest in the physics society. This interest was renewed in the year 2006 that Iron pnictide LaOFeAs was found to be superconducting at 26 K [50]. The transition temperature of this family of iron based superconductors soon reached 55 K in doped SmFeAsO [70]. Up until today, many important issues are still under debate for the pnictide superconductors. Infrared spectroscopy has provided valuable informations on the fundamental properties of superconductors [42] and it is applied to the pnictides.

4.1 Iron based superconductors

Magnetism tends to harm superconductivity through the following channels: (1) in ferromagnetic materials the macroscopic magnetic field induced Zeeman splitting of electronic states suppresses the formation or even breaks Cooper pairs when the splitting energy exceeds the binding energy of Cooper pair; (2) in magnetically ordered (ferromagnetic and anti-ferromagnetic) materials, the exchange of spin waves leads to a repulsion between electrons that can form Cooper pairs when phonon is exchanged; (3) in materials with localized magnetic moment on atoms, the two electrons in Cooper pairs have a (large) possibility to align their spins in the same direction due to scattering to magnetic moments. Electrons with same spin directions are less

likely to form Cooper pairs. It has been shown that several percent of paramagnetic ion concentration is sufficient to destroy superconductivity [71]. As a result, the discovery of superconductivity in pnictide, where transition metal iron is involved, is surprising. Many important properties of the iron pnictides are reminiscent of the cuprates therefore comparisons are sometimes made.

The iron based supeconductors belong to four category: 1111 REOFeAs (RE = La, Ce, Pr, Nd, Sm, $\cdots$), 122 AFe_2As_2 (A = Ba, Sr, $\cdots$), 111 AFeAs (A = Li, $\cdots$) and 11 FeSe(Te). Despite the various structures of the iron based superconductors, they all share the same basic structure: the FeAs square layer, which is believed to be the superconducting layer. In pnictides, the Fe atoms, tetrahedrally surrounded by As atoms, form a square lattice. The effect of intercalating layers are to provide carriers and/or to fine tune the structure of the $FeAs_4$ tetrahedra such as the bond length and bond angle. The highest transition temperature in pnictides are found in SmFeAsO [70] in 2008. It is believed that in SmFeAsO the tetrahedra have reached optimal structure that the transition temperature can no longer be increased.

For the non-superconducting parent compounds, both structural and magnetic transitions occur at low temperature, accompanied by the resistivity anomaly. Careful neutron scattering experiment [72] reveals a small temperature difference in the two transitions: structural phase transition $T_S \approx 138\ K$ and magnetic phase transition $T_N \approx 137\ K$. Upon phase transition, the crystal is distorted from tetragonal P4/nmm (1111, 111, 11) and I4/mmm (122) to orthorhombic Cmma (1111) and Fmmm (122) and the paramagnetic spin state is being aligned anti-ferromagnetically. Be the transition first or second order in nature is material dependent and is still under debate. The antiferromagnetism in the parent compound of iron pnictide is different compared with the cuprates: cuprates are Mott insulators with localized electrons

due to large Coulomb repulsion while the iron pnictides are spin density wave metals with delocalized electrons whose spins modulate periodically in real space. The spin density wave state in pnictides is a result of Fermi surface nesting. Upon doping, both transitions are suppressed and the difference in transition temperatures decrease as well. Superconductivity exist for certain amount of hole or electron doping. For 122 family the spin density wave persist upon entering superconducting phase while for 1111 family, the spin density wave is completely suppressed.

Numerical studies [73, 74] as well as optical measurement [75] have confirmed weak electron-phonon coupling constant that is not sufficient for the high transition temperature. Mazin [76] suggested that superconductivity of pnictides is mediated by antiferromagnetic spin fluctuation and the superconducting order parameter (gap) is "extended s-wave" or $s \pm$. Due to the five-fold degenerate $3d$ orbitals of Fe, five sheets of Fermi surface exist for the iron pnictides. Being isotropic on each sheet, the order parameter reverses it sign on different sheets of the Fermi surface. Although this scenario is generally accepted, later experiment showed relatively large isotope effect which indicates strong electron phonon coupling. More experiments and better samples are needed to clear those controversial.

The rich complexities of iron pnictides are fascinating yet present great challenges to the physics society. Many wonderful reviews exist on the iron based superconductors. General discussion can be found in Hosono [77], Sadovskii [78], Johnston [79] and Stewart [80]. Reviews on special topics include Hirschfeld on gap symmetry [81], Wang on IR and Raman [82], Jeff Lynn on neutron scattering [83] and many others.

4.2 Infrared study of $BaFe_{1.85}Co_{0.15}As_2$

All the data and analysis in this section can be found in J. J. Tu *et al.*, Phys. Rev. B **82,** 174509 (2010) [75].

4.2.1 DC resistivity

Large single crystals with nominal formula $BaFe_{2-x}Co_xAs_2$ (x = 0.15) were grown by a self flux method [84]. Energy Dispersive x-ray (EDX) microscope analysis indicates that the actual Co concentration is x = 0.15, which corresponds to the optimal doping level. The *ab*-plane resistivity was measured using a standard four-probe method and the magnetization measurements were done in a Quantum Design MPMS-5 system. The resistivity is shown in Fig. 4.1. The superconducting phase transition is clearly observed at 25 K. The narrow transition width $\delta T_c \simeq 0.7\ K$ indicates high quality of $BaFe_{1.85}Co_{0.15}As_2$ single crystal. The temperature dependence of resistivity is fit with Bloch-Gruneisen [85] formula:

$$\rho(T) = \rho_0 + \lambda_{ph}(m-1)(\frac{k_B\Theta_D}{\omega_{p,D}^2})(\frac{T}{\Theta_D})^m J_m(\frac{T}{\Theta_D}) \tag{4.1}$$

with

$$J_m(t) = \int_0^{1/t} \frac{x^m e^{-x}}{(1-e^{-x})^2}\mathrm{d}x \tag{4.2}$$

The Debye temperature Θ_D is taken as 250 K [86]. The plasma frequency $\omega_{p,D} = 0.972 \pm 0.05$ meV will be determined in later discussion. The best fit is achieved with transport electron-phonon coupling constant $\lambda_{ph} \simeq 0.2 \pm 0.02$, not in favor of the electron phonon coupling picture in conventional superconductors. The integer m, whose value is chosen to be 5, shows that the resistance is due to scattering of electrons by phonons [23] (as it is for simple metals).

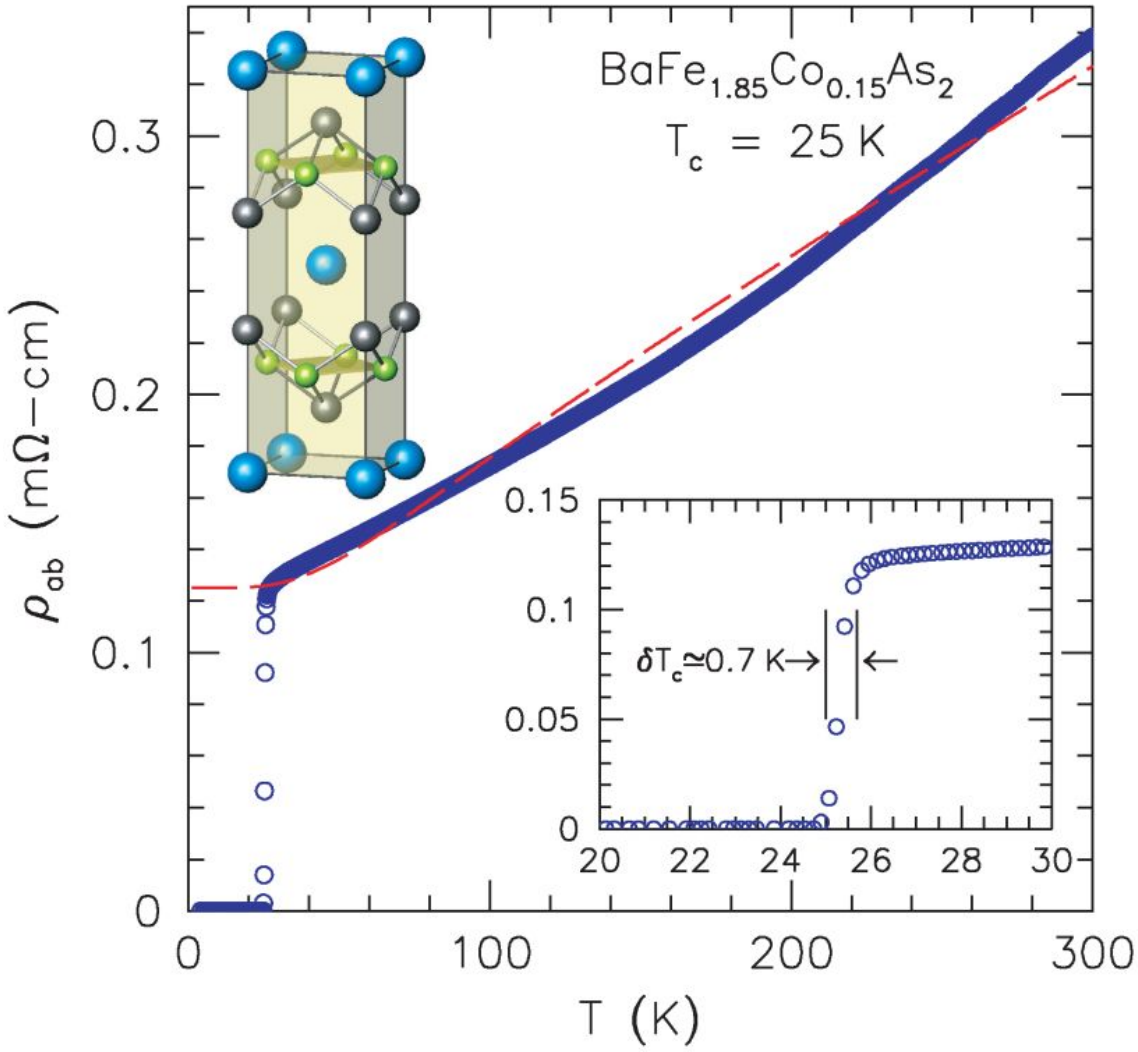

Figure 4.1 : Temperature dependence of *ab*-plane resistivity of $BaFe_{1.85}Co_{0.15}As_2$ single crystal. The unit cell of $BaFe_{1.85}Co_{0.15}As_2$ is shown in inset. The sharp transition at 25 K indicates high sample quality.

4.2.2 Reflectance and optical conductivity

The temperature dependent reflectance was measured in a near-normal-incidence arrangement from ∼20 cm^{-1} to over ∼25000 cm^{-1} on cleaved *ab*-plane surfaces on a Bruker IFS 66v/S and a Bruker IFS 113v. The absolute reflectivity was determined by evaporating a gold film *in situ* in high vacuum ($\sim 1 \times 10^{-8}$ Torr) over the sample [87]. The results are given in Fig. 4.2. The reflectance in the normal state behaves as a metal with $R(\omega) \propto 1 - \sqrt{\omega}$. Two kinks in the reflectance at 27 K and 5 K are marked by two arrows. They are due to scattering of the carriers with underlying bosonic excitations. At 6 K, the reflectance reaches unity at low frequency, a characteristic phenomenon for superconducting state.

To carry out a reliable Kramers-Kronig analysis, standard extrapolations were applied at higher and lower frequencies. Once the phase θ is obtained from reflectance R, both the real and imaginary part of the optical conductivity can be derived. The real part is more interesting and it is shown in Fig. 4.3 for different temperatures above and below T_c. As the temperature is lowered, the low frequency conductivity gets narrower and narrower, agrees with Drude model. Below T_c, the conductivity collapse. The reduction of spectral weight signals the formation of superconducting condensate. Also notable are the two phonon modes at $\simeq 94$ cm^{-1} and $\simeq 253$ cm^{-1}. They are infrared-active E_u mode that involves the movement of Ba atoms [88].

4.2.3 Normal state optical conductivity

To have a better understanding of the carrier dynamics, the normal state conductivity is studied in the Drude-Lorentz model. In Fig. 4.4 (a), two Drude terms and one Lorentian term are used to reproduce the experimental data. The complex Drude-

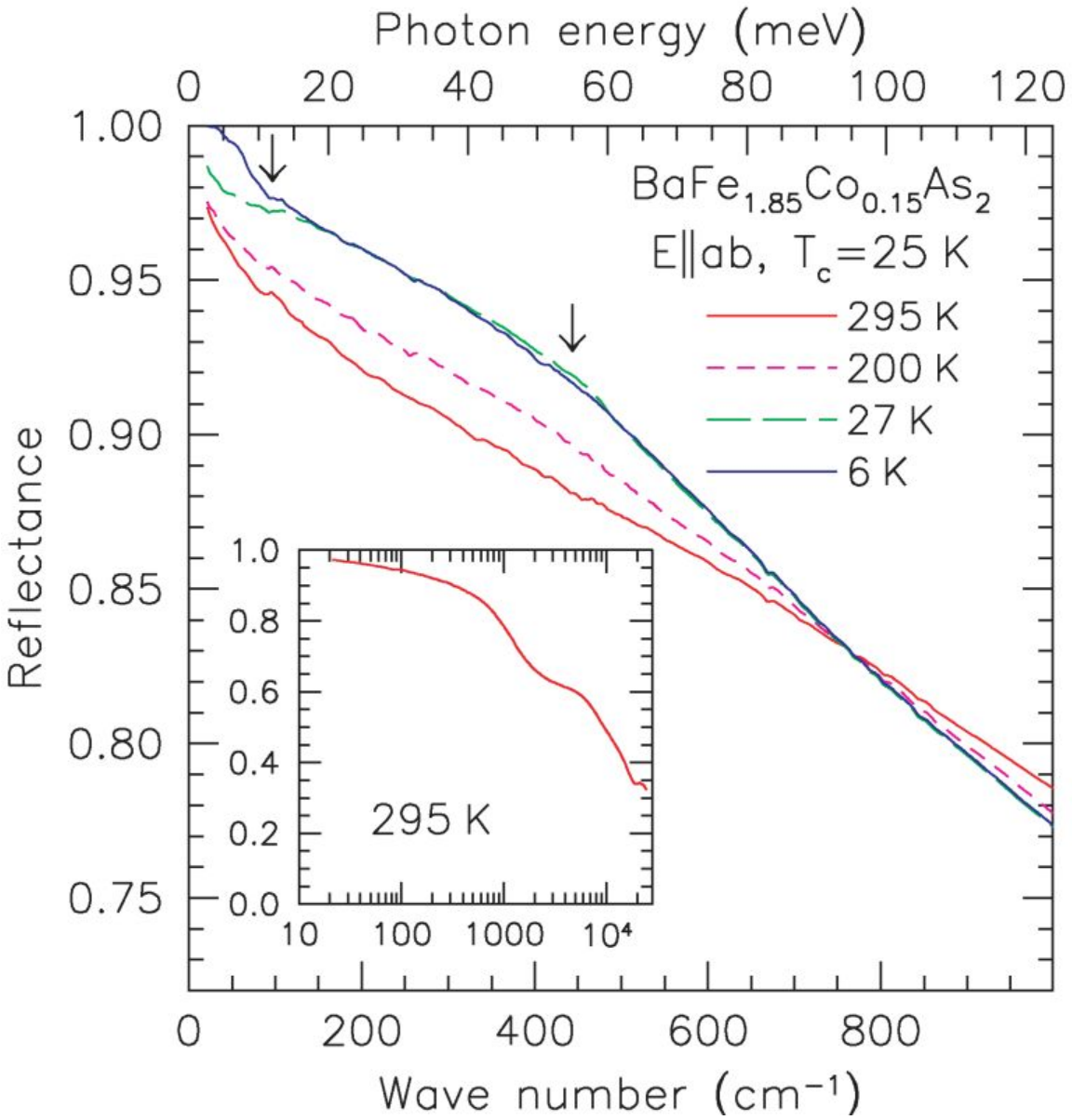

Figure 4.2 : Experimentally measured reflectance at different temperature as a function of photon frequency. Light is polarized in the *ab* plane. Two arrows mark two kinks in the reflectance at around 12 meV and 55 meV below and right above T_c. They are due to bosonic excitations whose interaction with electron is peaked at those positions. A semi-log plot of reflectance over a wide frequency range is shown in the inset.

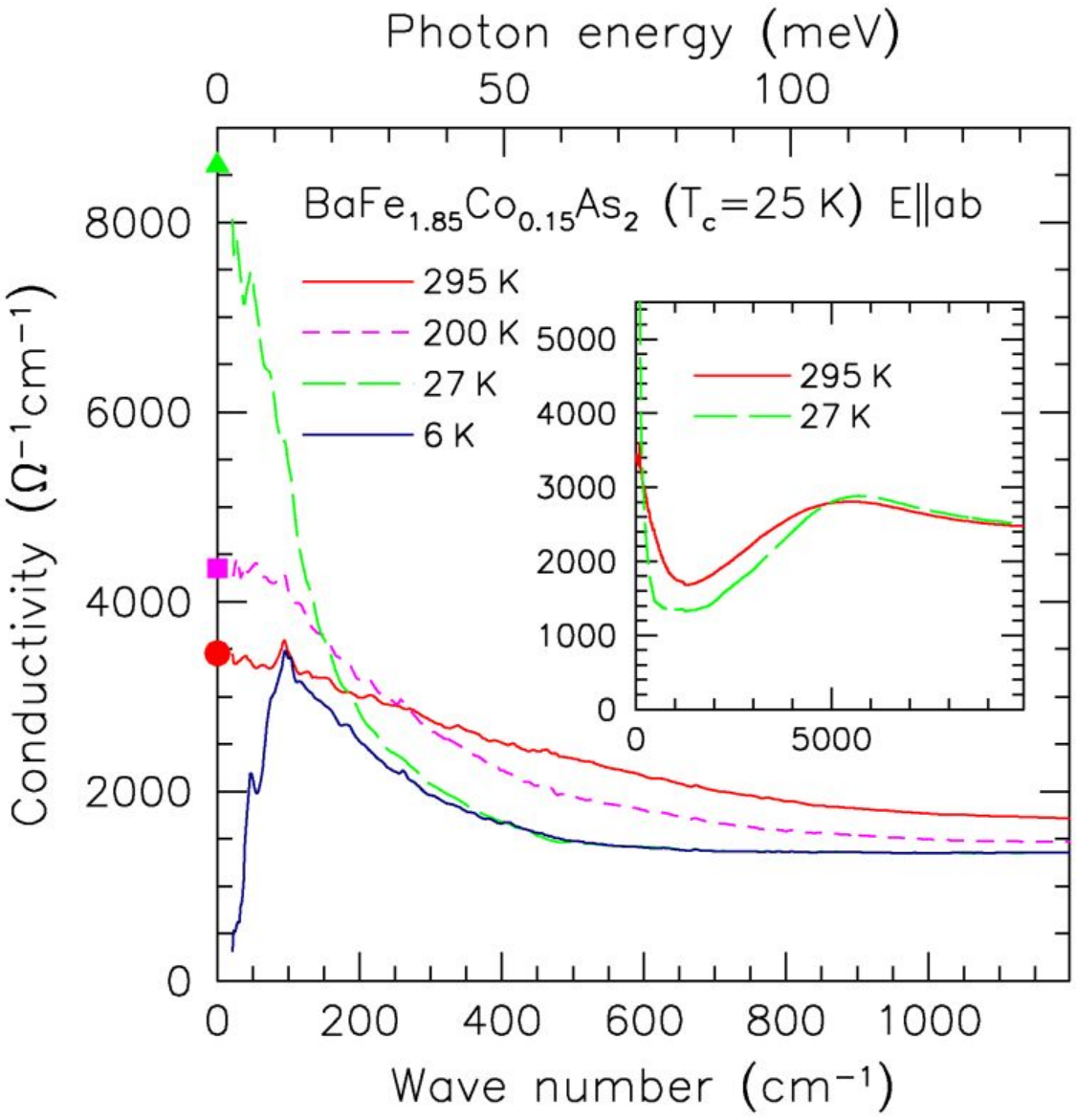

Figure 4.3 : The real part of the optical conductivity above and below T_c. In the normal state, upon reducing temperature, the Drude term becomes narrower and narrower. Below T_c there is a collapse of spectrum which is the sign of superconducting condensation. Extrapolations of optical conductivity agree with DC measurements at different temperatures.

Lorentz dielectric functions is:

$$\epsilon(\omega) = \epsilon_\infty - \sum_j \frac{\omega_{p,D;j}^2}{\omega^2 + i\omega/\tau_{D,j}} + \sum_k \frac{\Omega^2}{\omega_k^2 - \omega^2 - i\omega\gamma_k} \tag{4.3}$$

and the optical conductivity are closely defined. The iron pnictides have five sheets of Fermi surfaces and the fit with two Drude terms and one Lorentian term has physical meanings. The fitting parameters are:

$$\begin{aligned} 1/\tau_{D,1} &= 113 \text{ cm}^{-1}, & \omega_{p,D;1} &= 6943 \text{ cm}^{-1}; \\ 1/\tau_{D,2} &= 5720 \text{ cm}^{-1}, & \omega_{p,D;2} &= 19980 \text{ cm}^{-1}; \\ \omega_1 &= 5170 \text{ cm}^{-1}, & \gamma_1 &= 5730 \text{ cm}^{-1}, & \Omega_1 &= 22070 \text{ cm}^{-1}. \end{aligned}$$

The mean free path of the broad Drude term, $l_2 = 0.4$ Å, being less than the atomic distance casts doubt on the physical meaning of this term. This suggest that the conductivity of this band is neither metallic nor coherent and another bounded excitation is needed. The fit of the experimental data with two Drude terms and two Lorentzian term is given in Fig. 4.4 (b). The fitting parameters are now:

$$\begin{aligned} 1/\tau_{D,1} &= 126 \text{ cm}^{-1}, & \omega_{p,D;1} &= 7790 \text{ cm}^{-1}; \\ 1/\tau_{D,2} &= 608 \text{ cm}^{-1}, & \omega_{p,D;2} &= 1956 \text{ cm}^{-1}; \\ \omega_1 &= 1124 \text{ cm}^{-1}, & \gamma_1 &= 5560 \text{ cm}^{-1}, & \Omega_1 &= 18930 \text{ cm}^{-1}. \\ \omega_2 &= 5190 \text{ cm}^{-1}, & \gamma_2 &= 5780 \text{ cm}^{-1}, & \Omega_2 &= 22470 \text{ cm}^{-1}. \end{aligned}$$

The mean free path of the broad Drude term l_2 is now 3.5 Å. This value is still close to the Mott-Ioffe-Regal limit. If the two Drude component scenario is indeed intrinsic for $BaFe_{1.85}Co_{0.15}As_2$, the electron pockets dominates and the hole pocket represents a weak, possibly incoherent, background contribution. Nonlinear least-squares technique was used to fit the data.

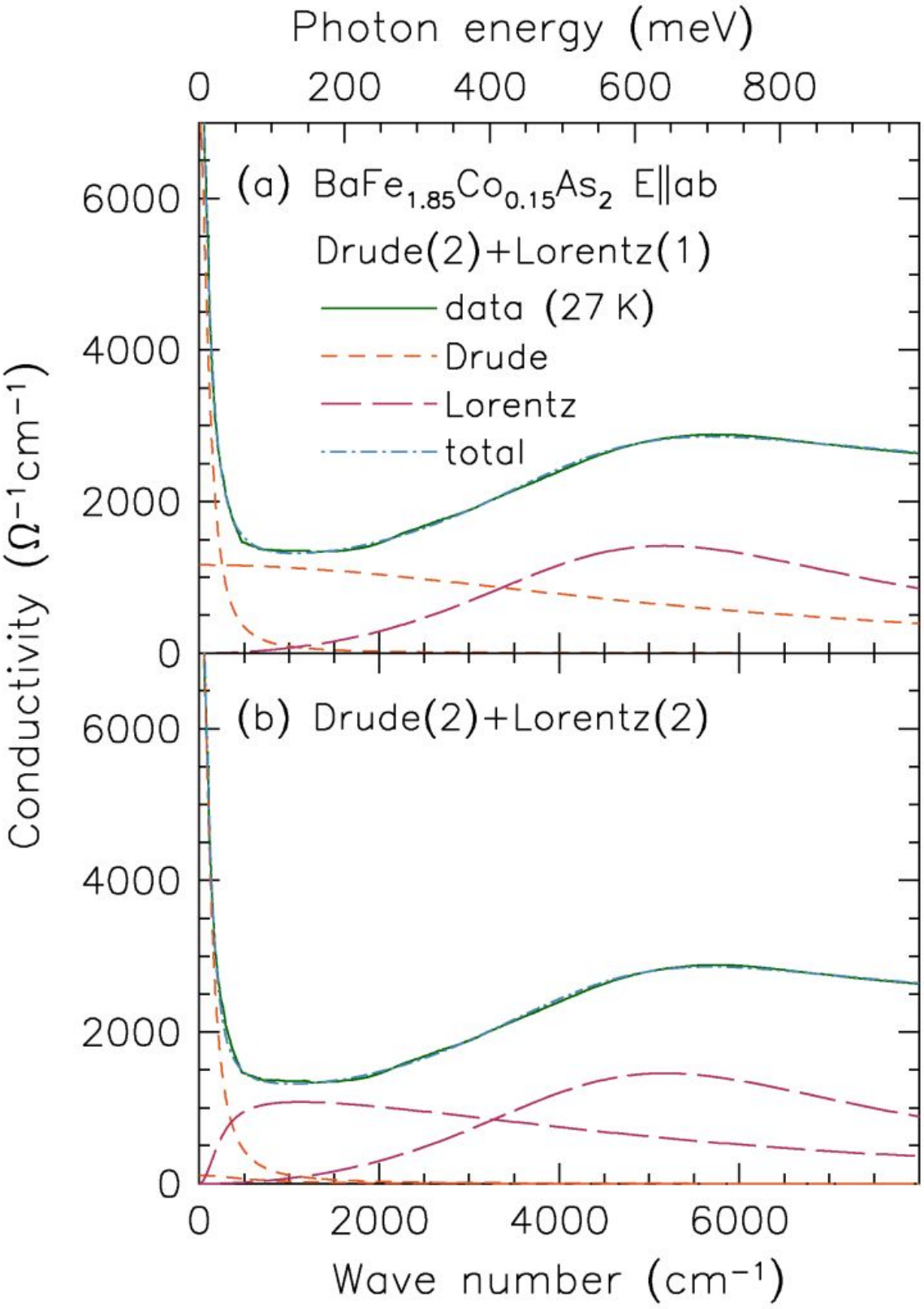

Figure 4.4 : Attempts to fit the normal state optical conductivity with Drude-Lorentz model. Two Drude terms and one Lorentzian term is used in (a); two Drude terms and two Lorentzian terms are used in (b).

4.2.4 Superconducting state optical conductivity

The "missing area" in the optical conductivity below T_c can be used to define the superconducting plasma frequency and super-fluid density through the Ferrell-Glover-Tinkham sum rule [89, 90]:

$$\int_0^{\omega_c} [\sigma_1(\omega', T \simeq T_c) - \sigma_1(\omega', T \ll T_c)] \mathrm{d}\omega' = \frac{\omega_{p,S}^2}{8} = \frac{\rho_S}{8} \tag{4.6}$$

The cut-off frequency ω_c is chosen to be 400 cm^{-1} to insure smooth convergence and the inferred superconducting plasma frequency is $\omega_{p,S} \simeq 5200 \pm 400$ cm^{-1}. Compared with Drude plasma frequency in the normal state, it is clear that less than one-half of the carriers have condensed. Equivalently, in Fig. 4.5, there is a significant amount of residue spectral in the superconducting state. This partial condensation indicate that $BaFe_{1.85}Co_{0.15}As_2$ is in the dirty limit.

Attempts to reproduce the optical conductivity below T_c are given in Fig. 4.5 within the Mattis-Bardeen formalism [44]. Clearly the data can not be fitted with a single gap. Two-gap fit with $\Delta_1 = 3.1$ meV and $\Delta_2 = 7.4$ meV reproduced the experimental data. Those values agrees with ARPES [91] and tunneling [92] results. The ratios between gap sizes and transition temperature are: $\frac{2\Delta_1}{k_B T_c} \simeq 2.9$ and $\frac{2\Delta_2}{k_B T_c} \simeq 7.3$. The former agrees with weak coupling BCS prediction and the latter indicates non-BCS behavior. In the "extended Drude model", both scattering rate and effective mass are taken as frequency dependent parameters. The results of such inversion technique is shown in Fig. 4.6. Above $\simeq 12$ meV, the abrupt increase in the scattering rate is due to the formation of one or many superconducting energy gaps.

In conclusion, the electron doped iron pnictide superconductor $BaFe_{1.85}Co_{0.15}As_2$ is more likely to be non-conventional superconductors. Due to the $3d$ orbitals of Fe atoms, $BaFe_{1.85}Co_{0.15}As_2$ has many sheets of Fermi surfaces in the normal state.

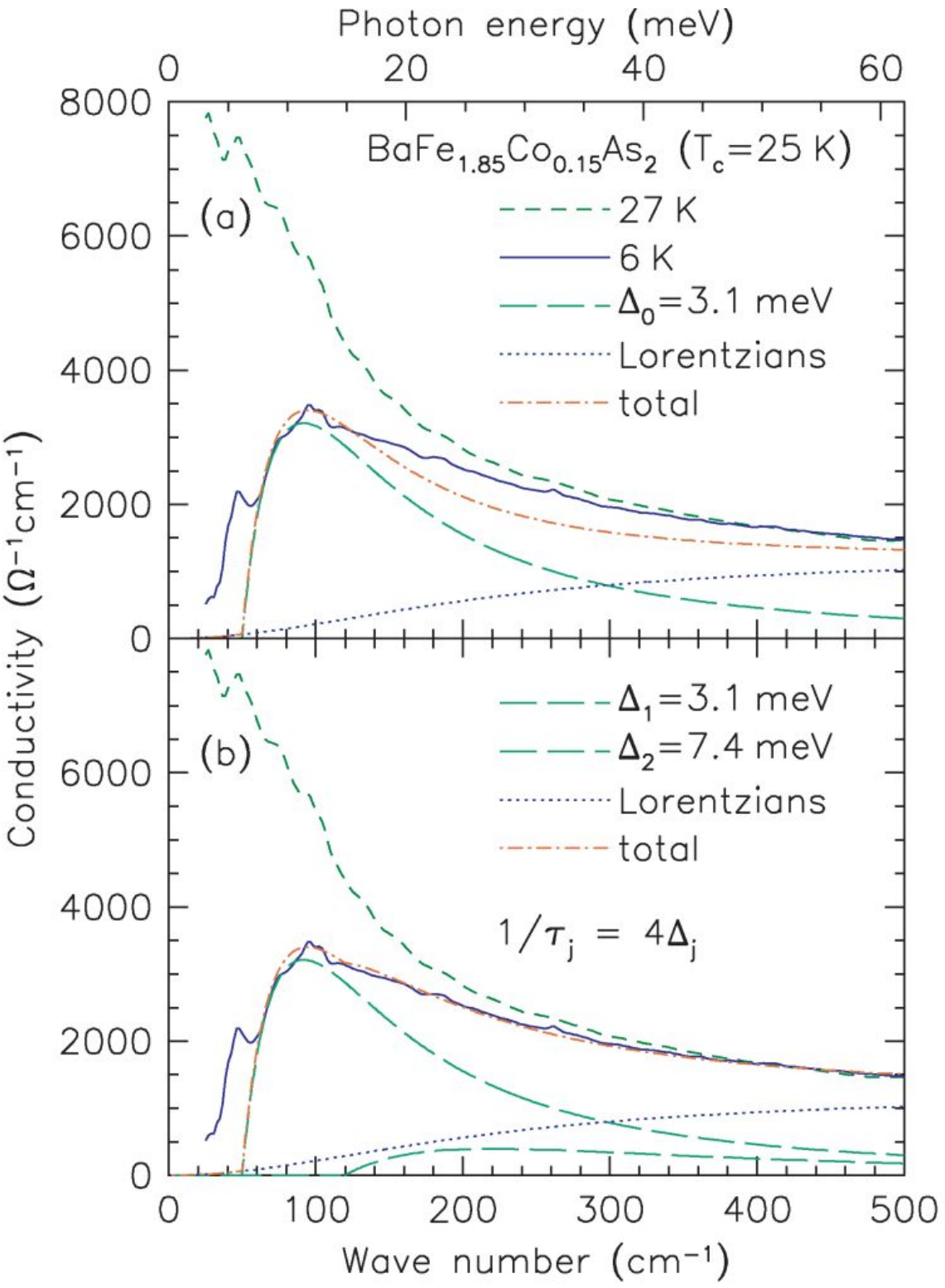

Figure 4.5 : Optical conductivity in the superconducting state. One-gap fit is presented in (a) and two-gap fit is given in (b) with $\Delta_1 = 3.1$ meV and $\Delta_2 = 7.4$ meV. Two-gap fit reproduces the experimental data, revealing the multi gap nature of pnictide superconductors.

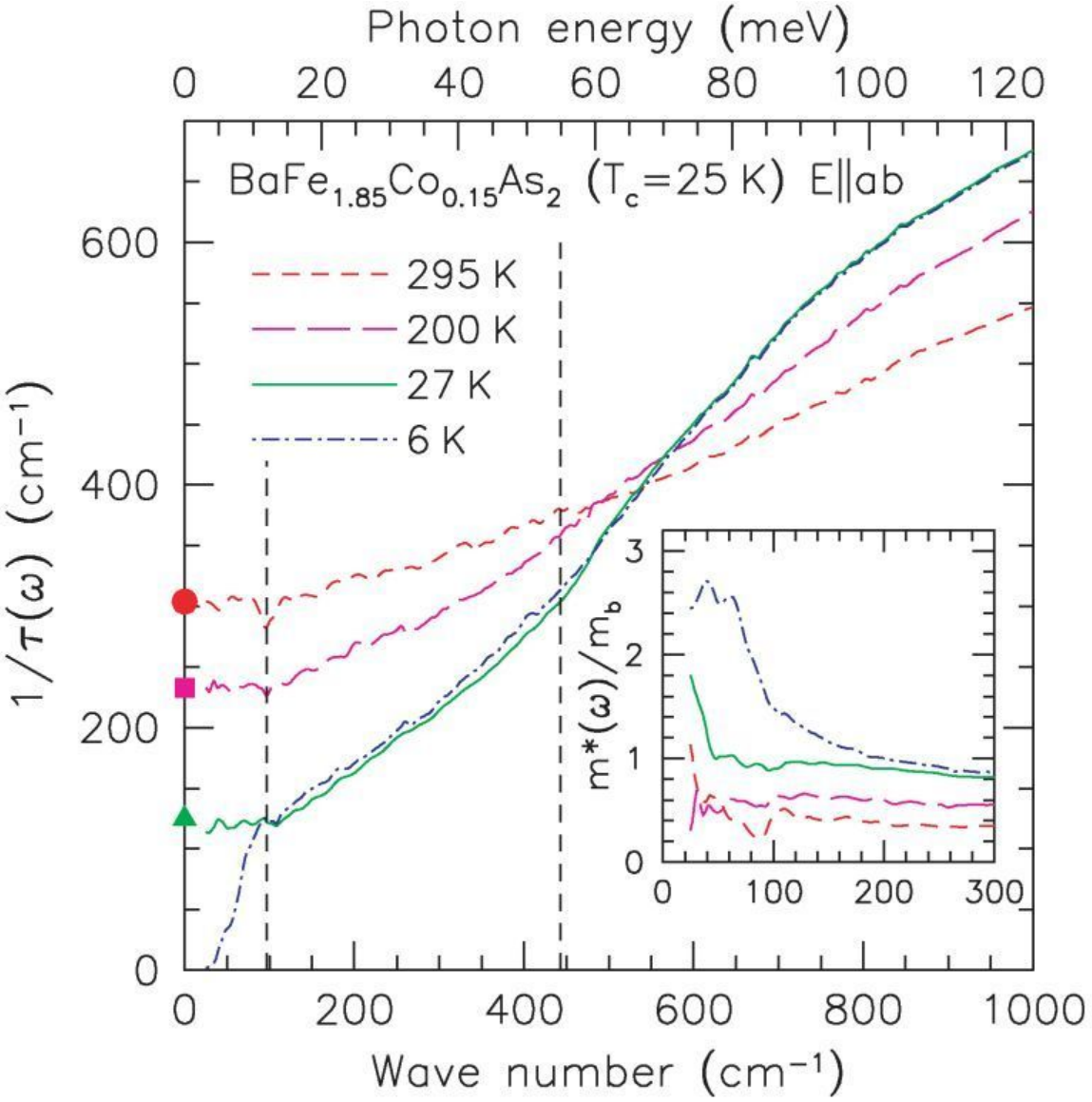

Figure 4.6 : The in-plane scattering rate as a function of frequency above and below T_c. Extrapolations of frequency dependent scattering rate $1/\tau$ agree with DC measurements. The renormalized mass is shown in the inset. The calculation, based on the *generalized Drude model*, is introduced in section 2.3.4, equation 2.61.

Below T_c, more than one superconducting gaps (3.1 meV and 7.4 meV) open at the Fermi surfaces. The ratio between one of the gap and transition temperature, $2\Delta_2/k_BT_c \simeq 7.3$, shows significant deviation from weak coupling BCS law. The normal state resistivity, when fitted with Bloch-Gruneisen formula, inform an electron phonon coupling constant that is too small to account for the large transition temperature and alternative pairing mechanisms may be needed. The Mattis-Bardeen formalism with two gaps indicates s-wave superconducting order parameter.

Chapter 5

Raman Scattering Using Vortex Light

In this chapter, we present our theoretical study of light scattering with vortex light. Based on interaction Hamiltonian, we derive Raman scattering tensors. To find a proper crystal that our proposed experiment can be tested is not an easy job. We make exhaustive study on the phonon structures in cubic crystals. After that it becomes clear that only relatively complicated crystals satisfy our experimental requirements. We choose $Bi_4Ge_3O_{12}$ crystal to carry out further analysis that two new features can be expected.

Light can carry both spin angular momentum (SAM) and orbital angular momentum (OAM) [93]. SAM determines the polarization of the beam while OAM describes its spatial profile. Light with non-zero OAM has a helical wavefront and Laguerre-Gaussian (LG) beams is one family of such light. The interaction between LG beam and small, yet macroscopic particles has been observed [94]. As suggest by many authors [95], the OAM is not only the property of the beam. Instead it is an intrinsic property of photons. This opens the possibility of spectroscopic applications. Experiments involving single photon absorption have been proposed [96, 97]. New selection rules due to non-zero OAM are presented for transitions between electronic states of a single atom. However, such proposals have not been experimentally realized. The lack of experimental confirmation may lies in the single atom absorption. Theoretical work [98] shows that the interactions between LG beam and electronic degree of free-

dom are higher order effects compared with interactions with atomic motions such as rotations or vibrations. The intensity of two photon scattering process involving atomic vibrations may be greater than single photon absorption involving electronic transitions. Therefore, we present the first study on the two photon scattering process with LG beam using group theory [99]. Group theory has the advantage that the analysis relies completely on symmetry consideration and no knowledge of the interaction is needed. The more symmetry operations there are in one system, the more powerful group theory is. We therefore confine ourselves to systems with O, T_d and O_h space groups, in the hope that most information can be extracted without dealing with the actual interaction. We also show our effort in identifing the proper crystal that the effect of vortex Raman can be tested [100].

5.1 Laguerre-Gaussian beams

Being second order differential equation, Maxwell equations have many possible solutions. Plane waves, either in vacuum or in medium, are solutions of Maxwell equations. Before the discovery of laser, Gaussian beams are only considered as a mathematical solution of the equations without physical meaning. Nowadays the Gaussian beams are well studied and there are higher orders Gaussian modes such as Hermite-Gaussian modes and Laguerre-Gaussian modes. Both higher order modes reduce to ordinary Gaussian mode when proper parameters are chosen. Usually when dealing with Gaussian beams away from the waist, the Helmholtz equations derived from Maxwell equations are simplified under the *paraxial approximation*.

The Laguerre-Gaussian modes are in the form of:

$$u(\rho,\phi,z;t) = \frac{C_{lp}^{LG}}{w(z)}\left(\frac{\rho\sqrt{2}}{w(z)}\right)^{|l|}\exp\left(-\frac{\rho^2}{w^2(z)}\right)L_p^{|l|}\left(\frac{2\rho^2}{w^2(z)}\right)\exp\left(ik\frac{\rho^2}{2R(z)}\right) \times \exp(il\phi)\exp\left[-i(2p+|l|+1)\Phi(z)\right]\exp(-i\omega t) \tag{5.1}$$

$L_p^{|l|}(x)$ are generalized Laguerre polynomials; l is the azimuthal index and sometimes referred as the "topological charge"; p is the radial index. ρ is the radial distance from the center axis of the beam; ϕ is the azimuthal angle; z is the axial distance from the waist. w_0 is the waist size; $w(z)$ is the radius at which the field amplitude drop to 1/e of their axial values. R_z is the radius of curvature of the beam's wavefronts; $\Phi(z)$ is the Gouy phase.

5.2 Raman tensor for LG beam

5.2.1 Hamiltonian for photon absorption and emission

Laguerre-Gaussian functions are a set of solutions of the Maxwell's equations in the paraxial approximation. Mathematically, LG beam is described by Laguerre polynomials with Gaussian envelope. The vector potential of LG beam in Lorentz-gauge is:

$$\mathbf{A}_{l,p} = A_0(\alpha\hat{x}+\beta\hat{y})\sqrt{\frac{2p!}{\pi(|l|+p)!}}\frac{w_0}{w(z)}L_p^{|l|}(\frac{2\rho^2}{w^2(z)})(\frac{\sqrt{2}\rho}{w(z)})^{|l|}e^{\frac{-\rho^2}{w^2(z)}+il\phi+i\frac{k_0\rho^2}{2R(z)}+i\Phi(z)-i\omega t+ikz} \tag{5.2}$$

α and β determine the polarization direction of the photon and $\alpha^2+\beta^2=1$. They are real parameters for linearly polarized light. No loss of generality, $p=0$ is chosen to simplify the analysis. Photons interact with matter through the electron-radiation coupling $\mathcal{H}_{eR} = \mathbf{A}\cdot\mathbf{p}$ term. Under dipole approximation, interaction $\mathcal{H}_{eR}$ becomes:

$$\mathcal{H}_{eR,l} = A_0(\alpha x+\beta y)\sqrt{\frac{1}{\pi|l|!}}\frac{w_0}{w(z)}L^{|l|}(\frac{2\rho^2}{w^2(z)})(\frac{\sqrt{2}\rho}{w(z)})^{|l|}e^{\frac{-\rho^2}{w^2(z)}+il\phi+i\frac{k_0\rho^2}{2R(z)}+i\Phi(z)-i\omega t}+c.c.$$

The part related to $e^{-i\omega t}$ is associated with photon absorption and it transforms according to $(\alpha x+\beta y)\rho^l e^{il\phi} \equiv (\rho\cdot\epsilon_I)\rho^l e^{il\phi}$; the complex conjugate part related to $e^{i\omega t}$ is associated with photon emission and it transforms according to $(\alpha x+\beta y)\rho^l e^{-il\phi} \equiv (\rho\cdot\epsilon_S)\rho^l e^{-il\phi}$. Notice the difference between $(\alpha x+\beta y)$ in $\mathcal{H}_{eR,l}$ and $(\alpha\hat{x}+\beta\hat{y})$ in $\mathbf{A}$.

5.2.2 Matrix element of Raman scattering

Under the third order perturbation theory the intensity of one-phonon Raman scattering is given by

$$I(\omega_1,\omega_2,\omega_0) \propto |\sum_{a,b} \frac{<f|\mathcal{H}_{eR}|a><a|\mathcal{H}_{eL}|b><b|\mathcal{H}_{eR}|i>}{(\omega_1-\omega_a)(\omega_1-\omega_b)}|^2$$

plus other time orders. $|a>$ and $|b>$ are intermediate states; $|i>$ and $|f>$ are initial and final states; $\mathcal{H}_{eR}$ and $\mathcal{H}_{eL}$ are electron-radiation interaction and electron-lattice interaction.

In ordinary Raman scattering, the interaction with matter does not change the OAM of photon: l remains zero before and after the scattering. We make the same *assumption* here that the scattering of LG beam does not change the OAM of photons. It is equivalent of saying that the topological charge of the LG beam remains the same in a scattering process. With this assumption, we can now proceed to define the Raman tensor P for the LG Raman scattering process. The first order Raman scattering intensity producing a phonon of symmetry (j,σ), is

$$I \propto C\sum_{\sigma}|\sum_{\alpha\beta\gamma\delta} k_{S\alpha}\epsilon_{S\beta}P_{\alpha\beta\gamma\delta}(\Gamma_j^{\sigma})k_{I\gamma}\epsilon_{I\delta}|^2$$

k_I and k_S are the propagating direction of the incident and scattered photons; ϵ_I and ϵ_S are the polarization direction of the incident and scattered photons. $P(\Gamma_j^{\sigma})$ is the Raman tensor.

5.2.3 Projection operator and Clebsch-Gordan coefficients

The Raman tensor $P_{\alpha\beta\gamma\delta}(\Gamma_j^\sigma)$ is determined by the Clebsch-Gordan coefficients of three representations: scattered photon $(\rho \cdot \epsilon_S)\rho^l e^{-il\phi}$, incident photon $(\rho \cdot \epsilon_I)\rho^l e^{il\phi}$ and phonon $\hat{O}(\Gamma_j^\sigma)$:

$$P_{z,\epsilon_s,\epsilon_I,z}(\Gamma_j^\sigma) = (\rho \cdot \epsilon_S)\rho^l e^{-il\phi} \otimes (\rho \cdot \epsilon_I)\rho^l e^{il\phi} \otimes \phi_\sigma^j$$

Complex conjugates come from absorption and emission part of the interaction $\mathcal{H}_{eR,l}$. For this moment only forward scattering is considered therefore the scattering geometry is $z(\epsilon_S, \epsilon_I)z$, in which case the 3 by 3 Raman tensors reduce to 2 by 2 tensors. Because of the equivalence of the (x, y, z) axis, the Raman tensors for $x(\epsilon_S, \epsilon_I)x$, $y(\epsilon_S, \epsilon_I)y$ are the same as $z(\epsilon_S, \epsilon_I)z$.

The Raman tensor analysis relies heavily on projection operators [101]. The analysis is carried out in O point group. T_d is isomorphic to O and O_h is the direct product of O and inversion group. They share the same Raman tensors with slight modification of notations. The Γ_1, Γ_2, Γ_3, Γ_4, Γ_5 representations of O point group are the Γ_1, Γ_2, Γ_3, Γ_4, Γ_5 representations of T_d point group and the Γ_{1+}, Γ_{2+}, Γ_{3+}, Γ_{4+}, Γ_{5+} representations of O_h point group. Only even representations are of interest in a Raman process.

Diagonal elements in Raman tensors are for situations in which both incident and scattered light polarize in x (or y) direction. $(x)\rho^l e^{-il\phi} \otimes (x)\rho^l e^{il\phi} = x^2(x^2+y^2)^l$ and $(y)\rho^l e^{-il\phi} \otimes (y)\rho^l e^{il\phi} = y^2(x^2+y^2)^l$. The off diagonal elements of the Raman tensor correspond to situations in which the incident photon is polarized in the x (or y) direction while the scattered photon is polarized in the y (or x) direction. $(x)\rho^l e^{-il\phi} \otimes (y)\rho^l e^{il\phi} = (y)\rho^l e^{-il\phi} \otimes (x)\rho^l e^{il\phi} = xy(x^2+y^2)^l$. Using projection operators, $x^2(x^2+y^2)^l$ and $y^2(x^2+y^2)^l$ can be decomposed into summation of basis functions

that transform according to one irreducible representation: $x^2(x^2+y^2)^l = \phi_1^1 + \phi_2^1 + \phi_3^{1,\gamma_1} + \phi_3^{2,\gamma_2}$ and $y^2(x^2+y^2)^l = \phi_1^1 - \phi_2^1 + \phi_3^{1,\gamma_1} - \phi_3^{2,\gamma_2}$. Each term in the expansion are defined by the following:

$$\begin{aligned}
\phi_1^1 &\equiv \frac{1}{6}[(x^2+y^2)^{l+1} + (y^2+z^2)^{l+1} + (z^2+x^2)^{l+1}]; \\
\phi_2^1 &\equiv \frac{1}{6}[(x^2-y^2)(x^2+y^2)^l + (y^2-z^2)(y^2+z^2)^l + (z^2-x^2)(z^2+x^2)^l]; \\
\phi_3^{1,\gamma_1} &\equiv \frac{1}{3}[(x^2+y^2)^{l+1} - \frac{1}{2}(y^2+z^2)^{l+1} - \frac{1}{2}(z^2+x^2)^{l+1}]; \\
\phi_3^{2,\gamma_2} &\equiv \frac{1}{3}[(x^2-y^2)(x^2+y^2)^l - \frac{1}{2}(y^2-z^2)(y^2+z^2)^l - \frac{1}{2}(z^2-x^2)(z^2+x^2)^l].
\end{aligned}$$

Apply the same method, it is shown that $xy(x^2+y^2)^l$ contains only Γ_5^3 part of the irreducible representation:

$$\phi_5^3 = xy(x^2+y^2)^l$$

One subtlety lies in the ϕ_3^{1,γ_2} and ϕ_3^{2,γ_1} functions. It can be shown that $\gamma_1 \neq \gamma_2$ for any $l \geq 1$. In other words, the two Γ_3^1 and Γ_3^2 functions contained in $x^2(x^2+y^2)^l$ and $y^2(x^2+y^2)^l$ belong to two inequivalent sets of Γ_3 representations except for $l = 0$. An intuitive example is the C_{3v} point group, where (x, y) and (xz, yz) are two inequivalent sets of basis functions for the E representation. x is connected with y and xz is connected with yz. But x can not be connected with xz or yz by symmetry. The result of $\gamma_1 \neq \gamma_2$ is that the two Raman tensors for Γ_3 phonon have different coupling coefficients (see table 5.1). It is in contrast with the $l = 0$ case where same coupling constant b is shared by the two Raman tensors for Γ_3 phonon.

Another point to be mentioned is $\phi_2^1 = \frac{1}{6}[(x^2-y^2)(x^2+y^2)^l + (y^2-z^2)(y^2+z^2)^l + (z^2-x^2)(z^2+x^2)^l]$. It becomes zero for $l = 0$ and 1. It is to say that the Raman tensors for Γ_2 phonon exist for only $l \geq 2$.

OAM	Γ_1^1	Γ_2^1	Γ_3^1	Γ_3^2	$\Gamma_4^{1,2,3,}$	$\Gamma_5^{1,2}$	Γ_5^3
$l=0$	$\begin{pmatrix} a & 0 \\ 0 & a \end{pmatrix}$	$\begin{pmatrix} 0 & 0 \\ 0 & 0 \end{pmatrix}$	$\begin{pmatrix} b & 0 \\ 0 & b \end{pmatrix}$	$\begin{pmatrix} -\sqrt{3}b & 0 \\ 0 & \sqrt{3}b \end{pmatrix}$	$\begin{pmatrix} 0 & 0 \\ 0 & 0 \end{pmatrix}$	$\begin{pmatrix} 0 & 0 \\ 0 & 0 \end{pmatrix}$	$\begin{pmatrix} 0 & c \\ c & 0 \end{pmatrix}$
$l=1$	$\begin{pmatrix} a & 0 \\ 0 & a \end{pmatrix}$	$\begin{pmatrix} 0 & 0 \\ 0 & 0 \end{pmatrix}$	$\begin{pmatrix} c & 0 \\ 0 & c \end{pmatrix}$	$\begin{pmatrix} -d & 0 \\ 0 & d \end{pmatrix}$	$\begin{pmatrix} 0 & 0 \\ 0 & 0 \end{pmatrix}$	$\begin{pmatrix} 0 & 0 \\ 0 & 0 \end{pmatrix}$	$\begin{pmatrix} 0 & e \\ e & 0 \end{pmatrix}$
$l \geq 2$	$\begin{pmatrix} a & 0 \\ 0 & a \end{pmatrix}$	$\begin{pmatrix} b & 0 \\ 0 & -b \end{pmatrix}$	$\begin{pmatrix} c & 0 \\ 0 & c \end{pmatrix}$	$\begin{pmatrix} -d & 0 \\ 0 & d \end{pmatrix}$	$\begin{pmatrix} 0 & 0 \\ 0 & 0 \end{pmatrix}$	$\begin{pmatrix} 0 & 0 \\ 0 & 0 \end{pmatrix}$	$\begin{pmatrix} 0 & e \\ e & 0 \end{pmatrix}$

Table 5.1 : Raman tensors $P_{z,\epsilon_s,\epsilon_I,z}(\Gamma_j^\sigma)$ for the σth branch of the Γ_j phonon mode in forward scattering geometry using Laguerre-Gaussian beam for crystals with O, T_d and O_h space groups symmetry.

5.2.4 Raman tensors

The Raman tensor are tabulated in Table 5.1 [99]. Quite surprisingly, the Raman tensors for $l \geq 2$ excitations have the same form therefore no difference would l make from symmetry point of view for $l \geq 2$. The constants a, b, c, d, e are of course different for different values of l therefore intensities vary. Compared with $l = 0$ ordinary Raman process, non-zero OAM brings new features: the appearence of the Γ_2 phonon for $l \geq 2$ photon excitation and the decoupling of the two Raman tensors for the Γ_3 phonon for $l \geq 1$ excitation. The next section will be devoted to setting up experiments for the realization of those new features. We also want to mention that Raman tensors for Γ_4 phonon do not nessisarily vanish. It is zero because of the forward scattering geometry. Γ_4 may be active under different polarization orientations such as right angle scattering.

5.3 $\Gamma_{2(+)}$ and $\Gamma_{3(+)}$ phonon modes in cubic crystal

Many well known crystals in O_h space group, such as silicon and perovskite, do not have Γ_{2+} phonons. A careful examination of those crystals shows that not only Γ_{2+}, but also all the one (Γ_{1+}, Γ_{2+}, Γ_{1-}, Γ_{2-}) and two (Γ_{3+}, Γ_3^-) dimensional phonons rarely happen while three dimensional phonons (Γ_{4+}, Γ_{5+}, Γ_{4-}, Γ_{5-}) always present. Instead of checking phonon structures of available crystals one by one, we perform a systematic study on the zone center phonon structures of O_h space groups. All one dimensional phonons are listed for different Wyckoff positions of the ten O_h space groups. Analysis shows that at least four inequivalent atoms in one set of Wyckoff positions are required to have one dimensional phonons. This explains the absence of the Γ_{2+} phonons in NaCl, diamond and other crystals with simple structures. The results are tabulated and, with the help of our tables, one can choose proper crystals when a certain one or two dimensional phonon is needed. The fact that crystals belonging to O_h space groups are the most common ones [102] makes this study useful.

5.3.1 Theoretical background

O_h space groups are space groups with O_h point group. They are O_h^1 ($Pm3m$), O_h^2 ($Pn3n$), O_h^3 ($Pm3n$), O_h^4 ($Pn3m$), O_h^5 ($Fm3m$), O_h^6 ($Fm3c$), O_h^7 ($Fd3m$), O_h^8 ($Fd3c$), O_h^9 ($Im3m$) and O_h^{10} ($Ia3d$). In those space groups, 48 rotational operations are associated with simple cubic, face-centered-cubic or body-centered-cubic lattices. The general form of a symmetry operation is $\{\hat{g}|\mathbf{R_L} + \tau_\mathbf{g}\}$: $\hat{g}$ is the rotational operation, $\mathbf{R_L}$ is the lattice translation. $\tau_\mathbf{g}$ is 0 for symmorphic space groups and some fractional translation(s) for nonsymmorphic space groups.

We now proceed to determine the phonon modes. Let γ denote any of the one

	E	$8C_3$	$3C_2$	$6C_4$	$6C_2$	I	$8S_6$	$3\sigma_h$	$3S_4$	$6\sigma_d$	$\otimes\ \Gamma_4^-$
Γ_1^+	1	1	1	1	1	1	1	1	1	1	Γ_4^-
Γ_2^+	1	1	1	-1	-1	1	1	1	-1	-1	Γ_5^-
Γ_3^+	2	-1	2	0	0	2	-1	2	0	0	$\Gamma_4^- + \Gamma_5^-$
Γ_4^+	3	0	-1	1	-1	3	0	-1	1	-1	$\Gamma_1^-+\Gamma_3^-+\Gamma_4^-+\Gamma_5^-$
Γ_5^+	3	0	-1	-1	1	3	0	-1	-1	1	$\Gamma_2^-+\Gamma_3^-+\Gamma_4^-+\Gamma_5^-$
Γ_1^-	1	1	1	1	1	-1	-1	-1	-1	-1	Γ_4^+
Γ_2^-	1	1	1	-1	-1	-1	-1	-1	1	1	Γ_5^+
Γ_3^-	2	-1	2	0	0	-2	1	-2	0	0	$\Gamma_4^+ + \Gamma_5^+$
Γ_4^-	3	0	-1	1	-1	-3	0	1	-1	1	$\Gamma_1^++\Gamma_3^++\Gamma_4^++\Gamma_5^+$
Γ_5^-	3	0	-1	-1	1	-3	0	1	1	-1	$\Gamma_2^++\Gamma_3^++\Gamma_4^++\Gamma_5^+$

Table 5.2 : The character table of O_h point group and the direct product of Γ_{4-} with all representations of O_h point group.

dimensional phonons ($\Gamma_1^+, \Gamma_2^+, \Gamma_1^-, \Gamma_2^-$). γ is carried by a set of n atoms labelled by their Wyckoff positions, such as $12(e)$ in O_h^2. Among the 48 rotational operations, $48/n$ of them, denoted by $\{\hat{\alpha}|\tau_\alpha\}$, do not move the atom or move the atom to its equvalent position: $\{\hat{\alpha}|\tau_\alpha\}\mathbf{r_i} = \mathbf{r_j}$ and $\mathbf{r_j} = \mathbf{r_i} + \mathbf{R_L}$ where$\mathbf{r_i}$ is the position of the original atom and $\mathbf{R_L}$ is any lattice vector; the rest $(48 - 48/n)$ operations, denoted by $\{\hat{\beta}|\tau_\beta\}$, would shift the original atom to its inequivalent positions: $\{\hat{\beta}|\tau_\beta\}\mathbf{r_i} = \mathbf{r_j}$ and $\mathbf{r_j} \neq \mathbf{r_i} + \mathbf{R_L}$. If a set of n atoms carry γ phonon, the atomic displacement vector $\mathbf{V}$ at atom $\mathbf{r_i}$ must satisfy: $\hat{g} \cdot \mathbf{V} = \chi^\gamma(\hat{\mathbf{g}}) \cdot \mathbf{V}$, where $\hat{g}$ is any of the 48 rotational operations. In general, $\mathbf{V}$ is in the form of (v_x, v_y, v_z) and any solution of $\mathbf{V} = (\mathbf{v_x}, \mathbf{v_y}, \mathbf{v_z})$ gives the allowed phonon mode. With the definition of $\hat{\alpha}$ the set of 48 equations can be simplified: $\hat{\alpha} \cdot \mathbf{V} = \chi^\gamma(\hat{\alpha}) \cdot \mathbf{V}$, which reduce the number of equations down to $48/n$. That is, only operations that shift the atom to itself or

its equivalent positions need to be considered. The existence of solutions for **V** is necessary and sufficient for the existence of one dimensional phonons.

5.3.2 Results

All Wyckoff positions in O_h space groups are considered in this section [100]. When dealing with phonons, the primitive cell is more suitable than the unit cell. Therefore, a slightly different notation is adopted, compared to the *International Table for Crystallography* [10]: although the letters of Wyckoff positions remain the same, we put down the number of atoms in one primitive cell instead of one unit cell. For example, in O_h^{10}, $48(h)$ in this note is the $96(h)$ in the *International Table for Crystallography*. Directions of phonon modes for (Γ_1^+, Γ_2^+, Γ_1^-, Γ_2^-) phonons are listed in below.

Table 5.3 : Possible one dimensional phonon modes in O_h space groups at different Wyckoff positions. Those without entity are Wyckoff positions that the one dimensional phonon cannot exist.

Wyckoff positions	Γ_{1+}	Γ_{2+}	Γ_{1-}	Γ_{2-}
O_h^1				
48, (n), (x, y, z)	(x, y, z)	(x, y, z)	(x, y, z)	(x, y, z)
24, (m), (x, x, z)	(x, x, z)	(x, -x, 0)	(x, -x, 0)	(x, x, z)
24, (l), (1/2, y, z)	(0, y, z)	(0, y, z)	(x, 0, 0)	(x, 0, 0)
24, (k), (0, y, z)	(0, y, z)	(0, y, z)	(x, 0, 0)	(x, 0, 0)
12, (j), (1/2, y, y)	(0, y, y)	(0, y, -y)		(x, 0, 0)
12, (i), (0, y, y)	(0, y, y)	(0, y, -y)		(x, 0, 0)
12, (h), (x, 1/2, 0)	(x, 0, 0)	(x, 0, 0)		
8, (g), (x, x, x)	(x, x, x)			(x, x, x)

6, (f), (x, 1/2, 1/2)	(x, 0, 0)			
6, (e), (x, 0, 0)	(x, 0, 0)			
3, (d), (1/2, 0, 0)				
3, (c), (0, 1/2, 1/2)				
1, (b), (1/2, 1/2, 1/2)				
1, (a), (0, 0, 0)				

O_h^2

48, (i), (x, y, z)	(x, y, z)	(x, y, z)	(x, y, z)	(x, y, z)
24, (h), (0, y, y)	(0, y, y)	(x, y, -y)	(0, y, y)	(x, y, -y)
24, (g), (x, 0, 1/2)	(x, 0, 0)	(x, 0, 0)	(x, 0, 0)	(x, 0, 0)
16, (f), (x, x, x)	(x, x, x)	(x, x, x)	(x, x, x)	(x, x, x)
12, (e), (x, 0, 0)	(x, 0, 0)		(x, 0, 0)	
12, (d), (1/4, 0, 1/2)		(x, 0, 0)		(x, 0, 0)
8, (c), (1/4, 1/4, 1/4)			(x, x, x)	(x, x, x)
6, (b), (0, 1/2, 1/2)				
2, (a), (0, 0, 0)				

O_h^3

48, (l), (x, y, z)	(x, y, z)	(x, y, z)	(x, y, z)	(x, y, z)
24, (k), (0, y, z)	(0, y, z)	(0, y, z)	(x, 0, 0)	(x, 0, 0)
24, (j), (1/4, y, y+1/2)	(0, y, y)	(x, y, -y)	(0, y, y)	(x, y, -y)
16, (i), (x, x, x)	(x, x, x)	(x, x, x)	(x, x, x)	(x, x, x)
12, (h), (x, 1/2, 0)	(x, 0, 0)	(x, 0, 0)		
12, (g), (x, 0, 1/2)	(x, 0, 0)	(x, 0, 0)		
12, (f), (x, 0, 0)	(x, 0, 0)	(x, 0, 0)		

8, (e), (1/2, 1/2, 1/2)		(x, x, x)		(x, x, x)
6, (d), (1/4, 1/2, 0)		(x, 0, 0)		
6, (c), (1/4, 0, 1/2)		(x, 0, 0)		
6, (b), (0, 1/2, 1/2)				
2, (a), (0, 0, 0)				

O_h^4

48, (l), (x, y, z)	(x, y, z)	(x, y, z)	(x, y, z)	(x, y, z)
24, (k), (x, x, z)	(x, x, z)	(x, -x, 0)	(x, -x, 0)	(x, x, z)
24, (j), (1/4, y, y+1/2)	(0, y, y)	(x, y, -y)	(0, y, y)	(x, y, -y)
24, (i), (1/4, y, -y+1/2)	(0, y, -y)	(x, y, y)	(0, y, -y)	(x, y, y)
24, (h), (x, 0, 1/2)	(x, 0, 0)	(x, 0, 0)	(x, 0, 0)	(x, 0, 0)
12, (g), (x, 0, 0)	(x, 0, 0)			(x, 0, 0)
12, (f), (1/4, 0, 1/2)		(x, 0, 0)		(x, 0, 0)
8, (e), (x, x, x)	(x, x, x)			(x, x, x)
6, (d), (0, 1/2, 1/2)				
4, (c), (3/4, 3/4, 3/4)				(x, x, x)
4, (b), (1/4, 1/4, 1/4)				(x, x, x)
2, (a), (0, 0, 0)				

O_h^5

48, (l), (x, y, z)	(x, y, z)	(x, y, z)	(x, y, z)	(x, y, z)
24, (k), (x, x, z)	(x, x, z)	(x, -x, 0)	(x, -x, 0)	(x, x, z)
24, (j), (0, y, z)	(0, y, z)	(0, y, z)	(x, 0, 0)	(x, 0, 0)
12, (i), (1/2, y, y)	(0, y, y)	(0, y, -y)		(x, 0, 0)
12, (h), (0, y, y)	(0, y, y)	(0, y, -y)		(x, 0, 0)

12, (g), (x, 1/4, 1/4)	(x, 0, 0)			(x, 0, 0)
8, (f), (x, x, x)	(x, x, x)			(x, x, x)
6, (e), (x, 0, 0)	(x, 0, 0)			
6, (d), (0, 1/4, 1/4)				(x, 0, 0)
2, (c), (1/4, 1/4, 1/4)				
1, (b), (1/2, 1/2, 1/2)				
1, (a), (0, 0, 0)				

O_h^6

48, (j), (x, y, z)	(x, y, z)	(x, y, z)	(x, y, z)	(x, y, z)
24, (i), (0, y, z)	(0, y, z)	(0, y, y)	(x, 0, 0)	(x, 0, 0)
24, (h), (1/4, y, y)	(0, y, y)	(x, y, -y)	(0, y, y)	(x, y, -y)
16, (g), (x, x, x)	(x, x, x)	(x, x, x)	(x, x, x)	(x, x, x)
12, (f), (x, 1/4, 1/4)	(x, 0, 0)	(x, 0, 0)		
12, (e), (x, 0, 0)	(x, 0, 0)	(x, 0, 0)		
6, (d), (0, 1/4, 1/4)			(x, 0, 0)	
6, (c), (1/4, 0, 0)		(x, 0, 0)		
2, (b), (0, 0, 0)				
2, (a), (1/4, 1/4, 1/4)				

O_h^7

48, (i), (x, y, z)	(x, y, z)	(x, y, z)	(x, y, z)	(x, y, z)
24, (h), (1/8, y, -y+1/4)	(0, y, -y)	(x, y, y)	(0, y, -y)	(x, y, y)
24, (g), (x, x, z)	(x, x, z)	(x, -x, 0)	(x, -x, 0)	(x, x, z)
12, (f), (x, 0, 0)	(x, 0, 0)			(x, 0, 0)
8, (e), (x, x, x)	(x, x, x)			(x, x, x)

4, (d), (5/8, 5/8, 5/8)				(x, x, x)
4, (c), (1/8, 1/8, 1/8)				(x, x, x)
2, (b), (1/2, 1/2, 1/2)				
2, (a), (0, 0, 0)				

O_h^8

48, (h), (x, y, z)	(x, y, z)	(x, y, z)	(x, y, z)	(x, y, z)
24, (g), (1/8, y, -y+1/4)	(0, y, -y)	(x, y, y)	(0, y, -y)	(x, y, y)
24, (f), (x, 0, 0)	(x, 0, 0)	(x, 0, 0)	(x, 0, 0)	(x, 0, 0)
16, (e), (x, x, x)	(x, x, x)	(x, x, x)	(x, x, x)	(x, x, x)
12, (d), (1/4, 0, 0)		(x, 0, 0)	(x, 0, 0)	
8, (c), (3/8, 3/8, 3/8)			(x, x, x)	(x, x, x)
8, (b), (1/8, 1/8, 1/8)		(x, x, x)		(x, x, x)
4, (a), (0, 0, 0)				

O_h^9

48, (l), (x, y, z)	(x, y, z)	(x, y, z)	(x, y, z)	(x, y, z)
24, (k), (x, x, z)	(x, x, z)	(x, -x, 0)	(x, -x, 0)	(x, x, z)
24, (j), (0, y, z)	(0, y, z)	(0, y, y)	(x, 0, 0)	(x, 0, 0)
24, (i), (1/4, y, -y+1/2)	(0, y, -y)	(x, y, y)	(0, y, -y)	(x, y, y)
12, (h), (0, y, y)	(0, y, y)	(0, y, -y)		(x, 0, 0)
12, (g), (x, 0, 1/2)	(x, 0, 0)	(x, 0, 0)		
8, (f), (x, x, x)	(x, x, x)			(x, x, x)
6, (e), (x, 0, 0)	(x, 0, 0)			
6, (d), (1/4, 0, 1/2)		(x, 0, 0)		
4, (c), (1/4, 1/4, 1/4)				(x, x, x)

3, (b), (0, 1/2, 1/2)				
1, (a), (0, 0, 0)				

O_h^{10}

48, (h), (x, y, z)	(x, y, z)	(x, y, z)	(x, y, z)	(x, y, z)
24, (g), (1/8, y, -y+1/4)	(0, y, -y)	(x, y, y)	(0, y, -y)	(x, y, y)
24, (f), (x, 0, 1/4)	(x, 0, 0)	(x, 0, 0)	(x, 0, 0)	(x, 0, 0)
16, (e), (x, x, x)	(x, x, x)	(x, x, x)	(x, x, x)	(x, x, x)
12, (d), (3/8, 0, 1/4)		(x, 0, 0)	(x, 0, 0)	
12, (c), (1/8, 0, 1/4)		(x, 0, 0)		(x, 0, 0)
8, (b), (1/8, 1/8, 1/8)		(x, x, x)		(x, x, x)
8, (a), (0, 0, 0)			(x, x, x)	(x, x, x)

The meaning of the notations are as follows: for a certain phonon mode belonging to a set of atoms, the number of free parameters in the phonon modes is the number of its appearances. For example, in O_h^{10}, Γ_2^+ phonon of Wyckoff position 24(g) $(1/8, y, -y + 1/4)$ is labelled (x, y, y). It means that Γ_2^+ phonon modes appear twice and the Γ_2^+ phonon modes on atom $(1/8, y, -y+1/4)$ are in the (1, 0, 0) direction and (0, 1, 1) direction. The actual atomic displacements are the linear combinations of the two phonon modes, the coefficients of which cannot be determined by symmetry alone. It is worth mentioning that the number of Γ_1^+ phonons equals the number of free parameters of the Wyckoff positions because totally symmetric distortions preserve the symmetry. For example, Wyckoff position 24(g) $(1/8, y, -y + 1/4)$ in O_h^{10} has only one Γ_1^+ phonon mode which is in the (0, 1, -1) direction. Also one can see

that any one dimensional phonon does not happen more than three times in one set of Wyckoff positions.

5.3.3 Two and three dimensional phonons

Additional informations about two and three dimensional phonons can also be obtained from the analysis on one dimensional phonons. In general, the phonon structure is determined by the decomposition of mechanical representation, which is the direct product of permutation group and the vector representation [11]. Permutation group is a group formed by taking atomic positions as basis functions. Its character under a certain symmetry operation equals the number of atoms unchanged or can be shifted back to itself by lattice vector. The vector representation is formed with basis functions (x, y, z) and it belongs to Γ_4^- in O_h space groups. The direct products of Γ_4^- with different representations are given in table 5.2.

Careful inspection of the tables shows many interesting results. There will always be three dimensional phonons, no matter how simple the structure is. Each one dimensional phonon is accompanied by one two dimensional phonon and two three dimensional phonons. This makes a restriction on the number of appearances of one dimensional phonons: $n \times 3 \geq \sum_\gamma m \times 9$, where n is the number of atoms in one set of Wyckoff position, and m is number of one dimensional phonons. Summation over γ means summation over all the one dimensional phonons.

The character of the permutation group must be non-negative. One dimensional phonons correspond to Γ_4^+, Γ_5^+, Γ_4^-, Γ_5^- in the permutation representation and they all have negative characters under C_2 symmetry operation (see table 5.2). Other one or two dimensional representations which have positive characters under C_2 operation must present in the permutation representation. It makes further restrictions on the

number of appearances of one dimensional phonons:

$$n \times 3 \geq \sum_{\gamma} m \times 12 \tag{5.4}$$

This means that at least four atoms are needed to carry a single one dimensional phonon, and this rule is indeed observed in all ten O_h space groups. The difference between $\sum_{\gamma} m \times 12$ and $m \times 3$ will be totally filled by three dimensional phonons.

5.3.4 Cubic lattice system

The same argument can be applied to other cubic lattice systems: T, T_h, T_d and O. The direct product tables of those point groups [8] show that any one dimensional phonon is accompanied by one two dimensional phonon and two three dimensional phonons, giving a total dimension of 9. Those 9 dimensional phonons correspond to one three dimensional representation in the permutation representation, and all three dimensional representations have negative characters under one set of C_2 operations (there are two sets of C_2 operations in O and O_h). Permutation representation must have non-negative characters, therefore other one or two dimensional representations with positive characters under C_2 must present. This makes the restriction for T, T_h, T_d, O and O_h space groups: $n \times 3 \geq \sum_{\gamma} m \times 12$ and the summation over γ is the summation over all one dimensional phonons in T, T_h, T_d, O and O_h space groups. It should be noticed that, for T and T_h, the two dimensional representation is actually two one dimensional representations forced to stick together due to time reversal symmetry.

The same analysis on one dimensional phonons in O_h space groups can be extended to T, T_h, T_d and O space groups. However, due to limitation of space, they are not tabulated.

5.3.5 Magnons for magnetic space groups with cubic unitary group

Without external magnetic field, time reversal operator θ is also a symmetry operation of the system. The inclusion of time reversal operator generates magnetic space group **M** which contains equal number of unitary and antiunitary elements: $\mathbf{M} = \mathbf{H} + \mathbf{AH}$. **H** is ordinary space group and **A** is antiunitary coset representative. The magnon symmetry is characterized within space group **H** [19]. Representations of magnons are contained in the direct product of permutation group and the "pseudo vector representation" (R_x, R_y, R_z).

For those magnetic space groups with **H** being one of the cubic space groups (#195 – #230), we find that the same analysis on phonons can also be applied. "Pseudo vector" belongs to one of the three dimensional representations in T, T_h, T_d, O and O_h point groups and any one or two dimensional representations must be contained in the direct product of "pseudo vector group" and a three dimensional representation of the permutation group. As for phonons, these three dimensional representations have negative character under C_2 operation therefore some one or two dimensional representations must present in the permutation group whose characters must be non-negative. This leads to the same restrictions that at least four atoms are needed to have one or two dimensional magnons if the unitary group **H** of the magnetic space group **M** belongs to cubic space groups (#195 – #230).

Compared with lattice systems of lower symmetry, the cubic system is peculiar in that the vector representation (x, y, z) belongs to a single three dimensional representation. This is the reason that one and two dimensional phonons happen rarely in crystals with cubic lattice. We have shown that some one dimensional phonons require as many as 24 atoms. Usually one does not go to such complicated structures before trying simpler ones. On the other hand, although any set of Wyckoff

positions with 48 inequivalent atoms, say, $48(h)$ of O_h^{10} space group, gives all one dimensional phonons ($\Gamma_1^{\pm}$, $\Gamma_2^{\pm}$), simpler crystal structures are better in that less phonon modes leads to larger separations in energy and resolution is always an issue in spectroscopy experiments. The number of one dimensional phonons equals the number of two dimensional phonons therefore the searching for two dimensional phonon modes is as difficult as the searching for one dimensional phonon modes. This is also the case for magnetic space groups with cubic unitary groups. Following our tables, one can choose the crystal that is complicated enough to have the required (one or two dimensional) phonon mode, yet keeps the structure as simple as possible.

In this section, four rules are obtained for phonon structure in T, T_h, T_d, O and O_h space groups and for magnon structure with magnetic space groups whose unitary space part belongs to T, T_h, T_d, O and O_h space groups [100]:

1. At least four inequivalent atoms are needed to produce one dimensional phonon (magnon).

2. The number of one dimensional phonons (magnons) equals the number of two dimensional phonons (magnons) therefore at least four inequivalent atoms are needed to produce two dimensional phonons (magnons).

3. Three dimensional phonons (magnons) always exist, no matter how simple the crystal is.

4. A restriction rule is obtained: $n \times 3 \geq \sum_\gamma m \times 12$, n being the number of atoms in one Wyckoff set and m the number of one dimensional phonons (magnons).

5.4 Bithmuth germanate($Bi_4Ge_3O_{12}$) crystal

Bithmuth germanate $Bi_4Ge_3O_{12}$ is one of the cubic crystals that have Γ_2 and Γ_3 phonons. It belongs to space group $I\bar{4}2d$ (T_d^6). The phonon modes are $4\Gamma_1+5\Gamma_2+9\Gamma_3+14\Gamma_4+15\Gamma_5$ [103]. Γ_1, Γ_3 and Γ_5 are Raman active and Γ_5 is also IR active. Interaction with crystal fields splits the IR active Γ_5 phonon into LO and TO phonons [34]. $Bi_4Ge_3O_{12}$ is transparent therefore the experiment can be done in forward scattering geometry. Pure $Bi_4Ge_3O_{12}$ is not fluoresence. Moderate photorefractive effect is observed in the UV range [104] therefore non-linear effect can be ignored for pure $Bi_4Ge_3O_{12}$ with visuable light excitation. Based on those reasons, pure $Bi_4Ge_3O_{12}$ single crystal is suitable for LG Raman experiment. Only part of phonon frequencies can be found [105]. For those phonons, symmetry assignment can be done using polarization dependence of the cross section, although the splitting of polar phonons must be handled with care.

Based on the Raman tensors, two effects are expected for LG Raman [99]. The appearence of the Γ_2 phonon modes and the change in polarization dependence of the cross section for the Γ_3 phonon.

5.4.1 Additional Γ_2 phonon mode

"Additional" means that although this phonon mode exists in the crystal regardless of experimental technique, it is silent in ordinary Raman process, and becomes active in Raman scattering with LG beam. Compared with $l = 0$, Γ_2 phonon is active for photons with $l \geq 2$ OAM. The Raman tensors for Γ_2 phonon are diagonal. This mode is observed as long as the incident polarization and scattered polarization are not perpendicular. Highest intensity is expected when the incident photons and scattered photons are polarized in the same direction.

5.4.2 Change of cross section dependence on polarization geometry for Γ_3 phonon

Γ_3 phonon is active in both ordinary Raman ($l = 0$) and LG Raman ($l \geq 1$). The Raman tensors for Γ_3 have similar forms except for that in $l = 0$ case two Raman tensors share the same coupling constant b and for $l \geq 1$ the two Raman tensors have two different coupling constants c and d. The two Raman tensors for γ_3 phonon are no longer connected by symmetry when LG beam is used. This leads to different cross section dependence on polarization orientations. The scattering cross section for Γ_3 phonon is $I(\Gamma_3) = [\epsilon_S \cdot P(\Gamma_3^1) \cdot \epsilon_I]^2 + [\epsilon_S \cdot P(\Gamma_3^2) \cdot \epsilon_I]^2$. Consider a special scattering geometry where the incident light is polarized in the $\epsilon_I = \frac{1}{\sqrt{2}}\hat{x} + \frac{1}{\sqrt{2}}\hat{y}$ direction and the scattered light is polarized in the $\epsilon_S = \cos\theta\hat{x} + \sin\theta\hat{y}$ direction. The Raman intensity for ordinary light is now

$$I_{l=0}(\Gamma_3) = 2b^2(1 - \cos\theta\sin\theta)$$

and the Raman intensity for LG beam is

$$I_{l\geq 1}(\Gamma_3) = \frac{c^2 + d^2}{2} + (c^2 - d^2)\cos\theta\sin\theta.$$

The intensity plots for $I_{l=0}(\Gamma_3)$ and $I_{l\geq 1}(\Gamma_3)$ are given in Figure 5.1a and 5.1b. The plots are in arbitrary units and a special value of $c = \sqrt{3}d$ is used for figure 5.1b. A clear difference in angular dependence of intensity on polarization is seen. Other ratios of c and d have less dramatic effect but in general the angular distribution of intensity has different patterns unless accidentally $d = \pm\sqrt{3}c$.

Figure 5.1 : Angular dependence of Raman scattering intensity for (a) ordinary Raman process and (b) LG Raman process with incident light polarized in the $(1/\sqrt{2})\hat{x} + (1/\sqrt{2})\hat{y}$ direction. The intensity is in arbitrary units. A special value of $c = \sqrt{3}d$ is used for (b).

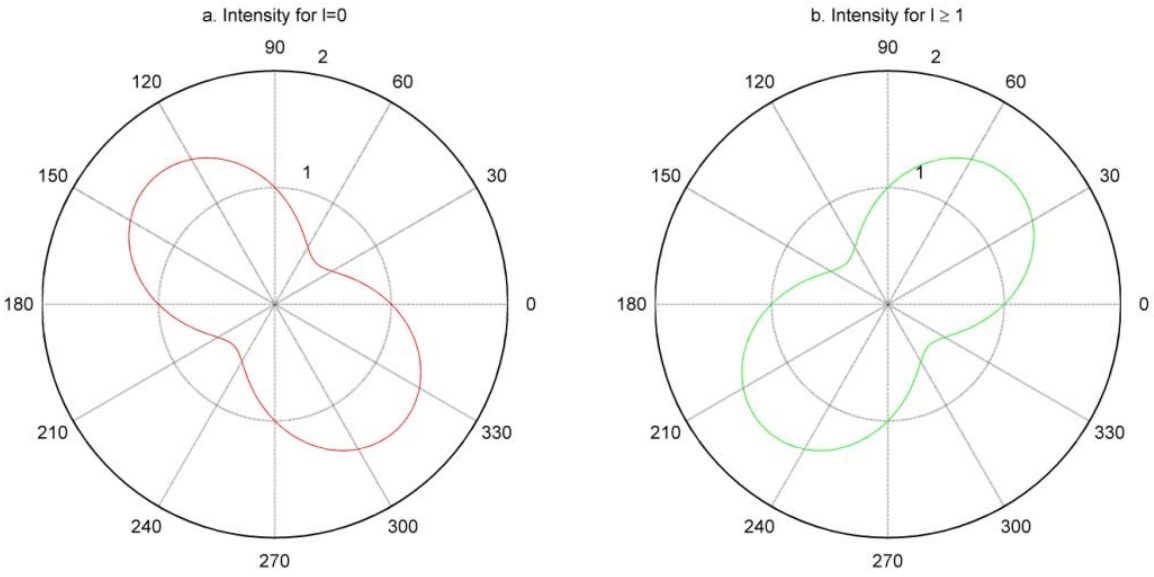

Chapter 6

Conclusions and Future Directions

6.1 Iron-based superconductor

The ultimate goal of superconductivity research is the realization of room temperature superconductor. To achieve that goal, a deep understanding of High-Temperature superconductivity (HTSC) is needed. The first family of HTSC was the cuprates [48]. The fact that the transition temperature lies well above liquid nitrogen boiling point [106] makes cuprates valuable in technological applications, such as producing high magnetic field. The cuprates has layered structure, anti-ferromagnetic parent compound, *d*-wave gap and very likely non-phonon mediated pairing mechanism. Those unique properties make it very distinguishable from conventional superconductors, including MgB_2 and heavy Fermion superconductors. A question arose whether or not high transition temperature requires all those peculiar properties (layered structure, anti-ferromagnetic parent compound, *d*-wave gap and non-phonon mediated pairing). This question is partial answered by the discovery of iron-based superconductors.

The discovery of the iron-based superconductors in 2006 broke the monopoly of cuprates in the world of HTSC. Same as the cuprates, it has layered structure, anti-ferromagnetic parent compound and likely non-phonon mediated Cooper pairs. However, there are significant differences between the two: the iron-based superconductors has multiple surfaces and $s \pm$ gaps. The study of iron-pnictide, together with

cuprates, will reveal more secret of HTSC.

We present results of transport measurements of $BaFe_{1.85}Co_{0.15}As_2$, an electron doped "122" system near optimal doping. The DC measurement shows clear superconducting transition at 25 K, An abrupt drop in resistivity indicates good quality of single crystal sample. A purely-phonon-mediated pairing mechanism is shown to be unlikely for $BaFe_{1.85}Co_{0.15}As_2$ that electron-phonon coupling constant derived from standard Bloch-Gruneisen is only 0.2.

The AC measurement data is collected at different temperatures above and below the superconducting transition. In the normal state, upon cooling down the sample, the Drude term in the real part of optical conductivity gets narrower. Drude-Lorentzian fits are carried out that two inter-band and two intra-band transitions are needed to accurately reproduce the experimental data. Detailed analysis of plasma frequency, scattering rate and mean free path shows that despite the multi-gap nature, the normal state conductivity of $BaFe_{1.85}Co_{0.15}As_2$ is dominated by one single electron pocket.

In the superconducting state, a clear "missing area" in optical conductivity is observed. That is a signature of super-fluid condensate. The remaining conductivity indicates that our $BaFe_{1.85}Co_{0.15}As_2$ sample is in the "dirty limit". Two superconducting gaps are required to fit the experimental data. The ratio between the larger gap and superconducting transition temperature is significantly higher than that of the BCS case ($2\Delta/kT_c = 3.5$) therefore puts $BaFe_{1.85}Co_{0.15}As_2$ in the strong coupling limit. Eliashberg theory [107] is used to extract electron-boson spectral function

$W(\omega)$. A peak at 45 meV is identified in $W(\omega)$, the position of which lies well beyond any phonon mode. This observation is in favor of spin-fluctuation over phonon as the paring mechanism for Cooper pairs.

Our experimental data shows that $BaFe_{1.85}Co_{0.15}As_2$ is a strong coupling, spin-mediated, multi-gap non-BCS superconductor in the dirty limit. Many topics, especially the possible mechanisms for superconductivity, are still the subject of considerable debate and further research.

6.2 Vortex Raman Spectroscopy

The field of vortex light is gaining more and more attention in physics. Beside polarization, light beams can carry orbital angular momentum. The helical wavefront and non-zero orbital angular momentum makes us seek potential applications of vortex light in the field of spectroscopy. It has been shown [98] that the interaction between vortex light and electronic degree of freedom is an higher order effect than the interaction between vortex light and atomic movement (rotation, vibration). We thus focus our attention on Raman scattering with vortex light.

The Hamiltonian for interaction between vortex light and matter is analyzed by group theory. Symmetry predicts certain go/no-go rules and they are summarized in the form Raman tensors. We show that, in cubic system with vortex light, previous silent Γ_2 phonon mode becomes active and the intensity dependence on polarization change for Γ_3 phonon modes.

The experiment should be carried out on a cubic crystal with Γ_2 or Γ_3 phonon. Many well known cubic systems, quite surprisingly, do not have those two phonons. The search of such crystal makes us conduct a study on phonon structure in cubic system. After this study the whole picture is clear that Γ_1, Γ_2 and Γ_3 phonons only appear in rather complicated crystals. $Bi_4Ge_3O_{12}$ crystal is one proper crystal that meets all requirements. Future experiments should be carried out to verify the proposed Raman scattering with vortex light.

Appendix

Appendix

The 32 crystallographic point groups are listed in different notations. The meaning of the symbols can be found in standard textbooks. For some point groups, other names exist such as V for point group D_2 and these are listed also under the Schoenflies notation column. O_h and D_{6h} are of the highest order and all other groups are subgroups of each or both of the two. This is helpful in some discussions that if certain rule holds for both O_h and D_{6h}, it holds for all crystallographic point groups. In fact the group multiplication table are given only to O_h and D_{6h} in the book of Kovalev [12].

Also tabulated are the 230 (3,3) Fedorov groups and the 17 (2,2) wallpaper groups. For Fedorov groups, each group is arranged in the order of group number, Schoenflies notation and international notation. For wallpaper group, each row represents one group. Due to historical reasons, other names exist for the wallpaper group and these are also listed.

Hermann-Mauguin (full)	Hermann-Mauguin (short)	Shubnikov	Schoenflies
1	1	1	C_1
$\bar{1}$	$\bar{1}$	$\tilde{2}$	$C_i = S_2$
2	2	2	C_2
m	m	m	$C_s = C_{1h}$
$\frac{2}{m}$	$2/m$	$2:m$	C_{2h}
222	222	$2:2$	$D_2 = V$
$mm2$	$mm2$	$2 \cdot m$	C_{2v}
$\frac{2}{m}\frac{2}{m}\frac{2}{m}$	mmm	$m \cdot 2 : m$	$D_{2h} = V_h$
4	4	4	C_4
$\bar{4}$	$\bar{4}$	$\tilde{4}$	S_4
$\frac{4}{m}$	$4/m$	$4:m$	C_{4h}
422	422	$4:2$	D_4
$4mm$	$4mm$	$4 \cdot m$	C_{4v}
$\bar{4}2m$	$\bar{4}2m$	$\tilde{4} \cdot m$	$D_{2d} = V_d$
$\frac{4}{m}\frac{2}{m}\frac{2}{m}$	$4/mmm$	$m \cdot 4 : m$	D_{4h}
3	3	3	C_3
$\bar{3}$	$\bar{3}$	$\tilde{6}$	$S_6 = C_{3i}$
32	32	$3:2$	D_3
$3m$	$3m$	$3 \cdot m$	C_{3v}
$\bar{3}\frac{2}{m}$	$\bar{3}m$	$\tilde{6} \cdot m$	D_{3d}
6	6	6	C_6
$\bar{6}$	$\bar{6}$	$3:m$	C_{3h}
$\frac{6}{m}$	$6/m$	$6:m$	C_{6h}
622	622	$6:2$	D_6
$6mm$	$6mm$	$6 \cdot m$	C_{6v}
$\bar{6}m2$	$\bar{6}m2$	$m \cdot 3 : m$	D_{3h}
$\frac{6}{m}\frac{2}{m}\frac{2}{m}$	$6/mmm$	$m \cdot 6 : m$	D_{6h}
23	23	$3/2$	T
$\frac{2}{m}\bar{3}$	$m\bar{3}$	$\tilde{6}/2$	T_h
432	432	$3/4$	O
$\bar{4}3m$	$\bar{4}3m$	$3/\tilde{4}$	T_d
$\frac{4}{m}\bar{3}\frac{2}{m}$	$m\bar{3}m$	$\tilde{6}/4$	O_h

Table .1 : The 32 crystallographic point groups.

1, C_1^1, $P1$	2, C_i^1, $P\bar{1}$	3, C_2^1, $P2$	4, C_2^2, $P2_1$	5, C_2^3, $B2$
6, C_s^1, Pm	7, C_s^2, Pb	8, C_s^3, Bm	9, C_s^4, Bb	10, C_{2h}^1, $P2/m$
11, C_{2h}^2, $P2_1/m$	12, C_{2h}^3, $B2/m$	13, C_{2h}^4, $P2/b$	14, C_{2h}^5, $P2_1/b$	15, C_{2h}^6, $B2/b$
16, D_2^1, $P222$	17, D_2^2, $P222_1$	18, D_2^3, $P2_12_12$	19, D_2^4, $P2_12_12_1$	20, D_2^5, $C222_1$
21, D_2^6, $C222$	22, D_2^7, $F222$	23, D_2^8, $I222$	24, D_2^9, $I2_12_12_1$	25, C_{2v}^1, $Pmm2$
26, C_{2v}^2, $Pmc2_1$	27, C_{2v}^3, $Pcc2$	28, C_{2v}^4, $Pma2$	29, C_{2v}^5, $Pca2_1$	30, C_{2v}^6, $Pnc2$
31, C_{2v}^7, $Pmn2_1$	32, C_{2v}^8, $Pba2$	33, C_{2v}^9, $Pna2_1$	34, C_{2v}^{10}, $Pnn2$	35, C_{2v}^{11}, $Cmm2$
36, C_{2v}^{12}, $Cmc2_1$	37, C_{2v}^{13}, $Ccc2$	38, C_{2v}^{14}, $Amm2$	39, C_{2v}^{15}, $Abm2$	40, C_{2v}^{16}, $Ama2$
41, C_{2v}^{17}, $Aba2$	42, C_{2v}^{18}, $Fmm2$	43, C_{2v}^{19}, $Fdd2$	44, C_{2v}^{20}, $Imm2$	45, C_{2v}^{21}, $Iba2$
46, C_{2v}^{22}, $Ima2$	47, D_{2h}^1, $Pmmm$	48, D_{2h}^2, $Pnnn$	49, D_{2h}^3, $Pccm$	50, D_{2h}^4, $Pban$
51, D_{2h}^5, $Pmma$	52, D_{2h}^6, $Pnna$	53, D_{2h}^7, $Pmna$	54, D_{2h}^8, $Pcca$	55, D_{2h}^9, $Pbam$
56, D_{2h}^{10}, $Pccn$	57, D_{2h}^{11}, $Pbcm$	58, D_{2h}^{12}, $Pnnm$	59, D_{2h}^{13}, $Pmmn$	60, D_{2h}^{14}, $Pbcn$
61, D_{2h}^{15}, $Pbca$	62, D_{2h}^{16}, $Pnma$	63, D_{2h}^{17}, $Cmcm$	64, D_{2h}^{18}, $Cmca$	65, D_{2h}^{19}, $Cmmm$
66, D_{2h}^{20}, $Cccm$	67, D_{2h}^{21}, $Cmma$	68, D_{2h}^{22}, $Ccca$	69, D_{2h}^{23}, $Fmmm$	70, D_{2h}^{24}, $Fddd$
71, D_{2h}^{25}, $Immm$	72, D_{2h}^{26}, $Ibam$	73, D_{2h}^{27}, $Ibca$	74, D_{2h}^{28}, $Imma$	75, C_4^1, $P4$
76, C_4^2, $P4_1$	77, C_4^3, $P4_2$	78, C_4^4, $P4_3$	79, C_4^5, $I4$	80, C_4^6, $I4_1$
81, S_4^1, $P\bar{4}$	82, S_4^2, $I\bar{4}$	83, C_{4h}^1, $4/m$	84, C_{4h}^2, $P4_2/m$	85, C_{4h}^3, $P4/n$
86, C_{4h}^4, $P4_2/n$	87, C_{4h}^5, $I4/m$	88, C_{4h}^6, $I4_1/a$	89, D_4^1, $P422$	90,D_4^2, $P42_12$
91, D_4^3, $P4_122$	92, D_4^4, $P4_12_12$	93, D_4^5, $P4_222$	94, D_4^6, $P4_22_12$	95, D_4^7, $P4_322$
96, D_4^8, $P4_32_12$	97, D_4^9, $I422$	98, D_4^{10}, $I4_122$	99, C_{4v}^1, $P4mm$	100, C_{4v}^2, $P4bm$
101, C_{4v}^3, $P4_2cm$	102, C_{4v}^4, $P4_2nm$	103, C_{4v}^5, $P4cc$	104, C_{4v}^6, $P4nc$	105, C_{4v}^7, $P4_2mc$
106, C_{4v}^8, $P4_2bc$	107, C_{4v}^9, $I4mm$	108, C_{4v}^{10}, $I4cm$	109, C_{4v}^{11}, $I4_1md$	110, C_{4v}^{12}, $I4_1cd$
111, D_{2d}^1, $P\bar{4}2m$	112, D_{2d}^2, $P\bar{4}2c$	113, D_{2d}^3, $P\bar{4}2_1m$	114, D_{2d}^4, $P\bar{4}2_1c$	115, D_{2d}^5, $P\bar{4}m2$
116, D_{2d}^6, $P\bar{4}c2$	117, D_{2d}^7, $P\bar{4}b2$	118, D_{2d}^8, $P\bar{4}n2$	119, D_{2d}^9, $I\bar{4}m2$	120, D_{2d}^{10}, $I\bar{4}2c$
121, D_{2d}^{11}, $I\bar{4}2m$	122, D_{2d}^{12}, $I\bar{4}2d$	123, D_{4h}^1, $P4/mmm$	124, D_{4h}^2, $P4/mcc$	125, D_{4h}^3, $P4/nbm$
126, D_{4h}^4, $P4/nnc$	127, D_{4h}^5, $P4/mbm$	128, D_{4h}^6, $P4/mnc$	129, D_{4h}^7, $P4/nmm$	130, D_{4h}^8, $P4/ncc$
131, D_{4h}^9, $P4_2mmc$	132, D_{4h}^{10}, $P4_2mcm$	133, D_{4h}^{11}, $P4_2nbc$	134, D_{4h}^{12}, $P4_2/nnm$	135, D_{4h}^{13}, $P4_2/mbc$
136, D_{4h}^{14}, $P4_2/mnm$	137, D_{4h}^{15}, $P4_2/nmc$	138, D_{4h}^{16}, $P4_2/ncm$	139, D_{4h}^{17}, $I4/mmm$	140, D_{4h}^{18}, $I4/mcm$
141, D_{4h}^{19}, $I4_1amd$	142, D_{4h}^{20}, $I4_1/acd$	143, C_3^1, $P3$	144, C_3^2, $P3_1$	145, C_3^3, $P3_2$
146, C_3^4, $R3$	147, C_{3i}^1, $P\bar{3}$	148, C_{3i}^2, $R\bar{3}$	149, D_3^1, $P312$	150, D_3^2, $P321$
151, D_3^3, $P3_112$	152, D_3^4, $P3_121$	153, D_3^5, $P3_212$	154, D_3^6, $P3_221$	155, D_3^7, $R32$
156, C_{3v}^1, $P3m1$	157, C_{3v}^2, $P31m$	158, C_{3v}^3, $P3c1$	159, C_{3v}^4, $P31c$	160, C_{3v}^5, $R3m$
161, C_{3v}^6, $R3c$	162, D_{3d}^1, $P\bar{3}1m$	163, D_{3d}^2, $P\bar{3}1c$	164, D_{3d}^3, $P\bar{3}m1$	165, D_{3d}^4, $P\bar{3}c1$
166, D_{3d}^5, $R\bar{3}m$	167, D_{3d}^6, $R\bar{3}c$	168, C_6^1, $P6$	169, C_6^2, $P6_1$	170, C_6^3, $P6_5$
171, C_6^4, $P6_2$	172, C_6^5, $P6_4$	173, C_6^6, $P6_3$	174, C_{3h}^1, $P\bar{6}$	175, C_{6h}^1, $P6/m$
176, C_{6h}^2, $P6_3/m$	177, D_6^1, $P622$	178, D_6^2, $P6_122$	179, D_6^3, $P6_522$	180, D_6^4, $P6_222$
181, D_6^5, $P6_422$	182, D_6^6, $P6_322$	183, C_{6v}^1, $P6mm$	184, C_{6v}^2, $P6cc$	185, C_{6v}^3, $P6_3cm$
186, C_{6v}^4, $P6_3mc$	187, D_{3h}^1, $P\bar{6}m2$	188, D_{3h}^2, $P\bar{6}c2$	189, D_{3h}^3, $P\bar{6}2m$	190, D_{3h}^4, $P\bar{6}2c$
191, D_{6h}^1, $P6/mmm$	192, D_{6h}^2, $P6/mcc$	193, D_{6h}^3, $P6_3/mcm$	194, D_{6h}^4, $P6_3/mmc$	195, T^1, $P23$
196, T^2, $F23$	197, T^3, $I23$	198, T^4, $P2_13$	199, T^5, $I2_13$	200, T_h^1, $Pm3$
201, T_h^2, $Pn3$	202, T_h^3, $Fm3$	203, T_h^4, $Fd3$	204, T_h^5, $Im3$	205, T_h^6, $Pa3$
206, T_h^7, $Ia3$	207, O^1, $P432$	208, O^2, $P4_232$	209, O^3, $F432$	210, O^4, $F4_132$
211, O^5, $I432$	212, O^6, $P4_332$	213, O^7, $P4_132$	214, O^8, $I4_132$	215, T_d^1, $P\bar{4}3m$
216, T_d^2, $F\bar{4}3m$	217, T_d^3, $I\bar{4}3m$	218, T_d^4, $P\bar{4}3n$	219, T_d^5, $F\bar{4}3n$	220, T_d^6, $I\bar{4}3d$
221, O_h^1, $Pm3m$	222, O_h^2, $Pn3n$	223, O_h^3, $Pm3n$	224, O_h^4, $Pn3m$	225, O_h^5, $Fm3m$
226, O_h^6, $Fm3c$	227, O_h^7, $Fd3m$	228, O_h^8, $Fd3c$	229, O_h^9, $Im3m$	230, O_h^{10}, $Ia3d$

Table .2 : The 230 (3,3) Fedorov groups.

Number	crystal system	IUC notations	alternative names
1	parallelogrammatic	$p1$	
2	parallelogrammatic	$p2$	$p211$
3	rectangle	pm	$p1m1$
4	rectangle	pg	$p1g1$
5	rhombus	cm	$c1m1$
6	rectangle	pmm	$p2mm$
7	rectangle	pmg	$p2mg$
8	rectangle	pgg	$p2gg$
9	rhombus	cmm	$c2mm$
10	square	$p4$	$p4mm$
11	square	$p4m$	
12	square	$p4g$	$p4gm$
13	hexagon	$p3$	
14	hexagon	$p31m$	
15	hexagon	$p3m1$	
16	hexagon	$p6$	
17	hexagon	$p6m$	$p6mm$

Table .3 : The 17 (2,2) wallpaper groups.

Bibliography

[1] H. Weyl, *Gruppentheorie und Quantenmechanik*. 1928.

[2] E. P. Wigner, *Gruppentheorie und ihre Anwendung auf die Quantenmechanik der Atomspektren*. F. Vieweg & Sogn Akt.-Ges, 1931.

[3] J. F. C. Hessel, "Krystallometrie oder Krystallonomie und Krystallographie," *Gehler's Physikalisches Worterbuch*, vol. 5, p. 1062, 1830.

[4] A. Schonflies, *Kirstallsysteme and Krisiallstruktur*. 1891.

[5] E. S. Fedorov, "Protokolnaia Zapis," *Zap. Min. Obshch.*, vol. 26, p. 455, 1891.

[6] N. Steno, *De solido intra solidum naturaliter contento dissertationis prodromus*. Jacobum Moukee, 1679.

[7] E. B. Wilson, J. C. Decius, and P. C. Cross, *Molecular Vibrations: The Theory of Infrared and Raman Vibrational Spectra*. Courier Dover Publications, 1955.

[8] G. F. Koster, J. O. Dimmock, R. G. Wheeler, and H. Statz, *The Properties of the Thirty-Two Point Groups*. The MIT Press, 1963.

[9] R. W. G. Wyckoff, *Crystal structures*. John Wiley & sons, New York, London, 1963.

[10] T. Hahn, ed., *International Tables for Crystallography Volume A: Space-group symmetry*. Springer, 2006.

[11] J. L. Birman, *Theory of Crystal Space Groups and Lattice Dynamics: Infra-Red and Raman Optical Processes of Insulating Crystals*. Springer-Verlag New York, LLC, 1984.

[12] O. V. Kovalev, *Irreducible representations of the space groups*. Gordon and Breach:New York, 1965.

[13] J. Zak, *The Irreducible representations of space groups*. W. A. Benjamin, 1969.

[14] S. C. Miller and W. F. Love, *Tables of irreducible representations of space groups and corepresentations of magnetic space groups*. Boulder, Colorado : Pruett, 1967.

[15] A. P. Cracknell and B. L. Davies, *Kronecker product tables*. IFI/Plenum, 1980.

[16] T. Terzibaschian and R. Enderlein, "The Irreducible Representations of the Two-Dimensional Space Group of Crystal Surfaces," *phys. stat. sol. (b)*, vol. 133, p. 433, 1986.

[17] A. V. Shubnikov, *Symmetry and Antisymmetry of Finite Figures*. Acad. Sci. U.S.S.R. Press, Moscow, 1951.

[18] E. P. Wigner, "Uber die Operation der Zeitumkehr in der Quantenmechanik," *Nachr. Akad. Ges. Wiss. Gottingen, Math.-Physik*, vol. 31, p. 546, 1932.

[19] J. O. Dimmock and R. G. Wheeler, "Irreducible representations of magnetic groups," *Zap. Min. Obshch.*, vol. 23, p. 729, 1962.

[20] G. Frobenius and J. Schur, "Uber die reellen darstellungen der endlichen gruppen," *Sitz. Ber. Preuss. Akad. Wiss.*, vol. 49, p. 186, 1906.

[21] G. Frobenius and J. Schur, "Uber die quivalenz der gruppen linearer substitutionen," *Sitz. Ber. Preuss. Akad. Wiss.*, vol. 49, p. 209, 1906.

[22] H. A. Kramers, "Theorie generale de la rotation paramagnetique dans les cristaux," *Proc. Acad. Sci. Amsterdam*, vol. 33, p. 959, 1930.

[23] N. W. Ashcroft and N. D. Mermin, *Solid State Physics*. Brooks Cole, 1976.

[24] D. C. Harris and M. D. Bertiolucci, *Symmetry and Spectroscopy: An Introduction to Vibrational and Electronic Spectroscopy*. Dover publications, 1989.

[25] M. Dressel and G. Gruner, *Electrodynamics of Solids: Optical Properties of Electrons in Matter*. Cambridge University Press, 2002.

[26] P. R. Griffiths and C. C. Homes, "Instrumentation for far-infrared spectroscopy," in *Handbook of Vibrational Spectroscopy, Volume 1 - Theory and Instrumentation*, John Wiley & sons, New York, London, 2001.

[27] L. Rosenfeld, *Theory of Electrons*. Dover, 1965.

[28] R. de L. Kronig, "On the theory of the dispersion of X-rays," *J. Opt. Soc. Am.*, vol. 12, p. 547, 1926.

[29] H. A. Kramers, "La diffusion de la lumiere par les atomes," *Atti Cong. Intern. Fisica*, vol. 2, p. 545, 1927.

[30] J. C. Maxwell, "A Dynamical Theory of the Electromagnetic Field," *Philosophical Transactions of the Royal Society of London*, vol. 155, p. 459, 1865.

[31] J. M. Ziman, *Priciples of the theory of solids*. Cambridge University Press, 1972.

[32] J. D. Jackson, *Classical Electrodynamics*. John Wiley & sons, New York, London, 1998.

[33] M. Born and E. Wolf, *Principles of Optics: Electromagnetic Theory of Propagation, Interference and Diffraction of Light*. Cambridge University Press, 1999.

[34] M. Born and K. Huang, *Dynamical Theory of Crystal Lattices*. Clarendon Press, 1954.

[35] W. Hayes and R. loudon, *Scattering of Light by Crystals*. Dover publication, 1978.

[36] R. Loudon, "The Raman effect in crystals," *Advances in Physics*, vol. 50, p. 813, 2001.

[37] G. D. Mahan, *Many Particle Physics (Physics of Solids and Liquids)*. Plenum Press, 1979.

[38] P. Drude, "Zur Elektronentheorie der metalle," *Annalen der Physik*, vol. 306, p. 566, 1900.

[39] J. D. G. H. R. O. A. Schilling, M. Cantoni, "Superconductivity above 130 K in the Hg-Ba-Ca-Cu-O system," *Nature*, vol. 363, p. 56, 1993.

[40] L. N. C. J. Bardeen and J. R. Schrieffer, "Theory of Superconductivity," *Phys. Rev.*, vol. 108, p. 1175, 1957.

[41] J. R. Schrieffer, *Theory Of Superconductivity*. Perseus Books, 1999.

[42] R. E. Glover and M. Tinkham, "Conductivity of Superconducting Films for Photon Energies between 0.3 and $40kT_c$," *Phys. Rev.*, vol. 108, p. 243, 1957.

[43] M. Tinkham, *Introduction to Superconductivity*. Dover publication, 1996.

[44] D. C. Mattis and J. Bardeen, "Theory of the Anomalous Skin Effect in Normal and Superconducting Metals," *Phys. Rev.*, vol. 111, p. 412, 1958.

[45] G. M. Eliashberg, "Interactions between electrons and lattice vibrations in a superconductor," *J. Exptl. Theoret. Phys. (U.S.S.R.)*, vol. 38, p. 966, 1957.

[46] W. L. McMillan, "Transition Temperature of Strong-Coupled Superconductors," *Phys. Rev.*, vol. 167, p. 331, 1968.

[47] S. V. Vonsovsky, Y. Izyumov, and E. Z. Kurmaev, *Superconductivity Of Transition Metals*. Springer-Verlag New York, Inc, 1982.

[48] J. G. Bednorz and K. A. Muller, "Possible high T_c superconductivity in the BaLaCuO system," *Zeitschrift fur Physik B Condensed Matter*, vol. 64, p. 189, 1986.

[49] Y. Kamihara, H. Hiramatsu, M. Hirano, R. Kawamura, H. Yanagi, T. Kamiya, and H. Hosono, "Iron-Based Layered Superconductor: LaOFeP," *J. Am. Chem. Soc.*, vol. 128, p. 10012, 2006.

[50] Y. Kamihara, T. Watanabe, M. Hirano, and H. Hosono, "Iron-Based Layered Superconductor La[$O_{1-x}F_x$]FeAs (x = 0.05-0.12) with T_c = 26 K," *J. Am. Chem. Soc.*, vol. 130, p. 3296, 2008.

[51] A. F. Hebard, M. J. Rosseinsky, R. C. Haddon, D. W. Murphy, S. H. Glarum, T. T. M. Palstra, A. P. Ramirez, and A. R. Kortan, "Superconductivity at 18 K in potassium-doped C_{60}," *Nature*, vol. 350, p. 600, 1991.

[52] F. Steglich, J. Aarts, C. D. Bredl, W. Lieke, D. Meschede, W. Franz, and H. Schafer, "Superconductivity in the Presence of Strong Pauli Paramagnetism: $CeCu_2Si_2$," *Phys. Rev. Lett.*, vol. 43, p. 1892, 1979.

[53] K. Bechgaard, K. Carneiro, M. Olsen, F. B. Rasmussen, and C. S. Jacobsen, "Zero-Pressure Organic Superconductor: Di-(Tetramethyltetraselenafulvalenium)-Perchlorate $[(TMTSF)_2ClO_4]$," *Phys. Rev. Lett.*, vol. 46, p. 852, 1981.

[54] F. Marsiglio, T. Startseva, and J. P. Carbotte, "Inversion of K_3C_{60} reflectance data," *Physics Letters A*, vol. 245, p. 172, 1998.

[55] J. P. Carbotte, E. Schachinger, and D. N. Basov, "Coupling strength of charge carriers to spin fluctuations in high-temperature superconductors," *Nature*, vol. 401, p. 356, 1999.

[56] L. Allen, M. W. Beijersbergen, R. J. C. Spreeuw, and J. P. Woerdman, "Orbital angular momentum of light and the transformation of Laguerre-Gaussian laser modes," *Phys. Rev. A*, vol. 45, p. 8185, 1992.

[57] D. N. Basov, R. D. Averitt, D. van der Marel, M. Dressel, and K. Haule, "Electrodynamics of correlated electron materials," *Rev. Mod. Phys.*, vol. 83, p. 471, 2011.

[58] L. Degiorgi, "The electrodynamic response of heavy-electron compounds," *Rev. Mod. Phys.*, vol. 71, p. 687, 1999.

[59] D. N. Basov and T. Timusk, "Electrodynamics of high-T_c superconductors," *Rev. Mod. Phys.*, vol. 77, p. 721, 2005.

[60] C. V. Raman and K. S. Krishnan, "A New Type of Secondary Radiation," *Nature*, vol. 121, p. 501, 1928.

[61] R. Loudon, "Theory of the first-order Raman effect in crystals," *Proc. Roy. Soc.*, vol. A 275, p. 218, 1963.

[62] J. R. Sandercock, "Brillouin-Scattering Measurements on Silicon and Germanium," *Phys. Rev. Lett*, vol. 28, p. 137, 1972.

[63] G. Placzek, "Rayleigh-streuung und raman-effekt," in *Handbuch der Radiologie*, Akademische Verlagsgesellschaft, Leipzig, 1934.

[64] P. Y. Yu and M. Cardona, *Fundamentals of Semiconductors: Physics and Materials Properties*. Springer-Verlag Telos, 2001.

[65] J. L. Birman and R. Berenson, "Scattering tensors and Clebsch-Gordan coefficients in crystals," *Phys. Rev. B*, vol. 9, p. 4512, 1974.

[66] A. Compaan and H. Z. Cummins, "Resonant Quadrupole-Dipole Raman Scattering at the 1S Yellow Exciton in Cu_2O," *Phys. Rev. Lett.*, vol. 31, p. 41, 1973.

[67] R. Loudon, "The Raman effect in crystals," *Adv. Phys.*, vol. 13, p. 423, 1964.

[68] J. F. Nye, *Physical Properties of Crystals*. Oxford:Clarendon Press, 1957.

[69] C. H. Henry and J. J. Hopfield, "Raman Scattering by Polaritons," *Phys. Rev. Lett.*, vol. 15, p. 964, 1965.

[70] Z. Ren, G. Che, X. Dong, J. Yang, W. Lu, W. Yi, X. Shen, Z. Li, L. Sun, F. Zhou, and Z. Zhao, "Superconductivity and phase diagram in iron-based

arsenic-oxides $ReFeAsO_{1-\delta}$ (Re = rare-earth metal) without fluorine doping ," *Europhysics Letters*, vol. 83, p. 17002, 2008.

[71] A. A. Abrikosov and L. P. Gor'kov, "Contribution to the theory of superconducting alloys with paramagnetic impurities," *Sov. Phys. JETP*, vol. 12, p. 1243, 1961.

[72] C. de la Cruz, Q. Huang, J. W. Lynn, J. Li, W. R. II, J. L. Zarestky, H. A. Mook, G. F. Chen, J. L. Luo, N. L. Wang, and P. Dai, "Magnetic order close to superconductivity in the iron-based layered $LaO_{1-x}F_xFeAs$ systems," *Nature*, vol. 453, p. 899, 2008.

[73] L. Boeri, O. V. Dolgov, and A. A. Golubov, "Is $LaFeAsO_{1-x}F_x$ an Electron-Phonon Superconductor?," *Phys. Rev. Lett.*, vol. 101, p. 026403, 2008.

[74] T. Yildirim, "Strong Coupling of the Fe-Spin State and the As-As Hybridization in Iron-Pnictide Superconductors from First-Principle Calculations," *Phys. Rev. Lett.*, vol. 102, p. 037003, 2009.

[75] J. J. Tu, J. Li, W. Liu, A. Punnoose, Y. Gong, Y. H. Ren, L. J. Li, G. H. Cao, Z. A. Xu, and C. C. Homes, "Optical properties of the iron-arsenic superconductor $BaFe_{1.85}Co_{0.15}As_2$," *Phys. Rev. B*, vol. 82, p. 174509, 2008.

[76] I. I. Mazin, D. J. Singh, M. D. Johannes, and M. H. Du, "Unconventional Superconductivity with a Sign Reversal in the Order Parameter of $LaFeAsO_{1-x}F_x$," *Phys. Rev. Lett.*, vol. 101, p. 057003, 2008.

[77] K. Ishida, Y. Nakai, and H. Hosono, "To What Extent Iron-Pnictide New Superconductors Have Been Clarified: A Progress Report," *J. Phys. Soc. Jpn.*, vol. 78, p. 062001, 2009.

[78] M. V. Sadovskii, "High-temperature superconductivity in iron-based layered iron compounds," *Physics-Uspekhi*, vol. 51, p. 1201, 2008.

[79] D. C. Johnston, "The puzzle of high temperature superconductivity in layered iron pnictides and chalcogenides," *Advances in Physics*, vol. 59, p. 803, 2010.

[80] G. R. Stewart, "Superconductivity in iron compounds," *Rev. Mod. Phys.*, vol. 83, p. 1589, 2011.

[81] P. J. Hirschfeld, M. M. Korshunov, and I. I. Mazin, "Gap symmetry and structure of Fe-based superconductors," *Reports on Progress in Physics*, vol. 74, p. 124508, 2011.

[82] W. Z. Hu, Q. M. Zhang, and N. L. Wang, "Optical and Raman spectroscopy studies on Fe-based superconductors," *Physica C: Superconductivity*, vol. 469, p. 545, 2009.

[83] J. W. Lynn and P. Dai, "Neutron studies of the iron-based family of high T_c magnetic superconductors," *Physica C: Superconductivity*, vol. 469, p. 469, 2009.

[84] L. J. Li, Y. K. Luo, Q. B. Wang, H. Chen, Z. Ren, Q. Tao, Y. K. Li, X. Lin, M. He, Z. W. Zhu, G. H. Cao, and Z. A. Xu, "Superconductivity induced by Ni doping in $BaFe_2As_2$ single crystals," *New J. Phys.*, vol. 11, p. 025008, 2009.

[85] E. Gruneisen, "Die Abhangigkeit des elektrischen Widerstandes reiner Metalle von der Temperatur," *Annalen der Physik*, vol. 408, p. 489, 1933.

[86] N. Ni, S. L. Budko, A. Kreyssig, S. Nandi, G. E. Rustan, A. I. Goldman, S. Gupta, J. D. Corbett, A. Kracher, and P. C. Canfield, "Anisotropic ther-

modynamic and transport properties of single-crystalline $Ba_{1-x}K_xFe_2As_2$ (x=0 and 0.45)," *Phys. Rev. B*, vol. 78, p. 014507, 2008.

[87] C. C. Homes, M. Reedyk, D. A. Cradles, and T. Timusk, "Technique for measuring the reflectance of irregular, submillimeter-sized samples," *Appl. Opt.*, vol. 32, p. 2976, 1993.

[88] A. P. Litvinchuk, V. G. Hadjiev, M. N. Iliev, B. Lv, A. M. Guloy, and C. W. Chu, "Raman-scattering study of $K_xSr_{1-x}Fe_2As_2$ (x=0.0,0.4)," *Phys. Rev. B*, vol. 78, p. 060503, 2008.

[89] R. A. Ferrell and R. E. Glover, III, "Conductivity of Superconducting Films: A Sum Rule," *Phys. Rev.*, vol. 109, p. 1398, 1958.

[90] M. Tinkham and R. A. Ferrell, "Determination of the Superconducting Skin Depth from the Energy Gap and Sum Rule," *Phys. Rev. Lett.*, vol. 2, p. 331, 1959.

[91] K. Terashima, Y. Sekiba, J. H. Bowen, K. Nakayama, T. Kawahara, T. Sato, P. Richard, Y.-M. Xu, L. J. Li, G. H. Cao, Z.-A. Xu, H. Ding, and T. Takahashi, "Fermi surface nesting induced strong pairing in iron-based superconductors," *PNAS*, vol. 106, p. 7330, 2009.

[92] F. Massee, Y. Huang, R. Huisman, S. de Jong, J. B. Goedkoop, and M. S. Golden, "Nanoscale superconducting-gap variations and lack of phase separation in optimally doped $BaFe_{1.86}Co_{0.14}As_2$," *Phys. Rev. B*, vol. 79, p. 220517(R), 2009.

[93] J. W. Allen and J. C. Mikkelsen, "Optical properties of CrSb, MnSb, NiSb, and NiAs," *Phys. Rev. B*, vol. 15, p. 2952, 1976.

[94] A. T. O'Neil, I. MacVicar, L. Allen, and M. J. Padgett, "Intrinsic and Extrinsic Nature of the Orbital Angular Momentum of a Light Beam," *Phys. Rev. Lett*, vol. 88, p. 053601, 2002.

[95] R. Loudon, "Theory of the forces exerted by Laguerre-Gaussian light beams on dielectrics," *Phys. Rev. A*, vol. 68, p. 013806, 2003.

[96] A. Alexandrescu, D. Cojoc, and E. D. Fabrizio, "Mechanism of Angular Momentum Exchange between Molecules and Laguerre-Gaussian Beams," *Phys. Rev. Lett.*, vol. 96, p. 243001, 2006.

[97] A. Picon, J. Mompart, J. R. V. de Aldana, L. Plaja, G. F. Calvo, and L. Roso, "Photoionization with orbital angular momentum beams," *Optics Express*, vol. 18, p. 3660, 2010.

[98] M. Babiker, C. R. Bennett, D. L. Andrews, and L. C. D. Romero, "Orbital Angular Momentum Exchange in the Interaction of Twisted Light with Molecules," *Phys. Rev. Lett*, vol. 89, p. 143601, 2002.

[99] Jian Li, Jiufeng J. Tu and Joseph L. Birman, "Raman scattering using vortex light." to be submitted.

[100] Jian Li, Jiufeng J. Tu and Joseph L. Birman, "One dimensional phonon modes in O_h space groups." to be submitted.

[101] M. Hamermesh, *Group Theory and Its Application to Physical Problems*. Dover publication, 1989.

[102] A. D. Mighell, H. M. Ondik, and B. B. Molino, "Crystal data spacegroup tables," *J. Phys. Chem. Ref. Data*, vol. 6, p. 675, 1977.

[103] A. A. Kaminskii, S. N. Bagayev, N. V. Kravtsov, S. N. Chekina, Y. V. Vasiliev, N. I. Ivannikova, K. Ueda, J. Lu, H. J. Eichler, G. M. A. Gad, J. Hanuza, J. Fernandez, and P. Reiche, "Spectroscopy and cw Laser Action, Magnetooptics and Nonlinear Optical Frequency Conversion in Ln^{3+} Doped and Undoped $Bi_4Ge_3O_{12}$ and $Bi_4Si_3O_{12}$ Crystals," *Laser Physics*, vol. 11, p. 897, 2001.

[104] B. Briat, A. Watterich, F. Ramaz, L. Kovacs, B. C. Forget, and N. Romanov, "Charge states and optical transitions of vanadium in $Bi_4Ge_3O_{12}$ identified by MCD and ODMR," *Optical Materials*, vol. 20, p. 253, 2002.

[105] R. Titorenkova1, B. Mihailova, R. Petrova, M. Gospodinov, and L. Konstantinov, "Effect of Doping on the Structure and Raman Spectra of $Bi_4Ge_3O_{12}$," *AIP Conf. Proc.*, vol. 1203, p. 289, 2009.

[106] M. K. Wu, J. R. Ashburn, C. J. Torng, P. H. Hor, R. L. Meng, L. Gao, Z. J. Huang, Y. Q. Wang, and C. W. Chu, "Superconductivity at 93 K in a new mixed-phase Y-Ba-Cu-O compound system at ambient pressure," *Phys. Rev. Lett.*, vol. 58, p. 908, 1987.

[107] E. Schachinger, J. J. Tu, and J. P. Carbotte, "Angle-resolved photoemission spectroscopy and optical renormalizations: Phonons or spin fluctuations," *Phys. Rev. B*, vol. 67, p. 214508, 2003.